A COMPUTATIONAL APPROACH TO HUMAN ADAPTIVE MOTOR CONTROL

Nikhil Bhushan

Dept. of Biomedical Engineering
Johns Hopkins University
720 Rutland Ave, 416 Traylor
Baltimore, MD 21205

A thesis submitted to the Johns Hopkins University
in conformity with the requirements for the degree of
Master's of Science in Engineering

August 25, 1998

Abstract

The aim of this thesis is to understand the computational process that underlie adaptive motor control capabilities of humans based on the study of reaching movements of the arm in the presence of novel force fields. An internal model of arm dynamics has been proposed as the computational unit in the CNS involved in learning control of novel dynamics. Based on computational principles, the internal model has been further divided into a forward and an inverse model. Co-existence of the two models has been proposed to facilitate learning of novel dynamics. However, there is as yet little evidence to support co-existence of the inverse and forward model, and little is known about their relative roles in adaptive motor control. In this thesis we develop a computational framework to simulate arm movements and analyze the properties of control methods based on these two models in the presence of novel force fields. We show that a control based exclusively on one of the two models is insufficient to explain performance characteristics of human subjects. However, a combination of the two models that relies on feedback control through a forward model and feedforward control through an inverse model is able to closely match the performance of human subjects. It is able to explain peculiar kinematic patterns in the movement trajectory during initial exposure to a novel field based on adapatation of the forward model. It is also able to mimic changes in key movement parameters during gradual learning of the force field, based on fast exponentially-decaying adaptation of both the inverse model and the forward model. This provides evidence that learning control in the CNS is accomplished through co-existence and co-adaptation of inverse and forward models. This adaptive control method based on both an inverse and a forward model provides a framework for further study of computational processes and learning mechanisms in the brain.

Contents

Introduction

Goal

The specific aim of this thesis work was to devise an adaptive control methodology which could explain results obtained from experiments where human subjects made rapid reaching movements of the arm in the presence of a novel dynamic perturbation called the curl force field. The broader implication of this work would be to provide a control framework that could explain the extraordinary ability of humans to perform motor tasks in unfamiliar interactive environments and acquire new motor skills through practice. The goal was to evaluate the control issues involved in the control of a nonlinear and complicated system like the human arm, develop a model of the human arm that incorporated these control issues, test the model with appropriate control methodologies based on the current theories of human motor control, and then determine the adaptive control method that could reasonably explain the force field adaptation study data. Then by studying this control method a greater insight could be gained about the computational problems faced by the brain to control the human arm and to understand the process of motor adaptation and learning.

Issues in Human Motor Control

Humans use their arms for simple tasks like moving objects from one point to another and for complicated tasks like playing tennis and sketching. Different tasks ideally require a form of control that is suited for that particular task. The main challange in the study of human motor system is that of understanding how a single control system can perform greatly different tasks. There are two elements of control that are involved in any task - planning and execution. For movements of the arm, planning refers to the computation of a desired trajectory for the arm, and execution refers to the computation of motor commands that will move the arm along the planned trajectory. Research in human motor control has focussed seperately on the issues of planning and execution. The main interest in this study is in the execution aspect of motor control given a planned trajectory. The problem of motor execution is difficult and extremely

challenging because of certain issues involved in the control of the arm.

The first control problem faced by the brain is that of controlling a nonlinear plant composed of a multi-joint arm and attached muscles. The output of the controller (or the brain) is a neural activation signal to the spinal cord that is then directed to muscles that move the arm. The plant receives the neural signal as input and generates force or arm movement as output. The input-output mapping of the plant is nonlinear beacuse the force or arm movement generated by the system is a nonlinear state-dependent function of the input neural activation. This nonlinearity is a result of the nonlinear force-length and force-velocity relations for the muscle, and the nonlinear dynamics of a multi-joint system.

The second control problem is that of time delays in the feedback pathways. The brain receives sensory inflow of information about the output of the arm from muscle spindles and golgi tendons and through visual feedback. In both cases, there is a time delay of nearly 150 msec, and is sufficient to cause instabilty in linear feedback control for rapid movements of the arm.

The third and most important control problem is that of changing dynamics of the arm because of different external environments. Different tasks alter the dynamics of the arm to a varying extent. Moving hand-held objects of different mass cause a shift in the center of mass and inertia of the lower arm depending on the mass of the object. This changes the relationship between input and output of the plant and a different neural activation is required to move an object of different mass along the same trajectory.

A fourth problem is that of noise in the system arising from inaccurate or noisy sensors, disturbances in the external environment, and noise in the output of the controller.

Current theories in Human Motor Control

The brain is able to overcome the control problems associated with a nonlinear time-delayed system, changing plant dynamics and noise in the system. This is evidenced in the ability of humans to perfectly control their arm movements and have the amazing ability to handle numerous objects and interact with new dynamic environments with their hand with ease. Conventional robots are stiff and clumsy in their operation compared to humans and can function only in familiar dynamic environments. It is not the technological limitation but the lack of suitable control methods that has prevented the robot from mimicking human motor behavior. Thus the human motor control system represents a highly developed controller, understanding of which will not only give a greater insight into the functioning of the brain but also new control methods for possible application in robotics. The main challenge in human motor control is then to understand this controller and the computational processes therein.

A great amount of research work in the last twenty years has focussed on trying to gain an insight into the brain control of movement, and has been divided into two different approaches - neurophysiological, based on the study of actual electrical signals and activity in different regions of the brain, and psychophysical, based on the study of movement behavior and hand trajectories. Behavioral neurophysiology has so far failed to reveal the nature of computations in the brain although it has provided knowledge of the signals that are represented in the brain and their locations. (Georgopoulos et al., 1982) showed that movement direction was encoded in M1 neurons and the firing of several neurons was sinusoidally modulated by movement direction. A population vector derived from the firing of individual cells could give a cue to the direction of movement even before the movement was initiated. Later studies by (Scott and Kalaska, 1997; Sergio and Kalaska, 1997) and (Fu et al., 1997) showed that movement parameters like movement position, velocity and acceleration were encoded by cells in both the motor and premotor areas as well as in the cerebellar cortex. The study of neuronal circuitry in the cerebellum has led to a hypothesis about a mechanism for learning and adaptation by (Kawato and Gomi, 1992) based on error related signals, but the exact biological nature of these signals is currently not known.

Psychophysical studies have on the other hand been far more successful in revealing properties of the controller used by the brain. Point-to-point reaching movements of the arm have been most commonly studied by reseachers. In one of the earliest experiments in human motor control done by (Feldman, 1966), it was shown how the elbow torque varied exponentially with elbow displacement from the desired joint angle. Since the subjects were instructed not to consciously interfere with the task, this was believed to represent a local circuit, possibly the spinal reflex loop, that functioned as a spring whose rest length could be adjusted. A theory for motor control that evolved out of this was the λ-equilibrium point hypothesis that required the controller in the brain to program only the mean resting lengths of the muscles. Later it was shown by (Bizzi et al., 1982) that muscles too had similar equilibrium properties that led to the α-equilibrium point theory. The equilibrium point hypothesis presented a control method that was simple, stable and independent of the dynamics of the plant. The equilibrium point hypothesis came under criticism by (Gomi and Kawato, 1996) because it required stiffness levels for straight movements that were higher than those observed physiologically. It was also found by (Shadmehr and Mussa-Ivaldi, 1994) that adaptation took place when subjects performed in a curl viscous force field. The subjects initially showed a large deviation from the desired straight path trajectory, but gradually with practice adapted to the field and converged to the straight path. When the force field was turned off after the subjects had adapted, the hand paths showed deviations that were a mirror image of their first movements in the field called 'aftereffects'. This led to the hypothesis of an internal model in the brain adapting to the force field. This could not be explained by the equilibrium point hypothesis because it required adapting to the dynamics of the environment. This reinforced a developing belief that

instead of equilibrium point control, an inverse dynamics model for the plant could be used for control of the arm. The inverse dynamics model translates desired states of the arm into motor commands and is an inverse mapping of the input-output relationship for the plant. The inverse model can be directly used as the controller in a feedforward path to control the plant. The inverse model is capable of learning new dynamics of the plant as in the case of force fields by modifying its internal representation to model the new dynamics based on errors in desired and actual performance.

Recent work by (Miall and Wolpert, 1996) has suggested the existence of another type of internal model, called the forward model, that allows the motor control system to predict the consequences of a motor action. The forward model mimics the plant directly and estimates the change in state of the plant given a copy of the motor commands being sent to the plant. Evidence for existence of a forward model was presented in a paper by (Wolpert et al., 1995). The most important use of having a forward model in control of arm movements is to allow feedback control in the presence of time delays. Smith predictor is one of the methods that can be used and has been proposed by (Miall et al., 1993). It will be discussed later why a simple smith predictor does not work in case of a nonlinear system like the human arm and the forward model has to be computationally more complex. Another use of the forward model is in distal supervised learning of the inverse model as proposed by (Jordan and Rumelhart, 1992). In this scheme, the forward model is initially learned from the error in predicted state from the forward model and actual state from the output of the plant, and is subsequently used to train the inverse model. This method also allows the inverse model to be trained during an offline period. This could be particularly relevant in the light of a recent result found by (Shadmehr and Holcomb, 1997) that suggests that changes occur in the internal representation of the plant during a period of rest following training in the force field. This is seen physiologically as a change in the regions of the brain being activated, and behaviorally as an improvement in performance, when subjects return to perform in the force field after a period of rest.

Tools from the Field of Robotics

Major advances have taken place in the field of robotics in the past several years. However, the control of time-delayed nonlinear systems has received only limited attention, and direct tools that can be readily considered for control of the human motor system are not available. Nonetheless, the concepts of observers, control of nonlinear systems, adaptive control and neural networks are important for understanding the computations that the brain must perform in order to control movements of the arm. These concepts have also been central to the development of current theories on human motor control. An observer is a subsystem that performs the observation of state variables of a system based on the information received from

measurement of the input and the output of the system. The observer has been proposed for the control of nonlinear systems ((Lohmiller and Slotine, 1996)) and for overcoming time delays in feedback loops ((Miall and Wolpert, 1996)). Adaptive control ((Slotine and Li, 1987)) refers to a control method where parameters of the controller can be modified in the presence of unmodeled changes in the plant and hence is an important tool for motor adaptation and learning. Neural networks have been shown to have the ability to approximate large classes of nonlinear maps sufficiently accurately, hence they can be used to construct controllers for nonlinear systems ((Narendra, 1990)). Neural networks also have the ability to learn new nonlinear maps and hence can be used for adaptive control. The origin of neural networks is related to the connectivity and computational processes in the brain, which makes it a particularly intersting tool in human motor study. Recent work by (Massaquoi and Slotine, 1996) on teleoperation has suggested a method based on wave variables for control of time delayed nonlinear systems, that could also provide a way to control the human arm.

Motivation for the Thesis

From previous work in human motor control, a single framework to study both human motor control and adaptation for reaching movements of the arm is not available. An adaptive controller for the human arm that incorporates nonlinear muscle properties and time delays in the feedback loop has not been tested for performance in unfamiliar dynamic environments. The concepts of inverse and forward models have been proposed as methods of dealing with the problems of control and learning related to arm movements, but have not been tested for actual performance and learning of novel dynamics. And little is known about the computational processes in the brain during control of arm movements, and in particular, about formation of motor memories and changes in the representation of these motor memories with time. The motivation behind this thesis was to develop a framework that could provide a means to study the control and learning of arm movements in the presence of novel dynamic environments, and then try to explain experimentally observed shifts in motor memories on the basis of changes in the controller.

In Chapter 1, an overview of control issues related to the human arm is provided and mainly involves a description of the time-delayed nonlinear plant represented by the arm. Methods to model the plant that retain its properties, are also discussed. Attempt is made to model the plant as accurately as possible, and simplifications are made only where they do not affect the properties of the plant.

In Chapter 2, a detailed account of various control methods based on concepts of equilibrium point control, inverse models and forward models is provided along with simulations with these controllers for reaching movements in the curl force field. The idea is to test the different

controllers in their ability to resolve the control problems faced by the system.

In Chapter 3, the results of actual experiments when human subjects make reaching movements of the arm in the presence of force field perturbations are provided.

In Chapter 4, two control methods, one based on purely a feedforward inverse model control, and the other on forward-inverse model feedback control, are compared and tested in their ability to explain human behavior in the presence of dramatic changes in expected dynamics.

In Chapter 5, an attempt is made to explain adaptation and learning data from Chapter 3 within the framework of forward-inverse model feedback control method. An attempt is also made to distinguish between the two types of internal models and in their rates of adaptation.

Chapter 1

Modeling of the Human Motor Apparatus

The human motor apparatus is the entire system involved in generating limb movements. In this chapter, the different components of the human motor apparatus and their features are described. Methods for developing reasonable computational models of these components are discussed. The human motor system under consideration here consists of the human arm, the muscles that control movement of the arm, spinal cord and reflex system, and supraspinal nervous system including the visual system. The first six sections in this chapter present a description of the human arm and its kinematic and dynamic properties, the muscles and their nonlinear behavior, the dynamics of the entire human arm with the musculature, a method of modeling the human arm assuming a simplified model of three pairs of muscles, sensory modalities including vision and proprioception, neural conduction pathways, and the spinal reflex mechanism. All relevant control issues concerned with each of these elements of human motor apparatus are explored and attempt is made to incorporate them in the simulation model. The last section of the chapter summarizes the model and parameter values used for simulations in this study. The brain control of movement and modeling of the brain function is the focus of this thesis and is dealt with separately in the remaining chapters.

1.1 The Human Arm - Kinematics and Passive Dynamics

The human arm is a simple mechanical system consisting of muscles and bones. For planar point to point reaching movements, the kinematics and passive dynamics of the human arm, governed by bone connectivity and the mass distributions, can be represented by a two-joint two-link mechanical system illustrated in Fig 1.1.
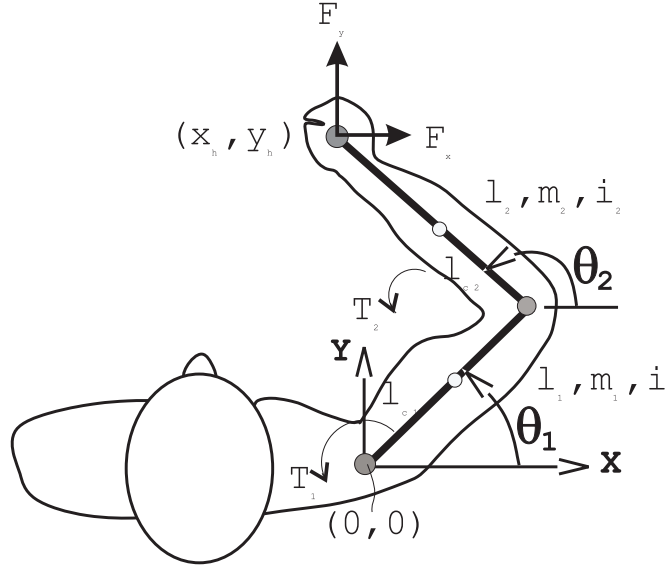
Figure 1.1: The human arm modeled as a two-joint two-link system

1.1.1 Kinematics of the Human Arm

The kinematics of the human arm refer to the configurational relationships between joint positions and hand positions and the transformation between these two coordinate systems. The following are the equations that govern the forward kinematics of the arm and represent Cartesian or hand state in terms of joint state:

$$
\begin{aligned}
x_h &= l_1 \cos\theta_1 + l_2 \cos\theta_2 \\
y_h &= l_1 \sin\theta_1 + l_2 \sin\theta_2 \\
\dot{x}_h &= -l_1 \sin\theta_1 \dot{\theta}_1 - l_2 \sin\theta_2 \dot{\theta}_2 \\
\dot{y}_h &= l_1 \cos\theta_1 \dot{\theta}_1 + l_2 \cos\theta_2 \dot{\theta}_2
\end{aligned}
$$

The last two equations can be represented in vector notation by:

$$\dot{\mathbf{x}} = J(\boldsymbol{\Theta})\dot{\boldsymbol{\Theta}} \tag{1.1}$$

$$
\mathbf{x} = \begin{bmatrix} x_h \\ y_h \end{bmatrix}; \quad
\boldsymbol{\Theta} = \begin{bmatrix} \theta_1 \\ \theta_2 \end{bmatrix}; \quad
J(\boldsymbol{\Theta}) = \frac{d\mathbf{x}}{d\boldsymbol{\Theta}} = \begin{bmatrix} -l_1 \sin\theta_1 & -l_2 \sin\theta_2 \\ l_1 \cos\theta_1 & l_2 \cos\theta_2 \end{bmatrix}
$$

where,

x_h, y_h are the cartesian x-y hand position

11

$\dot{x}_h$, $\dot{y}_h$ are the x-y hand velocity

θ_1, θ_2 are the absolute shoulder and elbow joint angles

$\dot{\theta}_1$, $\dot{\theta}_2$ are the absolute shoulder and elbow joint velocities

l_1, l_2 are the upper and lower arm lengths respectively

J is the Jacobian of joint to cartesian coordinate transform

The inverse kinematic relationship is given by the following equations,

$$
\begin{aligned}
\theta_{12} &= \cos^{-1}\left(\frac{x_h^2 + y_h^2 - l_1^2 - l_2^2}{2l_1 l_2}\right) \\
\theta_1 &= \theta_h - \sin^{-1}\left(\frac{l_2 \sin(\theta_{12})}{\sqrt{x_h^2 + y_h^2}}\right) \\
\theta_2 &= \theta_1 + \theta_{12} \\
\dot{\Theta} &= J^{-1}(\Theta)\dot{\mathbf{x}}
\end{aligned}
$$

where,

θ_{12} is the relative angle between the two links, and,

θ_h is the angle made by the hand with respect to the x-axis and is equal to $\arctan(x_h, y_h)$

The equation relating hand acceleration $\ddot{\mathbf{x}}$ to joint acceleration $\ddot{\Theta}$ is obtained by differentiating Eq. 1.1, which gives,

$$\ddot{\mathbf{x}} = J(\Theta)\ddot{\Theta} + \dot{J}(\Theta, \dot{\Theta})\dot{\Theta} \tag{1.2}$$

where,

$$\dot{J} = \frac{dJ}{dt} = \frac{dJ}{d\Theta}\frac{d\Theta}{dt}$$

1.1.2 Passive Dynamics of the Human Arm

The dynamics of the arm refers to the interaction between forces in the system and change of state of the system. A torque acting on the joints causes a change in the joint position and velocity. For the two-link two-joint system in Fig. 1.1, the dynamics can be represented in terms of the link lengths and mass and inertia of the links with these equations:

$$\tau_1 \quad = \quad (m_1 l_{c1}^2 + m_2 l_1^2 + i_1)\ddot{\theta}_1 + m_2 l_1 l_{c2} \cos(\theta_2 - \theta_1)\ddot{\theta}_2 - m_2 l_1 l_{c2} \sin(\theta_2 - \theta_1)\dot{\theta}_2^2$$

$$\tau_2 \quad = \quad (m_2 l_{c2}^2 + i_2)\ddot{\theta}_2 + m_2 l_1 l_{c2} \cos(\theta_2 - \theta_1)\ddot{\theta}_1 + m_2 l_1 l_{c2} \sin(\theta_2 - \theta_1)\dot{\theta}_1^2$$

These two equations can be jointly expressed in matrix form as,

$$\mathbf{T} = D(\mathbf{\Theta})\ddot{\mathbf{\Theta}} + C(\mathbf{\Theta}, \dot{\mathbf{\Theta}})\dot{\mathbf{\Theta}} \tag{1.3}$$

where,

$$d_{11} = m_1 l_{c1}^2 + m_2 l_1^2 + i_1$$

$$d_{22} = m_2 l_{c2}^2 + i_2$$

$$d_{12} = m_2 l_1 l_{c2} \cos(\theta_2 - \theta_1)$$

$$d_{21} = d_{12}$$

$$h = -m_2 l_1 l_{c2} \sin(\theta_2 - \theta_1);$$

$$D = \begin{bmatrix} d_{11} & d_{12} \\ d_{21} & d_{22} \end{bmatrix}$$

$$C = \begin{bmatrix} 0 & h\dot{\theta}_2 \\ -h\dot{\theta}_1 & 0 \end{bmatrix}$$

τ_1, τ_2 are the absolute shoulder and elbow torque, D is the Inertia matrix, and C is the Coriolis matrix. It is also posssible to represent the torque in terms of hand velocities and accelerations as,

$$\mathbf{T} = DJ^{-1}[\ddot{\mathbf{x}} - \dot{J}J^{-1}\dot{\mathbf{x}}] + CJ^{-1}\dot{\mathbf{x}} \tag{1.4}$$

The **forward dynamics** of the arm is the functional relationship that gives change in state of the hand in terms of the input joint torques. This is given by,

$$\ddot{\mathbf{x}} = JD^{-1}[\mathbf{T} - CJ^{-1}\dot{\mathbf{x}}] + \dot{J}J^{-1}\dot{\mathbf{x}}$$

and can be expressed in a simpler form by a nonlinear function f_D,

$$\ddot{\mathbf{x}} = f_D(\mathbf{T}, \mathbf{x}, \dot{\mathbf{x}})$$

The relationship that gives the torque required for moving the arm from one point to another along a certain trajectory is called the **inverse dynamics** of the arm and is represented by Eq.
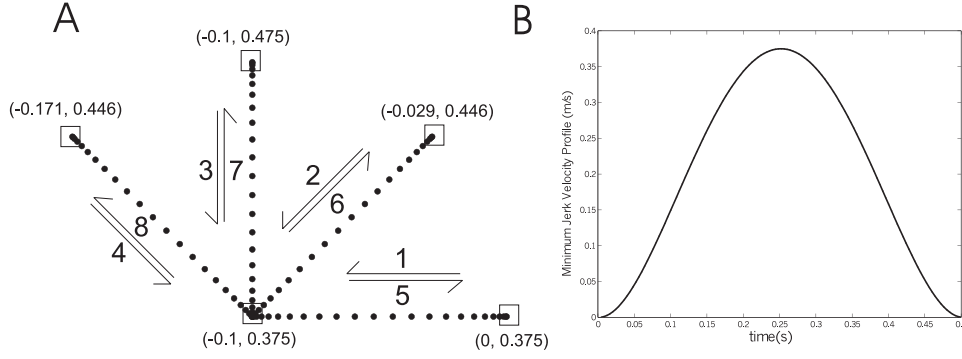
13

Figure 1.2: A, the hand paths for movements in eight different directions of movement. The movements are numbered 1 to 8. The start and end points for the movements are shown as boxes with coordinates in terms of hand position (x_h, y_h). B, the bell-shaped minimum jerk velocity profile in each direction.

1.4 or simply as f_D^{-1}. If the hand position, velocity, and acceleration are given for any instant of time then the torque can be computed using Eq. 1.4.

Note: The representation of kinematics and dynamics of the human arm is in absolute joint coordinate system throughout this thesis. This implies that the joint angles and joint torques are expressed in absolute joint coordinates

Consider eight hand paths (four pairs of outward and inward movements) shown in Fig. 1.2(A) that result in the hand moving a distance of 10 cm from the starting position ([-0.1 , 0.375] for outward movements) with a bell-shaped minimum-jerk speed profile (Fig. 1.2(B)) in eight equally spaced directions. The parameters for the arm assumed for simulating these movements are provided in Sec.1.7.

Note: A minimum jerk movement is considered because it has been experimentally found to best represent the trajectory for point-to-point reaching movements (Flash and Hogan, 1985). The minimum jerk trajectory is a straight line movement from the start point to the target with a symmetric bell-shaped velocity profile that minimizes the mean squared jerk for the movement. Jerk is defined as the derivative of hand acceleration.

Note: All simulations in the current study are based on the eight hand movements shown in Fig. 1.2(A) with the starting hand position at [-0.1 , 0.375] for outward movements. The eight movements are numbered 1 to 8 based on the direction of movement, starting with the movement in -180° leftward direction and proceding with other directions in an anticlockwise sequence. These movements and their numbering convention will be used consistently in the rest of the thesis.

The joint velocity in terms of $\dot{\theta}_1$, $\dot{\theta}_2$, for the eight directions is shown in Fig. 1.3. It can be seen that the movements in direction 2 and 6 require rotation of mainly the elbow whereas

14

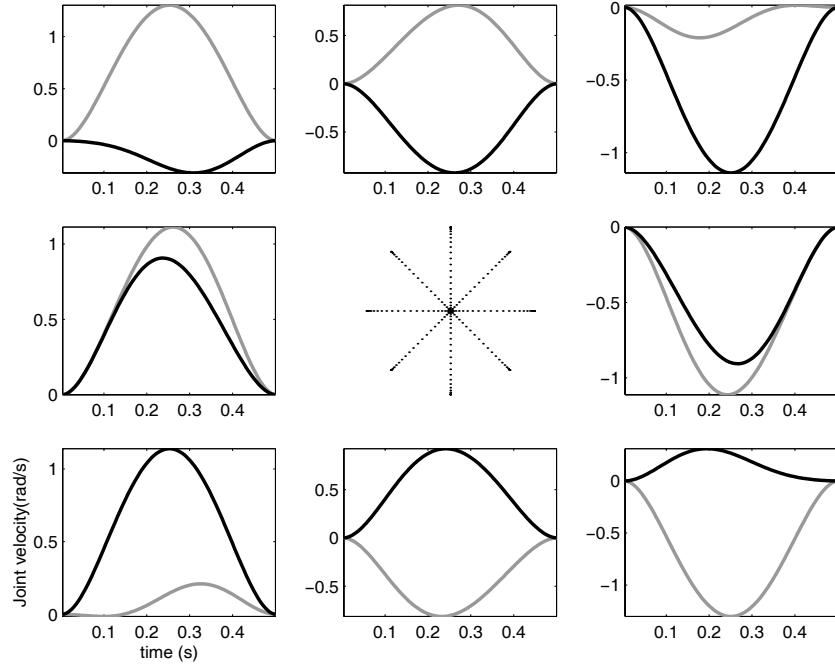Figure 1.3: The joint velocities for movements in eight different directions of movement as illustrated in Fig. 1.2. The gray line is the shoulder velocity and the black line is the elbow velocity.
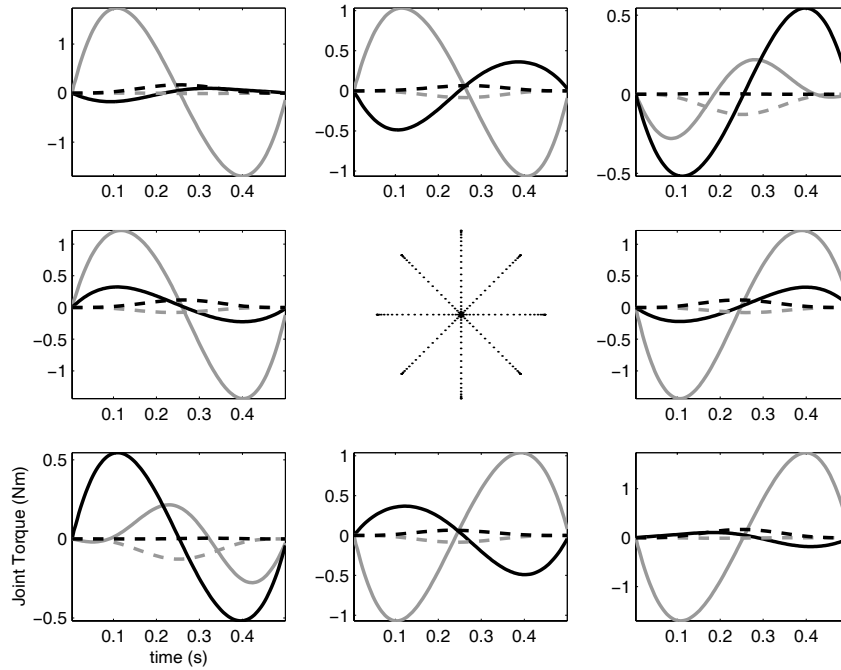

Figure 1.4: The joint torque for movements in eight different directions of movement. The gray line is the shoulder torque and the black line is the elbow torque. The dotted lines show the corresponding coriolis force components.
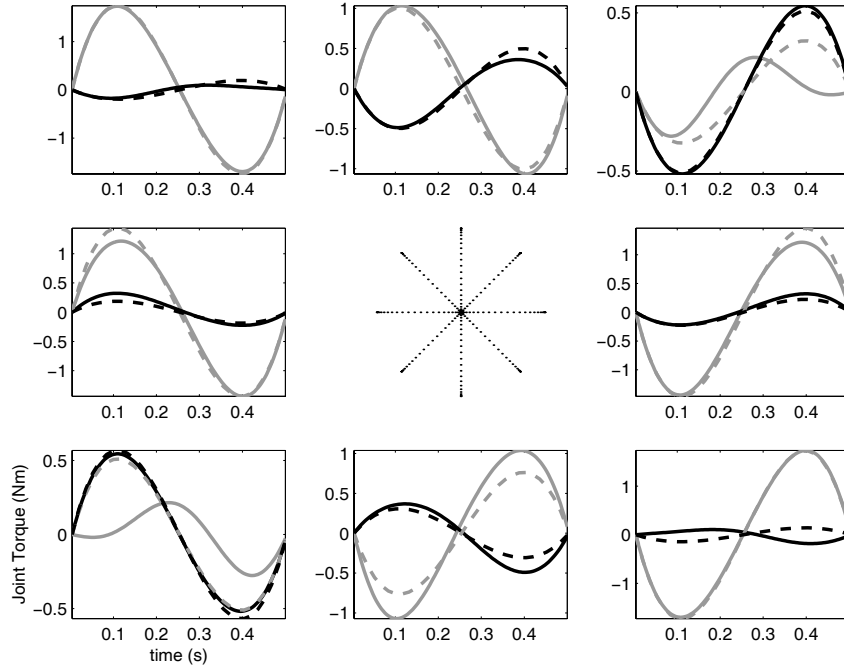
15

Figure 1.5: The joint torque for movements in eight different directions of movement computed using the simplified linear equation relating torque and hand acceleration (dotted line) and compared to the exact torque computed previously (solid) . The gray line is the shoulder torque and the black line is the elbow torque.

the movements in direction 4 and 8 require rotation of mainly the shoulder. The joint torques for these movements are given in Fig. 1.4. It is interesting to note that the torque profile for both the elbow and shoulder joint is biphasic and that the magnitude modulates almost sinusoidally with movement direction. In Eqn. 1.3, the contribution from the coriolis term is almost negligible compared to the inertia term. The dotted line in Fig. 1.4 shows the coriolis term component of torque which is small compared to the total torque (solid line). Since D and J are locally constant and can be assumed to be independent of θ for small movements, and the coriolis term is small, the torque required for a desired hand acceleration can be simply expressed as a linear function of hand acceleration. and approximately represented as,

$$\mathbf{T} = DJ^{-1}\ddot{\mathbf{x}}$$

The torque using this equation (dashed line) is compared in Fig. 1.5 with the torque (solid line) required for unloaded arm as computed earlier and shows a very close correspondence. This seems to indicate that the problem of arm control is simple in terms of torque generation for unloaded arm movements.

However the equations derived above apply only for the situation where the arm is making reaching movements in an unloaded situation. Typically, humans use their arm to pick and

16

place objects held in their hand or to move these objects along a desired trajectory. Holding objects of different shape, size and mass dramatically alter the dynamics of the arm and the simple task of making reaching movements becomes more complex. How do these objects alter the dynamics of the arm? The influence of external environment can be represented in most cases by an interaction force $\mathbf{F_x}$ acting on the hand as shown in Fig 1.1. The additional joint torque required to counteract this force is:

$$\mathbf{T} = -J^T(\mathbf{\Theta})\mathbf{F_x} \tag{1.5}$$

Any object held in the hand generates this interaction force when the hand moves. For a point mass, m , the force is $\mathbf{F_x} = m\ddot{\mathbf{x}}$. For other objects the relation can be more complex and may involve significant velocity terms which were small in the case of unloaded arm control. One thing to note however is the additive nature of this interaction force. The dynamics of the external environment can be decoupled from that of the arm itself when represented in terms of torque. This might make the task of learning and adaptation of different tasks easier. Consider interaction forces of the following structure:

$$\mathbf{F_x}(\mathbf{x}, \dot{\mathbf{x}}, t) = \Lambda(\mathbf{x})\ddot{\mathbf{x}} + \Gamma(\mathbf{x}, \dot{\mathbf{x}})\dot{\mathbf{x}} + \Delta(\mathbf{x})\mathbf{x} + \mathbf{F_x}(t) \tag{1.6}$$

where, Λ, Γ, Δ depend on the external environment dynamics. Almost all external dynamic interactions can be represented by this equation. Then, the net torque on the arm is,

$$\mathbf{T} = DJ^{-1}[\ddot{\mathbf{x}} - \dot{J}J^{-1}\dot{\mathbf{x}}] + CJ^{-1}\dot{\mathbf{x}} - J^T[\Lambda(\mathbf{x})\ddot{(\mathbf{x})} + \Gamma(\mathbf{x}, \dot{\mathbf{x}})\dot{\mathbf{x}} + \Delta(\mathbf{x})\mathbf{x} + \mathbf{F_x}(t)] \tag{1.7}$$

The first two terms on the right hand side of the equation represent the dynamics of the hand alone and the third term the dynamics of the external environment. Hence the torques required for interacting with the external environment are simply added to existing torques for moving just the arm.

1.1.3   Two Cases of Novel Dynamic Environments

The Robotic Manipulandum

A novel dynamic environment is provided when reaching movements of the arm are made while grasping a two degree of freedom robotic manipulandum as shown in Fig. 1.6. Coupling of the robotic system with the arm alters the dynamics of the system being controlled. The dynamics of the robotic arm is very similar to the human arm itself and can be expressed as,
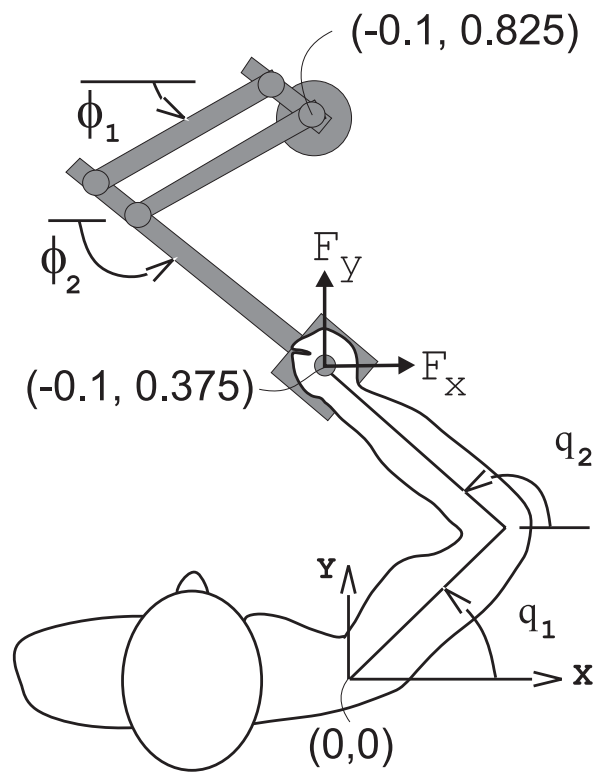
17

Figure 1.6: The robot manipulandum held in the hand. The figure shows the configuration of the robot used for actual experiments and simulations.
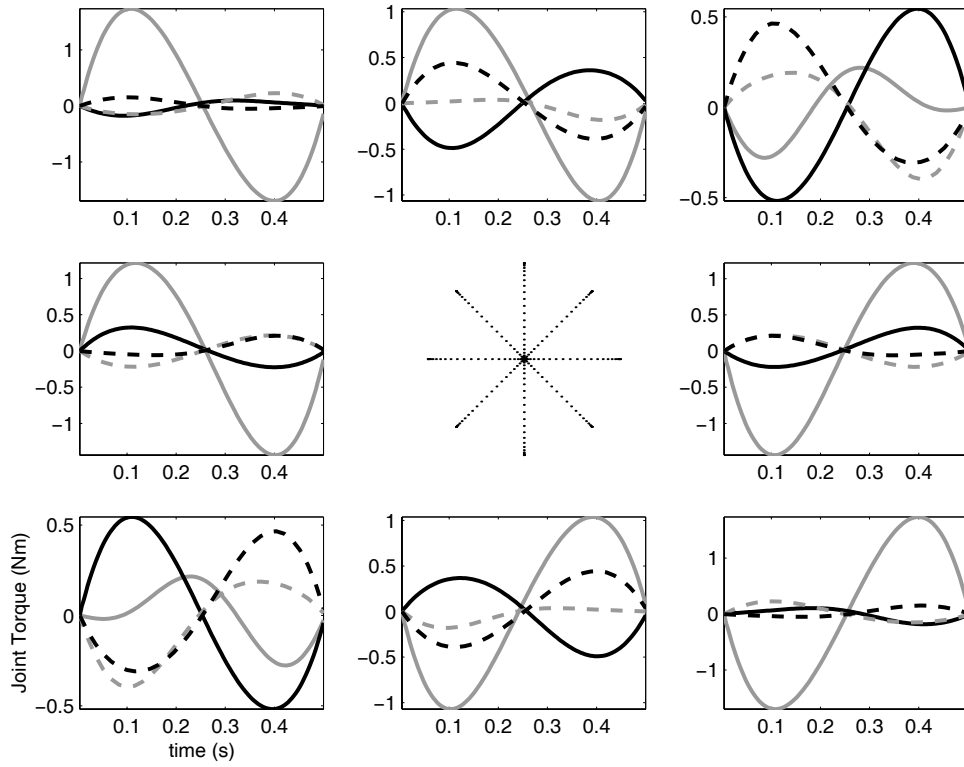
Figure 1.7: The additional joint torque (dotted line) required for movements due to the dynamics of the robot, compared to torque required for unloaded arm (solid line); the gray line is shoulder torque and the black line is elbow torque

$$
\begin{aligned}
\mathbf{T_r} &= D_r(\boldsymbol{\Phi})\ddot{\boldsymbol{\Phi}} + C(\boldsymbol{\Phi},\dot{\boldsymbol{\Phi}})\dot{\boldsymbol{\Phi}} \\
D_r &= \begin{bmatrix} K_{r1} & K_{r3}\cos(\phi_2 - \phi_1) \\ K_{r3}\cos(\phi_2 - \phi_1) & K_{r2} \end{bmatrix} \\
C_r &= \begin{bmatrix} 0 & -K_{r3}\sin(\phi_2 - \phi_1)\dot{\phi}_2 \\ K_{r3}\sin(\phi_2 - \phi_1)\dot{\phi}_1 & 0 \end{bmatrix}
\end{aligned}
$$

K_r are constants that depend on link lengths and mass distributions of the robotic arm. The interaction force acting on the hand as a result of this torque is $\mathbf{F_x} = -(J_r^T)^{-1}\mathbf{T_r}$. If we express the kinematics of the robot represented by $\boldsymbol{\Phi}$ in terms of kinematics of the human arm $\boldsymbol{\Theta}$ then the overall dynamics of the system can be expressed as,

$$
\mathbf{T} = A(\boldsymbol{\Theta})\ddot{\boldsymbol{\Theta}} + B(\boldsymbol{\Theta},\dot{\boldsymbol{\Theta}})\dot{\boldsymbol{\Theta}} \tag{1.8}
$$

where,

$$
\begin{aligned}
A &= D + J^T(J_r^T)^{-1}D_r J_r^{-1}J \\
B &= C + J^T(J_r^T)^{-1}C_r J_r^{-1}J + J^T(J_r^T)^{-1}D_r J_r^{-1}(\dot{J} - \dot{J}_r J_r^{-1}J)
\end{aligned}
$$

Assuming a $K_r = [0.3189, 0.0938, 0.1262]$, link lengths $r_1 = 0.46m, r_2 = 0.44m$ and the configuration of the robot arm as shown in Fig. 1.6, the torque required to be produced by the arm with added dynamics of the robot is shown in Fig. 1.7. The values of robot parameters used here are derived from the experimental robotic setup used for measuring arm movements in our laboratory and will be consistently used in all simulations with robot dynamics. Data from experiments using this setup will be presented in a later chapter. Therefore, it is important to account for dynamics of the robot in modeling of the system so that accurate comparisons can be made between experimental and simulated movements. As can be seen from the torque profile in Fig. 1.7, a significant change in torque is required to move the robot, and the dynamics of the robot are comparable to the human arm itself.

The Curl Force Field

The curl force field is another type of novel dynamic environment shown in Fig. 1.8. This force field is considered here because human motor behavior in this field is used as the main source of data for understanding human motor control and adaptation in this thesis. A wealth of data on human learning in this field has been collected in our laboratory and will be used
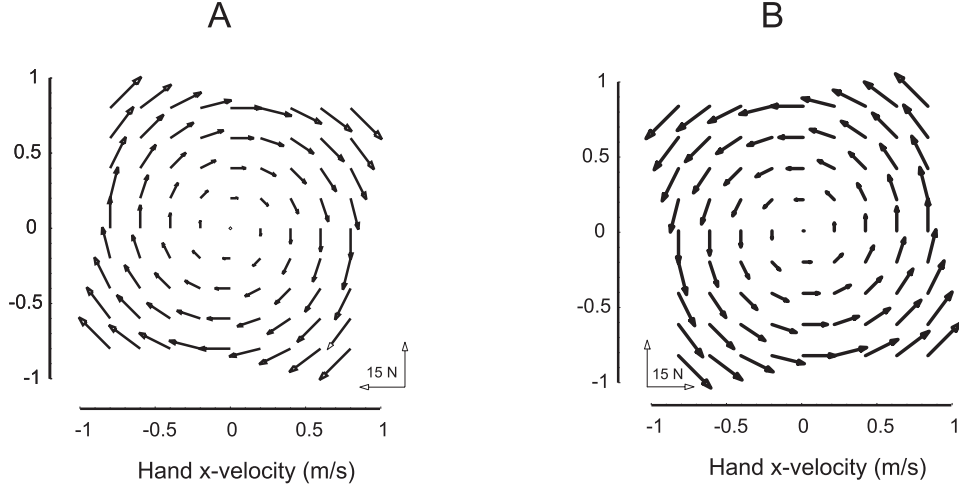
Figure 1.8: The curl force field for two cases (A) Force field B_1 with $K_x = [0\ 13;\ \text{-13}\ 0]$ (B) Force Field B_2 with $K_x = [0\ \text{-13};\ 13\ 0]$. External force vector (represented by arrows) shown as a function of x and y hand velocity.

in later chapters. Hence it is important to understand the structure and nature of this novel dynamic perurbation. The curl force field causes a force on the hand that is perpendicular and proportional to the hand velocity. The work done by the field is always zero, therefore it does not effect the energy of the system. The interaction force acting on the arm due to the curl force field can be mathematically represented as,

$$\mathbf{F_x} = K_x \dot{\mathbf{x}}$$
$$K_x = \begin{bmatrix} 0 & k \\ -k & 0 \end{bmatrix}$$

The overall dynamics of the arm is,

$$\mathbf{T} = D(\boldsymbol{\Theta})\ddot{\boldsymbol{\Theta}} + C(\boldsymbol{\Theta}, \dot{\boldsymbol{\Theta}})\dot{\boldsymbol{\Theta}} - J^T \mathbf{F_x} = D\ddot{\boldsymbol{\Theta}} + [C - J^T K_x J]\dot{\boldsymbol{\Theta}} \qquad (1.9)$$

Assuming $K_x = \begin{bmatrix} 0 & 13 \\ -13 & 0 \end{bmatrix}$ (units in Ns/m), the torque change required with the altered dynamics for reaching movement in the 8 directions is shown in Fig. 1.9 and compared to the torque required for the unloaded arm. The torque change is significant compared to the torque required for moving the arm. The net torque required is the sum of the solid and dotted line as is changed significantly by the addition of the force field.
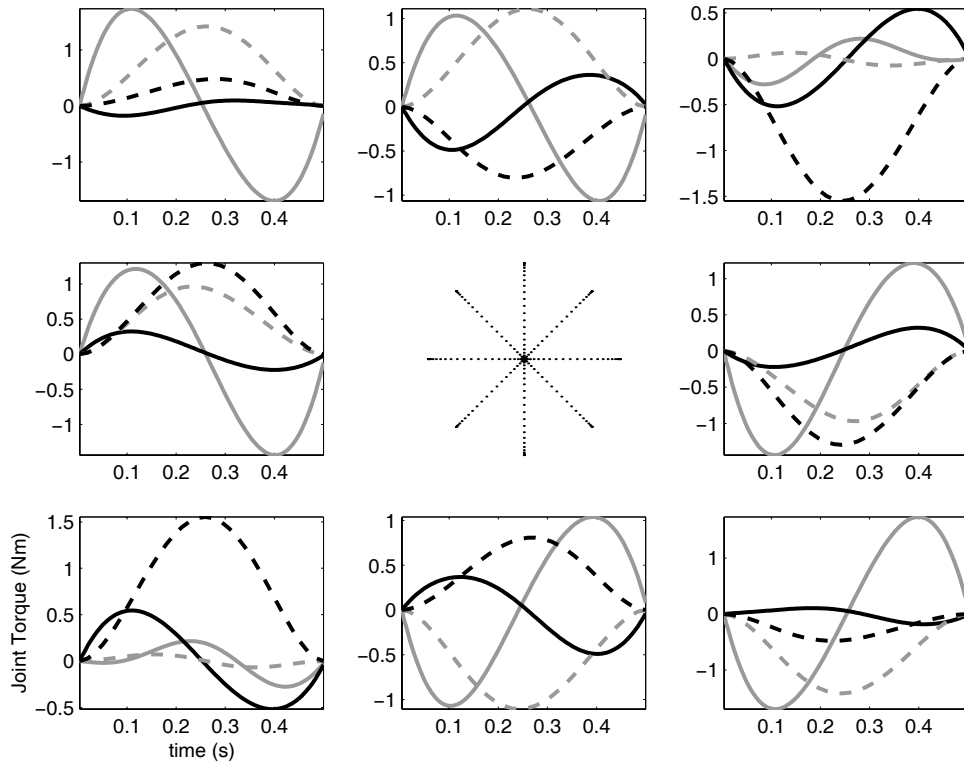
Figure 1.9: The additional joint torque (dotted line) required for movements in the force field, compared to torque required for unloaded arm (solid line); the gray line is shoulder torque and the black line is elbow torque

22

Note: This force field will be used for simulations in Chapter 2 to test different controllers for their stability and robustness when faced with an unfamiliar dynamic environment. In actual experiments with human subjects and for simulations in Chapter 4 and 5, the novel dynamic environment will be a combination of robot dynamics and the force field presented above and the overall dynamics will be determined by the sum of external forces due to the robot and the force field.

1.2 The Muscles and their Active Dynamic Properties

In the previous section the relationship between kinematic trajectory and joint torque was established based on dynamics of the arm and the environment. In this section the dynamics of the muscle actuators that generate joint torques are discussed. Starting with description of a single muscle as a state dependent force generator, it is shown how a group of muscles can be used to generate joint torques as well as equilibrium states for control of the two-joint arm.

1.2.1 A Single Muscle

A muscle is made up of muscle fibers. Within the muscle fiber, the site of muscle contraction is the sarcomere. When an action potential is applied to the muscle fiber there is release of calcium ions from the sarcoplasmic reticulum to the myofibrils and the sarcomeres. The calcium ions initiate attractive forces between the actin and myosin filaments on the sarcomeres causing them to slide together and contract. This generates the force of contraction. After a fraction of a second, the calcium ions are pumped back to the reticulum and the muscle contraction ceases until the next action potential comes along. Each muscle is innervated by a number of motoneurons receiving activation from the spinal cord. Each motoneuron in turn, excites hundreds of muscle fibers. The force generated by the muscle as a whole is governed by the frequency of muscle stimulation and the number of motor units recruited at any time, as well as the length and velocity of contraction of the muscle. The spinal cord coordinates the activation pattern to individual motor units to generate the desired force.

When the muscle fiber is given a short electrical stimulus it elicits a single muscle twitch. This is the force response produced by an impulse of motor activation and is termed the *force-activation impulse response*. The time duration of the twitch depends on the muscle type which can be either fast or slow. When the muscle fiber is stimulated by a series of electrical impulses at a certain frequency it elicits multiple contractions resulting in a sustained muscle force output. The force output by a muscle fiber is the additive sum of the force due to individual contractions and the net force produced by a muscle is the summation of the force output of individual muscle fibers that make up the muscle. If we represent the normalized force response of a single fiber to an electrical impulse by $h_i(s)$ such that $\int_{t=0}^{\infty} h_i(t) = 1$, then the net force
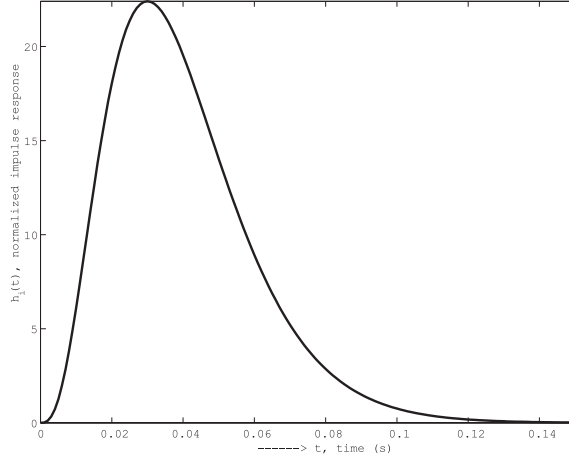
Figure 1.10: The force activation impulse response function for the muscle

$F(t)$, produced by a muscle composed of n_m fibers, each having a maximum twitch force c_n and receiving electrical impulse activity A_n, is:

$$
\begin{aligned}
F(t) &= \sum_{n=1}^{n_m} h_i * [c_n A_n](t) = \sum_{n=1}^{n_m} \int_0^t h_i(\rho) c_n A_n(t-\rho)\, d\rho \\
&= h_i * \sum_{n=1}^{n_m} [c_n A_n](t)
\end{aligned}
$$

where * denotes the convolution operation. If we now denote the summated force activity of muscle fibers as $\mathcal{F}(t) = \sum_{n=1}^{n_m}[c_n A_n(t)]$ and define a normalized electrical muscle activity $R = \frac{\mathcal{F}}{\mathcal{F}_{max}}$, then we can write,

$$
F(t) = \mathcal{F}_{max}[h_i * R](t) = \alpha N(t)
$$

where, $\mathcal{F}_{max}$ corresponds to α, the maximum force generated by the muscle. $N(t)$ is the filtered normalized electrical activity to the muscle equal to $[h_i * R]$. N directly controls the force produced by the whole muscle and hence will be used as the variable to represent the central motor command to the muscle. The activation-force impulse response function of the muscle is modeled as shown in Fig. 1.10 using the following third order equation:

$$
h_i(t) = \frac{t^3 e^{\left(\frac{-t}{0.01}\right)}}{6 \times 10^{-8}}
$$

The results above are derived for an isometric muscle and hence F is the isometric force produced by the muscle for a given neural activation. The force produced by an active muscle also depends on muscle length and rate of change of length at that instant. For a fixed neural
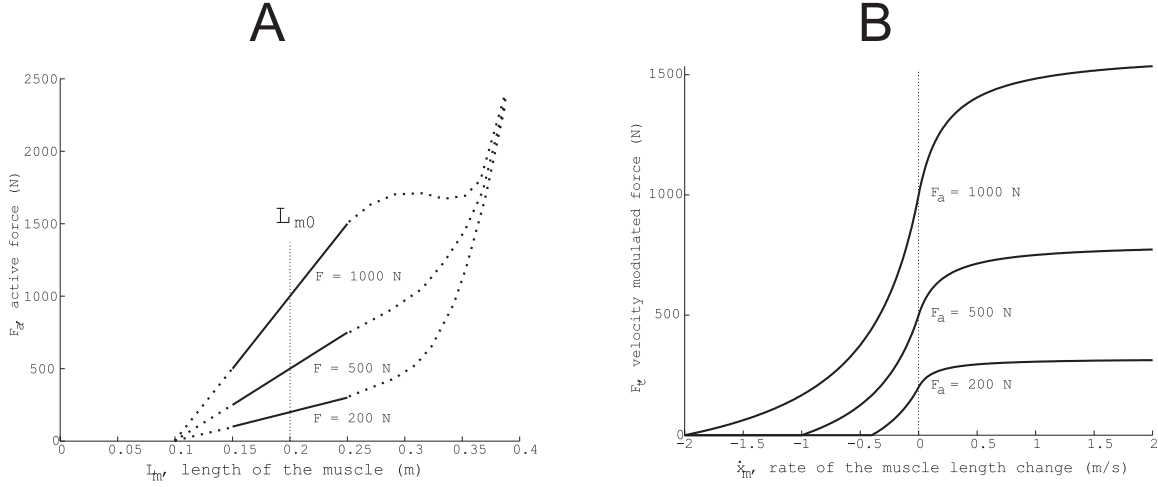
24

Figure 1.11: A, the force-length characteristics for the muscle. B, the force-velocity relationship for the muscle

activation, the muscle force changes in proportion to the muscle length in the normal operating region of muscle length. If the muscle lengthens, the force of contraction increases and vice versa. This represents a mechanical action analogous to a spring. The slope of this force-length relation modulates with the level of activation and increases for greater activations. The force-length relationship can be modeled as an active elastic element whose stiffness changes proportionately to neural activation. If we denote the length of the muscle as L_m and the mean isometric muscle length as L_{m0}, then we can represent the length-modulated force output F_a as,

$$F_a = F + K(L_m - L_{m0})$$

Since the stiffness is proportional to neural activation and the isometric force, and also varies with muscle length, we can write $K = FC_m(L_m)$, where F is the isometric force and C_m is a nonlinear function of muscle length. If we also define a muscle displacement $x_m = L_m - L_{m0}$ as the change in the length of the muscle from the isometric or mean muscle length, then we get,

$$F_a = F[1 + C_m(L_m)(L_m - L_{m0})] = F[1 + C_m(x_m)x_m] \tag{1.10}$$

For most muscles the force reduces to zero at half the mean length. Hence if we assume a constant C_m, and L_{m0}=0.2 m then at half the mean length x_m=-0.1 m and the force F_a=0. This gives a value for C_m equal to 10. The value of C_m is later derived from joint stiffness properties of the human arm observed by (Gomi and Kawato, 1996) and found to reasonably close to this hypothesized value. The modeled force-length relation is shown in Fig. 1.11(A) for α=1000N, L_{m0}=0.2m and $C_m = 10$.

The velocity of muscle contraction or expansion further affects the force generated by a muscle. The force drops off rapidly as the contraction velocity increases and goes to zero at the maximum attainable velocity. When the muscle is expanding, the force increases and saturates at some value (assumed to be 1.6 times the length-modulated force in the model). The muscle therefore behaves like a viscous element with variable viscosity. This can be modeled adequately by a Hill parametrized model ((Krylow et al., 1995)) that treats this force-velocity relation as a contractile element (CE) with the following equations governing its characteristics:

$$
\begin{aligned}
F_t &= \frac{bF_a + a\dot{x}_m}{b - \dot{x}_m} & \dot{x}_m \leq 0 \quad (shortening) \\
F_t &= \frac{b'F_a - (a' + 2F_a)\dot{x}_m}{b' - \dot{x}_m} & \dot{x}_m > 0 \quad (lengthening) \\
a' &= -0.4F_a \\
b' &= -b\frac{a' + F_a}{a + F_a}
\end{aligned}
$$

F_t is the velocity-modulated force of the muscle given a length-modulated force F_a and muscle velocity $\dot{x}_m$. a and b are constants that govern viscosity of the muscle. Two different models are used for contraction and expansion of the muscle to obtain the experimentally observed behavior. The value of b' is derived to ensure continuity at $\dot{x}_m=0$. The following values for constants a and b have been quoted in a paper by (Soechting and Flanders, 1997):

Wilkie (1954)	$\frac{a}{F_{max}}$	$= 0.25$	
	$\frac{\dot{x}_{m\,max}}{L_{m0}}$	$= \frac{bF_{max}}{aL_{m0}}$	$= 6$
Zajac (1989)	$\frac{\dot{x}_{m\,max}}{L_{m0}}$	$= \frac{bF_{max}}{aL_{m0}}$	$= 10$

Fig. 1.11(B) shows the force-velocity relationship for three different values of F_a. A value of $a = 250$ and $b = 0.5$ is used in the model and is obtained by assuming $F_{max} = 1000N$, $L_{m0} = 0.2m$ and the ratio $\frac{\dot{x}_{m\,max}}{L_{m0}} = 10$.

F_t is the output force of the muscle and is transmitted to the tendon. The tendon is an elastic tissue with a very high stiffness and transfers the force from the muscle to the bone. It can be modeled as a series elastic element. However, the dynamics of the tendon is negligible compared to that of the muscle and it is reasonable to omit its effect when considering dynamics of the arm. Similarly, the passive elastic properties of the muscle visible during extreme muscle stretch, can be neglected in an intact muscle with normal operating length. For this reason, the tendons and passive elasticity of the muscles are ignored in the current study.

The overall input-output relation for the nonlinear muscle, relating the activation N with the force F_t, can be represented by a function f_M,

$$\begin{aligned} F_t &= F + K_m(F, x_m)x_m + B_m(F, x_m, \dot{x}_m)\dot{x}_m \\ &= \alpha N + K_m(N, x_m)x_m + B_m(N, x_m, \dot{x}_m)\dot{x}_m \\ &= f_M(N, x_m, \dot{x}_m) \end{aligned} \tag{1.11}$$

where, K_m represents the nonlinear stiffness due to force-length relationship and B_m the non-linear viscosity due to force-velocity relationship for the muscle.

Inverse of the Force-Activation relationship

It is possible to compute the inverse of the relationship in the last equation. For a given muscle force F_t at a certain state of the muscle, there exists a unique muscle activation N that will generate that force. Hence it is possible to define an inverse muscle function f_M^{-1} as,

$$N = f_M^{-1}(F_t, x_m, \dot{x}_m) \tag{1.12}$$

The significance of existence of an inverse is that neural activation to the muscle can be directly determined for generating a desired force using the inverse relation. In the model the inverse is analytically computed by inverting the modeled force-velocity and force-length relationships. In reality, where the exact mathematical structure of these relationships is not known, the inverse can be implemented as a neural network or a series of basis functions, and might be the way that the inverse, if it exists, is represented in the brain.

However there is one problem with the inverse relationship derived here. The neural activation is represented in terms of the filtered neural signal N. In section 1.2.1, the actual signal to the muscles is the unfiltered neural signal R. Hence to generate a desired force, it is important to invert the filter function or the force-activation impulse response function. This may not be possible if the filter has significant high order terms. The inverse used in the current study is achieved by assuming the response function to be a pure time delay of 20 ms and modeling the inverse as a time-lead element that precomputes the neural signal R, 20 ms in advance of N. This is the best approximation to the impulse response and works reasonably well.

Baseline or Tonic activation and force in the muscle

The muscles receive a baseline level of neural activity or muscle tone even at rest, which causes the muscle to be in a constant state of contraction and to generate a tonic force. The baseline activity increases when producing arm movements. The baseline activity also results in cocontraction of a muscle pair acting on a joint that allows changes in the joint stiffness as will be discussed later. In the model we assume that each muscle maintains a constant baseline activity
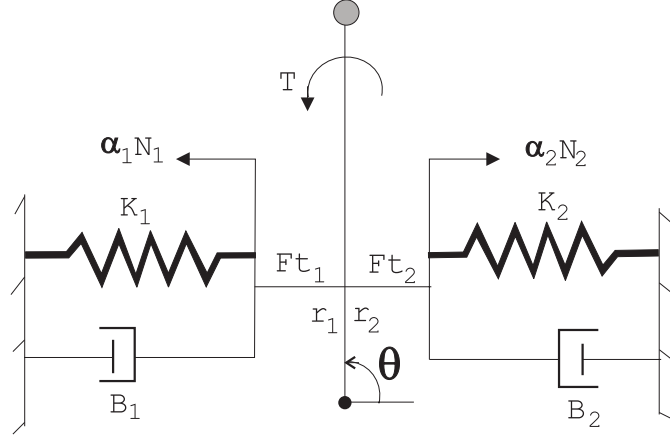
Figure 1.12: A model representing a single joint attached by two muscles

throughout the movement in order to generate a tonic force that equals 10-20% of F_{max} or α, and a specified stiffness.

1.2.2 Linearization of the muscle

For the purpose of simplifying the study of the muscle and its dynamic behavior and to derive certain equilibrium properties, we will consider a linearized muscle model for the next two sections. It is important to realize that linearization is perfectly valid when considering small changes in the state of the muscle and hence the relationships are true locally. The non-linearity in the system arises from nonlinear force-length and force-velocity relationships. If we linearize the system around the normal operating state of the muscle, mean length L_{m0} and zero velocity $\dot{x}_m = 0$, then we obtain the following relationships:

$$
\begin{aligned}
F_t &= F + K_m x_m + B_m \dot{x}_m = \alpha N + K_m x_m + B_m \dot{x}_m & (1.13) \\
K_m &= \left. \frac{d}{dx_m} F_a \right|_{x_m = L_{m0}} = F C_m = \alpha N C_m \\
B_m &= \left. \frac{d}{d\dot{x}_m} F_t \right|_{\dot{x}_m = 0} = \frac{a + F_a}{b} \approx \frac{a + \alpha N}{b}
\end{aligned}
$$

This linearized model consists of two model elements K_m and B_m that are positive and depend only on the neural activation N. K_m is modulated multiplicatively and B_m additively by N.

1.2.3 A Muscle pair attached to a Joint and Equilibrium properties

So far we have only looked at an individual muscle. But in most situations and atleast for the relevant case of human arm, the muscles act in agonist-antagonist pairs around the elbow

and shoulder joints. It is this configuration that gives rise to two important properties of the muscles - (1) the capability to generate torques about a joint, and (2) the capability to control the equilibrium state of the joint. A model of a muscle pair acting on a joint is represented in Fig. 1.12. The following equations, derived using linearized muscles, govern the dynamics of the joint:

$$
\begin{aligned}
F_{t1} &= \alpha_1 N_1 + K_{m1} x_{m1} + B_{m1} \dot{x}_{m1} \\
F_{t2} &= \alpha_2 N_2 + K_{m2} x_{m2} + B_{m2} \dot{x}_{m2} \\
\tau &= F_{t1} r_1 - F_{t2} r_2 \\
&= [\alpha_1 N_1 + K_{m1} x_{m1} + B_{m1} \dot{x}_{m1}] r_1 - [\alpha_2 N_2 + K_{m2} x_{m2} + B_{m2} \dot{x}_{m2}] r_2 \qquad (1.14)
\end{aligned}
$$

τ is the torque produced at the joint and $r1$, $r2$ are the moment arms for the two muscles about the joint. If we assume that the mean angle for the joint is θ_0, then we can represent x_{m1} and x_{m2} as $(\theta_0 - \theta) r_1$ and $(\theta - \theta_0) r_2$ respectively. This gives,

$$
\begin{aligned}
\tau &= [\alpha_1 N_1 + K_{m1}(\theta_0 - \theta) r_1 - B_{m1} \dot{\theta} r_1] \, r_1 - [\alpha_2 N_2 + K_{m2}(\theta - \theta_0) r_2 + B_{m2} \dot{\theta} r_2] \, r_2 \\
&= (\alpha_1 N_1 r_1 - \alpha_2 N_2 r_2) + [K_{m1} r_1^2 + K_{m2} r_2^2] \, (\theta_0 - \theta) - [B_{m1} r_1^2 + B_{m2} r_2^2] \dot{\theta} \qquad (1.15)
\end{aligned}
$$

This equation represents a classical second order feedback control system for maintaining the joint at its mean joint angle θ_0 when the two muscle activations balance each other. If now, we program the activations to the two muscles such that,

$$
\alpha_1 N_1 r_1 - \alpha_2 N_2 r_2 = [K_{m1} r_1^2 + K_{m2} r_2^2] \, (\theta_d - \theta_0) + [B_{m1} r_1^2 + B_{m2} r_2^2] \dot{\theta}_d \qquad (1.16)
$$

we obtain,

$$
\begin{aligned}
\tau &= -[K_{m1} r_1^2 + K_{m2} r_2^2] \, (\theta - \theta_d) - [B_{m1} r_1^2 + B_{m2} r_2^2] \, (\dot{\theta} - \dot{\theta}_d) \\
&= -K_\theta (\theta - \theta_d) - B_\theta (\dot{\theta} - \dot{\theta}_d) \qquad (1.17)
\end{aligned}
$$

This shows that it is possible to program a desired equilibrium trajectory for the joint in terms of a series of desired joint angle θ_d and joint velocity $\dot{\theta}_d$ by choosing appropriate muscle activations based on a knowledge of B_m and K_m. The system will asymptotically track the desired trajectory in a stable manner because K_θ and B_θ are positive definite. This is the property that governs the equilibrium of the joint and is used in the *equilibrium control hypotheis* of the arm proposed by (Bizzi et al., 1982) and discussed in a later section.

From Eqn. 1.16 it follows that for any given activation of the two muscles, there exists a stable equilibrium position for the muscle where the joint will come to a rest and remain indefinitely. The torque τ and velocity $\dot{\theta}$ will be zero at this position. This equilibrium position θ_q is given by,

$$\theta_q = \theta_0 + \frac{\alpha_1 N_1 r_1 - \alpha_2 N_2 r_2}{K_{m1} r_1^2 + K_{m2} r_2^2} \tag{1.18}$$

It is possible that for very large differences in N_1 and N_2, this equilibrium position will lie outside the physiological space of the muscle or the joint. In such a situation the joint will be driven to the mechanical limit for the joint. The *virtual trajectory hypothesis* proposed by (Hogan, 1984) uses the idea of a complex equilibrium position trajectory to generate straight line movements.

The muscle activations can also be used to produce a desired torque τ_d around the joint. This can be achieved if,

$$\alpha_1 N_1 r_1 - \alpha_2 N_2 r_2 = \tau_d + [K_{m1} r_1^2 + K_{m2} r_2^2](\theta - \theta_0) + [B_{m1} r_1^2 + B_{m2} r_2^2]\dot{\theta} \tag{1.19}$$

in which case,

$$\tau = \tau_d$$

This is based however on accurate knowledge of the current state of the arm $(\theta, \dot{\theta})$ required in Eqn. 1.19. This is a representation of the muscles in the form of a state-dependent torque controller. If the state of the muscle is known then the neural input can be programmed to produce any desired torque. In control literature an observer is used to supply the state information to the controller. It will be shown later how torque control seems to be the strategy used by the brain to control the arm and how a forward model (similar to an observer) is used to provide accurate estimates of current state of the arm.

To summarize, the muscle is a force generating element but by using a combination of two muscles it is possible to control an equilibrium state of a joint or alternately the torque generated at a joint.

Muscle Co-contraction, Tonic Force, and Effect on Stiffness and Viscosity

In the previous section, it was shown how the *difference* in muscle activations, $\alpha_1 N_1 r_1 - \alpha_2 N_2 r_2$, can be used for arm movements by controlling the equilibrium trajectory or the torque produced at the joint. Since α_1, α_2 are two independent variables, and there is one constraint, there exists a degree of freedom that can be controlled independentally. This can be the *sum* of

the activations or their baseline levels of activity. Eqn. 1.19 relates the joint stiffness K_θ and viscosity B_θ to K_m and B_m and further on muscle activation N for the two muscles,

$$\begin{aligned}
K_\theta &= [K_{m1}r_1^2 + K_{m2}r_2^2] = \alpha_1 N_1 C_{m1} r_1^2 + \alpha_2 N_2 C_{m2} r_2^2 \\
B_\theta &= [B_{m1}r_1^2 + B_{m2}r_2^2] = \frac{a_1 + \alpha_1 N_1}{b_1} r_1^2 + \frac{a_2 + \alpha_2 N_2}{b_2} r_2^2
\end{aligned}$$

For simplicity of equations, assume that the two joint muscles are identical, i.e. $r_1 = r_2$, $C_{m1} = C_{m2}$, $a_1 = a_2$, $b_1 = b_2$ and $\alpha_1 = \alpha_2$. This reduces the equations to:

$$\begin{aligned}
\tau &= \alpha(N_1 - N_2)r - K_\theta(\theta - \theta_0) - B_\theta \dot{\theta} & (1.20) \\
K_\theta &= \alpha C_m r^2 (N_1 + N_2) \\
B_\theta &= \frac{ar^2}{b} + \alpha r^2 \frac{N_1 + N_2}{b}
\end{aligned}$$

These equations show that the torque τ generated at the joint is controlled by the difference in the activations, $N_1 - N_2$, whereas, stiffness or viscosity of the joint or some combination of both is independently controlled by the sum of muscle activations, $N_1 + N_2$. If we define a muscle cocontraction or baseline activation, $N_b = 0.5(N_1 + N_2)$ and desired torque activation, $N_t = N_1 - N_2$, then,

$$N_1 = N_b + 0.5N_t \qquad (1.21)$$

$$N_2 = N_b - 0.5N_t \qquad (1.22)$$

An interesting thing to note here is that if the cocontraction is kept constant, then to produce a certain torque there is increased activation of the agonist and a inhibition of the antagonist by the same amount. This inhibition of the antagonist is seen physiologically in EMG measurements. A problem with this definition arises when $N_b < 0.5N_t$. To overcome this we can define the activations such that,

$$N_1 = \frac{N_b^2}{N_2}$$

and solve it with the constraint that $N_1 - N_2 = N_t$. This is known as reciprocal inhibition and is depicted in Fig. 1.13.

This approach is justifiable as long as the linear muscle model is considered. For a nonlinear muscle, it is easier to define the co-contraction in terms of muscle force instead of muscle activation, such that,
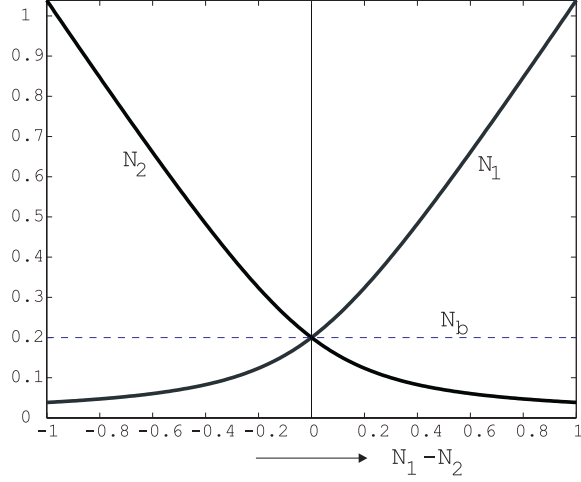
31

Figure 1.13: Reciprocal inhibition of the agonist-antagonist muscle pair

$$F_{t1} = \frac{F_c^2}{F_{t2}}$$

and,

$$(F_{t1} - F_{t2})r = \tau_d$$

F_c is the cocontractive or tonic force in each muscle. This relationship is used for modeling in the presented study and F_c assumes a value that is 10%-20% of F_{max} depending on the stiffness desired during the movement.

1.3   Dynamics of the Two-joint Human Arm

It is possible to extend the dynamics and properties derived for one joint connected by two linearized muscles in the previous section, to the real case of a two-joint arm attached by several nonlinear muscles.

1.3.1   The Input-Output relationship for the Human Arm

The human arm is composed of several muscles. If muscles receive neural activation $\mathbf{N}$, and produce an acceleration of the hand $\ddot{\mathbf{x}}$, then the overall dynamics of the arm can be written as a combination of muscle dynamics and passive arm dynamics derived earlier.

$$\mathbf{F_t} = \alpha\,\mathbf{N} + K_m(\mathbf{N}, \mathbf{x_m})\,\mathbf{x_m} + B_m(\mathbf{N}, \mathbf{x_m}, \dot{\mathbf{x}_m})\,\dot{\mathbf{x}_m} = f_M(\mathbf{N}, \mathbf{x_m}, \dot{\mathbf{x}_m}) \qquad (1.23)$$

$$\mathbf{T} \quad = \quad -J_m^T \mathbf{F_t} \tag{1.24}$$

$$\ddot{\mathbf{x}} \quad = \quad D^{-1}(\mathbf{x})[\mathbf{T} - C(\mathbf{x}, \dot{\mathbf{x}}) + J^T \mathbf{F_x}] \tag{1.25}$$

f_M is the muscle dynamics function and J_m is the Jacobian of muscle length to joint position transformation defined as $J_m = \frac{d\mathbf{x_m}}{d\mathbf{\Theta}}$. J_m also corresponds to the moment arms for the muscles. The negetive sign relating $\mathbf{T}$ to $\mathbf{F_t}$ arises because $\mathbf{F_t}$ is a contractive force and opposite to the coordinates of muscle length in direction. The overall forward dynamics of the plant can be represented by a nonlinear function f_p,

$$\ddot{\mathbf{x}} = f_p(\mathbf{N}, \mathbf{x}, \dot{\mathbf{x}})$$

This is a general representation of the plant (the human arm) that will be useful when we look at control methodoligies for this plant in a later section.

1.3.2   Equilibrium properties of the human arm

The equilibrium property for a single joint as derived earlier, shows that the activation to the muscles determine an equilibrium position for the joint, or alternately, that activations can be programmed to move the arm along an equilibrium trajectory. It is possible to define similar equilibrium properties for the multi-joint human arm under certain constraints. An equilibrium is defined as the state of the system where the rate of change of the state is zero. The equilibrium point is locally [or globally] stable, if additionally, a small [or any] displacement from the equilibrium state will bring the system back to the same equilibrium state. Local stability for the human arm follows from the result that a nonlinear system can be linearized locally and the linear muscle model has already been shown to yield stable equilibrium. Now we want to show existence of a globally stable equilibrium point for a given activation of the muscles.

At the equilibrium point, the torque on the arm and arm velocity have to be zero. Hence,

$$\mathbf{T}_q \quad = \quad -J_m^T \mathbf{F_t}_q = 0$$

$$\mathbf{F_t}_q \quad = \quad \alpha\, \mathbf{N} + K_m(\mathbf{N}, \mathbf{x_m}_q)\, \mathbf{x_m}_q$$

and therefore,

$$-J_m^T[\alpha\, \mathbf{N} + K_m(\mathbf{N}, \mathbf{x_m}_q)\, \mathbf{x_m}_q] \quad = \quad 0$$

$$J_m^T K_m(\mathbf{N}, \mathbf{x_m}_q)\, \mathbf{x_m}_q \quad = \quad -J_m^T \alpha\, \mathbf{N}$$

The solution of the last equation will give the equilibrium muscle state $\mathbf{x_{m}}_q$ or the corresponding equilibrium joint position $\mathbf{\Theta_q}$. Stability of the system will be ensured if the torque is greater than zero for $\mathbf{\Theta} < \mathbf{\Theta_q}$ and less than zero for $\mathbf{\Theta} > \mathbf{\Theta_q}$. This will definitely be true if $\frac{d\mathbf{T}}{d\mathbf{\Theta}} < 0$ for all $\mathbf{\Theta}$.

$$\frac{\delta \mathbf{T}}{\delta \mathbf{\Theta}} = -J_m^T \frac{\delta \mathbf{F_t}}{\delta \mathbf{\Theta}} - \mathbf{F_t} \frac{\delta J_m^T}{\delta \mathbf{\Theta}}$$

The first term on the on the right hand side of the above equation can be further written as:

$$J_m^T \frac{\delta \mathbf{F_t}}{\delta \mathbf{\Theta}} = J_m^T \frac{\delta \mathbf{F_t}}{\delta \mathbf{x_m}} \frac{\delta \mathbf{x_m}}{\delta \mathbf{\Theta}} = J_m^T \frac{\delta \mathbf{F_t}}{\delta \mathbf{x_m}} J_m$$

Consider the shoulder joint angle θ_1 and n muscles connected to the shoulder. The lengths of these muscles are $x_{m[1..n]}$ and the force generated by them $F_{t[1..n]}$. J_m^T is a vector of n terms corresponding to the moment arms for the muscles around the shoulder, $r_{[1..n]} = \frac{\delta x_{m[1..n]}}{\delta \theta_1}$. One can represent the above equation for just the shoulder as:

$$\frac{\delta \tau_1}{\delta \theta_1} = - \begin{bmatrix} r_1 & r_2 & \cdots & r_n \end{bmatrix} \begin{bmatrix} \frac{\delta F_{t1}}{\delta x_{m1}} r_1 \\ \frac{\delta F_{t2}}{\delta x_{m2}} r_2 \\ \vdots \\ \frac{\delta F_{tn}}{\delta x_{mn}} r_n \end{bmatrix} - \begin{bmatrix} \frac{\delta r_1}{\delta \theta_1} & \frac{\delta r_2}{\delta \theta_1} & \cdots & \frac{\delta r_n}{\delta \theta_1} \end{bmatrix} \begin{bmatrix} F_{t1} \\ F_{t2} \\ \vdots \\ F_{tn} \end{bmatrix}$$

$$= - \begin{bmatrix} r_1^2 & r_2^2 & \ldots & r_n^2 \end{bmatrix} \begin{bmatrix} K_{m1} \\ K_{m2} \\ \vdots \\ K_{mn} \end{bmatrix} - \begin{bmatrix} \frac{\delta r_1}{\delta \theta_1} & \frac{\delta r_2}{\delta \theta_1} & \ldots & \frac{\delta r_n}{\delta \theta_1} \end{bmatrix} \begin{bmatrix} F_{t1} \\ F_{t2} \\ \vdots \\ F_{tn} \end{bmatrix}$$

For stable equilibrium, the RHS should be negetive for all θ_1. This is ensured if slopes of the force length relation for all muscle $K_{m[1..n]}$ are positive and slopes of their moment arm with respect to joint angle, $\frac{\delta r_{[1..n]}}{\delta \theta_1}$, are positive. This is true in the case of a linearized muscles with constant moment arms. However in reality, the values of K_m and $\frac{\delta r_{[1..n]}}{\delta \theta_1}$ may not always be positive at all θ_1. In this situation, the constraint on the system for stable equilibrium is that atleast the total sum of the terms on the left hand side be negetive for all θ_1. For real muscles, the majority of K_m are positive and the magnitude of the first term on RHS of the equation above is much larger than the second term with moment arm derivatives.

1.3.3 Parameters for major muscles in the human arm

The values for parameters of muscles in the human arm that play an important role in the flexion and extension of the shoulder and elbow joint are outlined here. The values for mean
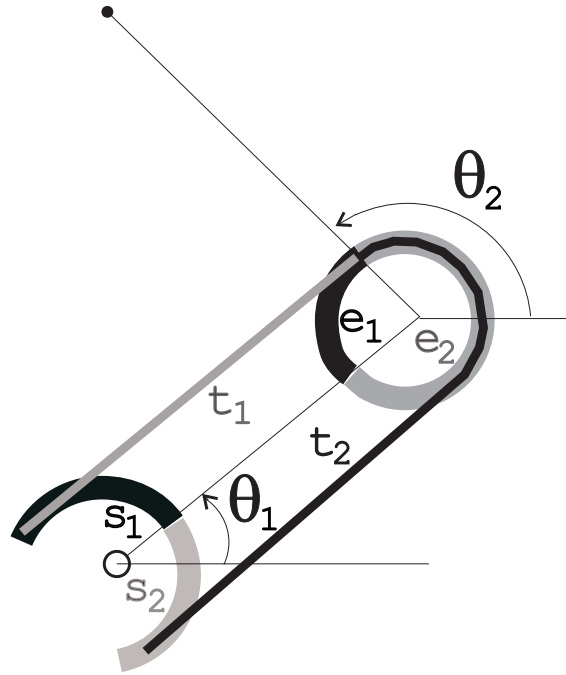
Figure 1.14: The simplified three muscle pair model. s1, s2 - shoulder single joint muscles. t1, t1 - two-joint muscles. e1, e2 - elbow single-joint muscles

length have been taken from origin/insertion data from (Soechting and Flanders, 1997), the moment arm from (Murray et al., 1995), and F_{max} from (Karniel and Inbar, 1997).

Muscle	(L_{m0},cm)	PCSA (cm^2)	F_{max} (N)	Moment arm (r,cm)
Anterior Deltoid	6.1	14.9	800	5
Posterior Deltoid	5.3	14.9	800	5
Brachialis/Brachioradialis	-	-	700	1.5-3.5
Triceps (short)	4.7	12.1	700	2.5-3.5
Biceps	11.2	11.0	1000	2-4
Triceps (Long)	16.4	6.7	1000	2.5-3.5

1.4   Modeling the human arm using three pairs of muscles

Since it is very difficult to model the exact musculature of the arm, several researchers ((Karniel and Inbar, 1997; Gribble et al., 1998) have used a simplified model that has three pairs of muscles attached to the arm. This is shown in Fig 1.14. The three pairs are:

- Single joint shoulder muscles (s) - correspond to the anterior and posterior deltoid that

connect the upper arm to the body

- Single joint elbow muscles (e) - brachialis/brachioradialis and the short head of triceps that connect the lower arm to the upper arm

- Two joint muscles (t) - biceps and the long head of triceps that span both the elbow and shoulder joints and connect the lower arm to the body

For further simplicity we can assume that the two muscles constituting each pair are identical. But it is important to establish that this simplified representation does not undermine any significant dynamics of the real arm. Since this study does not seek to compare actual muscle activations (EMG) with the model, and is instead focused on the dynamics of the arm, any simplification of the actual musculature can be assumed as long as the dynamics of the arm are preserved. The dynamics of the arm are fully described by the following factors - lengths and mass distributions of the upper and lower arm, stiffness and viscosity of the elbow and shoulder joints, and muscle contraction dynamics. When assuming a simplified arm muscle structure we have to ensure that the joint stiffness and viscosity are modeled correctly, the other factors not being affected. We show that the simple model is indeed capable of producing the stiffness and viscosity patterns found experimentally in humans.

It is first important to find the relation between muscle dynamics and joint dynamics. This has already been derived for a single-joint in the previous section and can be easily extended to the two-joint arm. In the simplified musculature, the two muscles in each pair are assumed to be identical and to have the same moment arms. From Fig. 1.14, the relation between muscle lengths for the three pairs and joint angles is,

$$
\begin{aligned}
x_{s1} &= -x_{s2} = -(\theta_1 - \theta_{s0})r_s \\
x_{e1} &= -x_{e2} = -(\theta_{12} - \theta_{e0})r_e \\
x_{t1} &= -x_{t2} = -(\theta_2 - \theta_{t0})r_t
\end{aligned}
$$

where, x denotes the muscle length, s, e, t are subscripts for shoulder, elbow and two joint muscles respectively, and 1, 2 are subscripts for the flexor and extensor muscle respectively. θ_0 is the rest position for the joint. The torque generated by a muscle pair about the joint at which they are acting was derived in Eqn 1.15 and can be computed for the three muscle pairs in this case:

$$
\begin{aligned}
\tau_s &= \alpha_s(N_{s1} - N_{s2}) - K_{\theta s}(\theta_1 - \theta_{s0}) - B_{\theta s}\dot{\theta_1} \\
\tau_e &= \alpha_e(N_{e1} - N_{e2}) - K_{\theta e}(\theta_2 - \theta_{e0}) - B_{\theta e}\dot{\theta_2} \\
\tau_t &= \alpha_t(N_{t1} - N_{t2}) - K_{\theta t}(\theta_{12} - \theta_{t0}) - B_{\theta t}\dot{\theta_{12}}
\end{aligned}
$$

36

The net joint torque in terms of individual muscle torque is given by,

$$\mathbf{T} = \left[\begin{array}{c} \tau_s - \tau_e \\ \tau_e + \tau_t \end{array} \right] \tag{1.26}$$

The stiffness about the joint the rate of change of torque with joint angle and can be derived from the equation above as,

$$K_\theta = \frac{\delta}{\delta\Theta}\mathbf{T} = \left[\begin{array}{cc} -K_{\theta s} - K_{\theta e} & K_{\theta e} \\ K_{\theta e} & -K_{\theta e} - K_{\theta t} \end{array} \right] \tag{1.27}$$

Observe that the cross diagonal terms in the stiffness matrix are equal.

The following values of joint stiffness have been reported by different researchers,

(Mussa-Ivaldi et al., 1985)

$$K_\theta = \left[\begin{array}{cc} -41 & 23 \\ 23 & -38 \end{array} \right]$$

(Flash, 1987)

$$K_\theta = \left[\begin{array}{cc} -25 & 14 \\ 14 & -19 \end{array} \right]$$

(Gomi and Kawato, 1996)

$$K_\theta = \left[\begin{array}{cc} -30 & 10 \\ 10 & -15 \end{array} \right]$$

It is important to note that these stiffness matrices are in absolute joint coordinate system and may have been converted from the value reported by these authors if they used relative coordinate systems. The cross-diagonal terms in these experimentally determined stiffness matrices are indeed equal as desired and hence the stiffness can be represented by a simplified three muscle-pair model.

For the model, the stiffness reported by Kawato is chosen because their experiment was done while subjects actually performed reaching movmements with the arm. One of the factors that contributes to stiffness and viscosity of the arm and has not been discussed yet, is the spinal reflex. The role of the spinal cord will be discussed in a later section. In order to derive the stiffness parameters for the muscles, we have to know the contribution from the spinal reflex. From values of stiffness reported by (Sanes and Shadmehr, 1995) for deafferented patients, who presumably have no spinal reflex, the values of the stiffness matrix are close to 50% of the normal subjects. This implies that the spinal reflex contributes 50% of the stiffness and the other 50% comes from muscle properties. Hence,

$$K_\theta = \begin{bmatrix} -(K_{m_{s1}} + K_{m_{s2}})r_s^2 - (K_{m_{e1}} + K_{m_{e2}})r_e^2 & (K_{m_{e1}} + K_{m_{e2}})r_e^2 \\ (K_{m_{e1}} + K_{m_{e2}})r_e^2 & -(K_{m_{e1}} + K_{m_{e2}})r_e^2 - (K_{m_{t1}} + K_{m_{t2}})r_t^2 \end{bmatrix}$$

$$= 0.5 \begin{bmatrix} -30 & 10 \\ 10 & -15 \end{bmatrix}$$

We assume the following values for moment arms of the muscle pairs, $r_s = 0.05$, $r_e = 0.03$, and $r_t = 0.03$ based on the average values of muscle moments described earlier for the real muscles. This gives,

$$K_{m_{s1}} + K_{m_{s2}} = \alpha_s C_{ms}(N_{s1} + N_{s2}) = 4000$$
$$K_{m_{e1}} + K_{m_{e2}} = \alpha_e C_{me}(N_{e1} + N_{e2}) = 5500$$
$$K_{m_{t1}} + K_{m_{t2}} = \alpha_t C_{mt}(N_{t1} + N_{t2}) = 2750$$

At the baseline level of activity during movement, and for the given α for each muscle-pair, we get,

$$C_{ms} = 10.00$$
$$C_{me} = 18.33$$
$$C_{mt} = 13.75$$

The joint viscosity of the arm is typically 15-20% of the joint stiffness (Shadmehr and Mussa-Ivaldi, 1994). Since the viscosity of spinal reflex is only 10% of spinal stiffness as will be shown later, this implies that muscle viscosity should be close to 25% of the muscle stiffness. The viscosity for the muscle is approximately given by $B_m = \frac{a + F_a}{b}$. Values of a and F_a at baseline level of activity are,

$$a = 0.25 F_{max} = 0.25\alpha$$

$$F_a = 0.1 F_{max} = 0.1\alpha$$

For $B_m = 0.25 K_m$ one gets,

$$b_s = \frac{0.35\alpha_s}{0.25 K_{ms}} = 1.39$$
$$b_e = \frac{0.35\alpha_e}{0.25 K_{me}} = 0.76$$
$$b_t = \frac{0.35\alpha_s}{0.25 K_{mt}} = 1.01$$

This successfully completes the task of specifying the observed dynamics of the arm musculature in terms of a simplified model consisting of only three muscle pairs.

1.4.1 Torque generation about elbow and shoulder joint (the inverse problem)

So far we have only looked at forward dynamics of the system that gives the torque generated by the arm for a neural activation input. If a certain torque is desired at the joints, then the forward dynamics have to be inverted to arrive at the appropriate neural activations to the muscles. This relationship was derived for the single joint case and is extended here for the two joint human arm connected by three pairs of muscles. The inverse problem involves determining the three single joint torque τ_s, τ_t, τ_e, given desired elbow and shoulder joint torque $\mathbf{T_d}$. The relation between them is,

$$\mathbf{T} = \begin{bmatrix} \tau_s - \tau_e \\ \tau_e + \tau_t \end{bmatrix}$$

The problem is that of inverting this equation. There are two variables on left hand side and three on right hand side of the equation. Hence it is not a unique one-to-one mapping. Physiologically it is found that around the elbow joint, the single-joint elbow muscles and the two-joint muscles, that is the short head and long head of biceps and triceps, produce forces that complement each other. The elbow torque is thus distributed between the single-joint and two-joint muscles. The exact distribution for these torques is not known, so it is assumed that 50% of the desired torque comes from single-joint muscles ($\tau_e = 0.5\tau_2$) and the remaining 50% from two-joint muscles ($\tau_t = 0.5\tau_2$) which gives,

$$\begin{bmatrix} \tau_s \\ \tau_e \\ \tau_t \end{bmatrix} = \begin{bmatrix} 1 & -0.5 \\ 0 & 0.5 \\ 0 & 0.5 \end{bmatrix} \mathbf{T_d}$$

The following equations can then be solved simultaneously for the three pairs of muscles ($m = s, e, t$) to give the force to be generated by each muscle pair $F_{t_{m1}}, F_{t_{m2}}$,

$$F_{t_{m1}} = \frac{F_{c_m}^2}{F_{t_{m2}}}$$

and,

$$(F_{t_{m1}} - F_{t_{m2}})r_m = \tau_m$$

where, F_{c_m} is the cocontractive or tonic force and has a value equal to 0.1α. This gives,

$$F_{t_{m1}} = \frac{\tau_m}{2r_m} + \sqrt{\frac{\tau_m^2}{4r_m^2} + F_{c_m}}$$

$$F_{t_{m2}} = \frac{F_{c_m}^2}{F_{t_{m1}}}$$

The muscle activations to each muscle is obtained from the inverse of the muscle dynamics in Eqn 1.13 and can be expressed as $N = f_M^{-1}(F_t, x_m, \dot{x}_m)$.

1.5 Sensory feedback to the brain

1.5.1 Muscle Spindles and Proprioception

Muscle spindles refer to a group of intrafusal muscle fibres that sense the length of the muscle and the velocity of length change of the muscle and transmit this information to the spinal cord which eventually reaches the brain. This knowledge of muscle state can be integrated for the whole arm to determine the position of the limb and the velocity at which it is moving. The feedback delay for this information to reach the brain is assumed to be 150 ms (Turrell et al., 1998). This implies that during movement of the arm, the brain does not have exact knowledge of the state of the arm during the 150 ms preceding the current time. The afferent signals are also affected by noise and may not be very accurate. However, for the simulations, we assume a perfect proprioceptive system that provides accurate and precise measurement of muscle length and muscle velocity with a time delay of 150 ms. We also assume the existence of accurate internal kinematic transformforms from which joint state and hand state can be determined. Noise in the measurement and robustness of the system to noise will be considered in a later chapter.

1.5.2 Visual Feedback

Vision plays a major role in the control of arm movements. Reaching movements are usually directed towards a visual target. To move the hand from one point to another, a trajectory has to be planned. There is evidence to show that this plan is executed in the perceived visual space and is a minimum jerk hand path connecting the two points. (Wolpert et al., 1994) and (Flanagan and Rao, 1995) have shown that when curvature of the perceived hand path is visually altered, subjects adapt their arm movements in order to preserve straight line paths in visually perceived space.

In another recent study done by (Conditt et al., 1997), it was found that if a visual-proprioceptive mismatch was introduced during a practiced fast reaching movement, then the

movement was controlled by visual feedback. In the experiment subjects were trained to make fast reaching movement while grasping a robotic manipulandum. During certain movements the curl force field was turned on. A group of subjects received altered visual feedback during this movement that restricted vision to a straight line path to the target, while another control group received unaltered visual feedback. The control group produced hand movements that were deflected in a clockwise direction by the field and then hooked back to the target. In the experimental group, however, the movement terminated when the perceived visual hand postion reached the target, although the actual position of the hand was still in the deviated position observed in controls just prior to the corrective hook. This provided evidence for online control of arm movements by visual feedback even during fast reaching movements.

Vision seems to play a role in the plan of movement in the visually perceived space and then in feedback correction during the arm movement if there is an error in perceived and planned visual movement. Vision provides information about the state of the arm in terms of hand position and velocity. However, there are significant delays in the visuomotor pathways as in the case of proprioception. We assumed a delay of 150 ms in the model that is the same as proprioceptive delay. Whether vision provides any more information than proprioception has not been established although it seems to play a dominating role in control of visually-guided movements as evidenced by the two experiments cited above. Experiments on control of arm movements in deafferented subjects who suffer loss of proprioception ((Gordon et al., 1995)) reveal that arm movements are affected in the deafferented subjects, but in the presence of vision the subjects are able to perform reasonably well.

Note: In the simulations considered in this thesis, no distinction is made between proprioception adnd visual information and both are assumed to provide accurate state information to the brain with a time delay of 150 ms. This is also based in part on the observation that movements in the force field considered in the current study are not affected in the absence of vision and show the same behavior

1.5.3   Efferent conduction delays from the brain

There is a delay in motor commands reaching the muscles in the arm from the brain because of conduction path delays and synaptic delays in the spinal cord. This delay is an important consideration in the problem of motor control because it adds to feedback loop delays and can cause instability in the system. For the current study a delay of 60 ms is assumed between the issuance of motor commands by the brain and their reaching the muscles in the arm.

1.6   The Spinal Reflex

The spinal reflex is a feedback mechanism that tries to correct for unexpected perturbations to the arm. It works at the individual muscle or muscle pair level and increases the activation to the muscle and thereby the contraction force if it senses an increase in the length of the muscle. A nonlinear model of the relation between change in activation and change in length is provided in a study by (Gielen and Houk, 1987). In the current study a linear relation between activation and muscle length is assumed for simplicity. The activation to the muscle N_r, through the spinal reflex pathway is based on reciprocal inhibition of a muscle pair and is the solution of,

$$N_{r1} - N_{r2} = K_s(x_m - x_{ms}) + B_s(\dot{x}_m - \dot{x}_{ms}) \; and, \tag{1.28}$$

$$N_{r1} = \frac{N_{rc}^2}{N_{r2}} \tag{1.29}$$

where, $x_{ms}, \dot{x}_{ms}$ are the set-point muscle length and velocity, K_s is the reflex stiffness, B_s the reflex viscosity, and N_{rc} the reciprocal inhibition constant. The ratio of B_s to K_s has been reported to be 0.1 by (Gielen and Houk, 1987) and is assumed in the model here. The reflex pathway is modeled as a time delay of 0.03 s based on results of (Gielen and Houk, 1987), which implies that proprioceptive information about muscle length and velocity takes 30 msec to reach the spinal cord and affect the activation.

As was mentioned earlier, the reflex mechanism contributes to 50% of the muscle stiffness. Hence for the three muscle pairs the values of K_s are,

$$K_{ss} = \frac{4000}{\alpha_s} = 2.0$$

$$K_{se} = \frac{5500}{\alpha_e} = 3.67$$

$$K_{st} = \frac{2750}{\alpha_t} = 2.75$$

For the model the values of K_s and $B_s = 0.1K_s$ were taken as,

$$K_s = \begin{bmatrix} 2.0 \\ 4.0 \\ 3.0 \end{bmatrix} \qquad B_s = \begin{bmatrix} 0.2 \\ 0.4 \\ 0.3 \end{bmatrix}$$

The net activation going to the muscles is the sum of the activations from the brain N_C and activation from the spinal reflex N_R
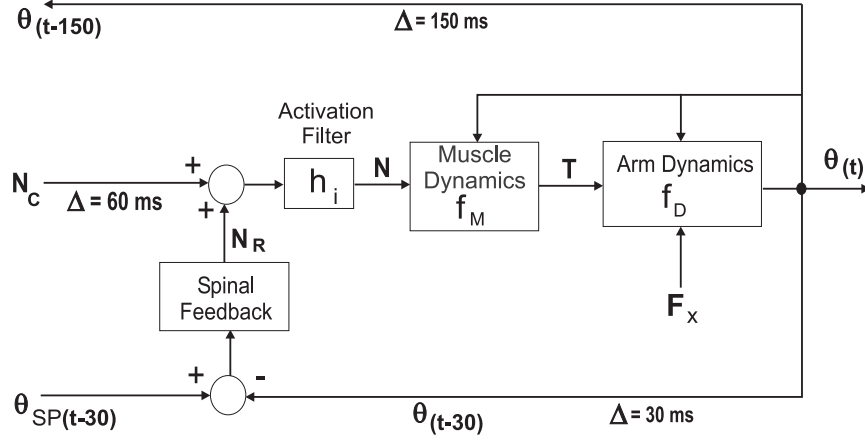
Figure 1.15: Block diagram of the plant represented by the human arm

$$N = N_C + N_R$$

The spinal reflex provides a fast feedback corrective loop to achieve the state specified by the set point muscle length and velocity. If the gain for a zero-delay feedback loop is infinity, then it can be easily shown that the output of the two-joint system is equal to the set-point at all times. However, the gain of the spinal reflex is limited by 30 msec plus muscle activation delay in the feedback loop. It was determined through simulations that a feedback gain that was 3 times the physiologically determined values, caused the system to be unstable. Hence the values determined here seem to be close to the maximum allowable without causing instability in the system.

1.7   Model of the Human Arm used for Simulations

In the previous sections a general overview of the plant and its properties was provided. The physiological parameters controlling dynamics of the human arm and methods for modeling them were discussed. A summary of the equations and parameter values used in the computational model for simulating arm movements in the current study are presented here. The block diagram of the plant is shown in Fig. 1.15.

The arm is modeled as a two-joint inertial system with kinematics and dynamics derived in Sec. 1.1. f_D represents the nonlinear forward dynamics function of the two-joint arm and $\mathbf{F_x}$ is the external force acting on the hand. The following parameter values for the human arm are used and taken from (Jordan et al., 1994):

$$l_1 = 0.33m$$
$$l_2 = 0.32m$$
$$l_{c1} = 0.165m$$
$$l_{c2} = 0.16m$$
$$m_1 = 2.52kg$$
$$m_2 = 1.6kg$$
$$i_1 = 0.023kgm^2$$
$$i_2 = 0.011kgm^2$$
$$d_{11} = 0.255kgm^2$$
$$d_{22} = 0.052kgm^2$$

The three muscle pair model of the arm (Sec. 1.3) is used for torque generation at the joints. The muscles in each pair are assumed to be identical and modeled as nonlinear elements with dynamics modeled in Sec. 1.2.1. The muscle dynamics are represented by the nonlinear function f_M that transforms the filtered neural input $\mathbf{N}$ to the muscles into joint torque $\mathbf{T}$. The activation filter h_i acts on the neural signals from the brain $\mathbf{N_C}$ and the spinal reflex path $\mathbf{N_R}$ to give $\mathbf{N}$. The muscles have the following parameters:

$$\begin{bmatrix} \alpha_s \\ \alpha_e \\ \alpha_t \end{bmatrix} = \begin{bmatrix} 2000 \\ 1500 \\ 1000 \end{bmatrix}$$

$$\begin{bmatrix} a_s \\ a_e \\ a_t \end{bmatrix} = \begin{bmatrix} 500 \\ 375 \\ 250 \end{bmatrix}$$

$$\begin{bmatrix} b_s \\ b_e \\ b_t \end{bmatrix} = \begin{bmatrix} 1.3 \\ 0.7 \\ 0.7 \end{bmatrix}$$

$$\begin{bmatrix} C_{ms} \\ C_{me} \\ C_{mt} \end{bmatrix} = \begin{bmatrix} 10 \\ 16 \\ 15 \end{bmatrix}$$

$$\begin{bmatrix} r_s \\ r_e \\ r_t \end{bmatrix} = \begin{bmatrix} 0.05 \\ 0.03 \\ 0.03 \end{bmatrix}$$

$$
\begin{bmatrix} \theta_{0s} \\ \theta_{0e} \\ \theta_{0t} \end{bmatrix} = \begin{bmatrix} \frac{\pi}{2} \\ \frac{\pi}{2} \\ \frac{4\pi}{5} \end{bmatrix}
$$

The gains for the spinal reflex are chosen to be the same as those derived earlier. The set-point for the reflex is specified by the brain as Θ_{SP} and is a combination joint angle position and velocity signal.

$$
\begin{bmatrix} K_{ss} \\ K_{se} \\ K_{st} \end{bmatrix} = \begin{bmatrix} 2.0 \\ 4.0 \\ 3.0 \end{bmatrix} \qquad \begin{bmatrix} B_{ss} \\ B_{se} \\ B_{st} \end{bmatrix} = \begin{bmatrix} 0.2 \\ 0.4 \\ 0.3 \end{bmatrix}
$$

The total time delay in the spinal reflex loop is equal to 0.03 s. The cortical feedback time delay is modeled as 0.15 s and the efferent motor command path delay as 0.06 s.

Note:The simulations of arm movements are performed by discretizing the signals in the system with time interval of 0.004 s and then using a first order iterative procedure to solve the nonlinear equations governing the dynamics of the system. A first order approximation is used because it is found to be reasonably immune to quantization noise, and higher order methods are not required.

Chapter 2

Methods for Control of the Human Arm and Simulation Results

In the prevous chapter the properties of the human arm system were outlined. This included a description of the arm dynamics, muscle properties, visual and proprioceptive feedback available to the brain and delays associated with them, and spinal reflex mechanism; components of the system that received neural activation from the brain. In this chapter, control methods based on feedforward and feedback modalities that the brain can use for controlling arm movements are investigated.

2.1   Requirements for a Control Method

For point-to-point reaching arm movements the hand moves along a predetermined trajectory from the start point to the target. The controller has to generate motor commands to the muscles to execute this planned movement. A method to control human arm movements has to be capable of meeting for the following requirements:

- Generate a movement of the arm along any desired trajectory expressed in terms of cartesian hand position and velocity

- Provide stable control and correct movements of the arm in the presence of perturbations or external forces on the hand, for example not to spill the contents of a glass when accidently pushed on the hand.

- Be robust to noise in sensory feedback and errors in the controller

- Track the desired trajectory in the presence of deterministic novel dynamic environments, for example when objects of different weights have to be moved along the same trajectory.

This may require it to have adaptive capabilities.

2.2 Properties of the human arm important for design of control methods and their incorporation in the simulations

- Equilibrium properties of the muscle pair around a joint and capability to adjust joint stiffness by changing the cocontraction to the muscle pair. This is represented by an additional *desired coactivation* control block providing input to the inverse muscle model that can adjust the coactivation of muscles based on the desired stiffness.

- Fast but limited and fixed gain local feedback loop through the spinal reflex with a time delay of 30 ms and whose set point can be adjusted by the brain. The set-point is sent as a joint position and velocity signal from the brain and delayed through the neural pathway by 90 ms in order to arrive in synchrony with the feedback from the sensors.

- Feedback delay from vision and proprioception to the brain of about 150 ms because of which conventional feedback control does not work, specially for fast movements.

- Nonlinearities of the plant that have to be compensated for in control loops. This is a problem because the inverse of such nonlinear functions may not exist. The muscle inverse can invert the nonlinear force-length and force-velocity relation for the muscle, but cannot model the muscle activation-force impulse response function h_i. The best compensation to this impulse function without causing instabilty is achieved by assuming it to be a pure time delay of 20 ms and modeling its inverse as a time-lead element that precomputes the signals 20 ms in advance.

- Descending neural path delay of 60 ms from the brain to the muscle, which requires the motor command from the brain to be precomputed 60 ms in advance. This includes the 20 ms compensation for activation-force response. All signals in the brain used for computation of the desired behavior of the system like the desired trajectory and torque have to lead the current time by 60 ms.

2.3 Simulation Methods

The control methods outlined in this section are used for simulating arm movements to test the properties of each controller. The desired trajectory for all controllers is a minimum jerk trajectory with a movement time of 0.5 s to a target placed 10 cms away in one of eight equally spaced directions. Each method is tested under two cases of arm dynamics:

47

1. Null field B_0 : Unloaded arm with only the dynamics of the arm.

2. Force Field B_1 : A curl force field with $K_x = \begin{bmatrix} 0 & 13 \\ -13 & 0 \end{bmatrix}$ acting on the hand and altering the dynamics of the arm

In the two cases, the controller expects a null field and hence the force field B_1 acts as an external perturbation to the arm. The idea is to test stability and robustness of the controller to unmodeled changes in arm dynamics. In some cases, a third dynamic situation is created where the controller expects field B_1 but has to perform in an opposite field B_2 with $K_x = \begin{bmatrix} 0 & -13 \\ 13 & 0 \end{bmatrix}$.

2.3.1 Glossary of terms and symbols used in block diagrams

- $\mathbf{x}_{md}$, $\dot{\mathbf{x}}_{md}$ - the desired trajectory in terms of muscle position and velocity respectively

- Θ_d, $\dot{\Theta}_d$ - the desired trajectory in terms of angular position and velocity for the joints respectively

- $\mathbf{x}_d$, $\dot{\mathbf{x}}_d$ - the desired trajectory in terms of hand position and velocity respectively

- $\hat{\mathbf{x}}_m$, $\dot{\hat{\mathbf{x}}}_m$ - the estimated trajectory from the forward model in terms of muscle position and velocity respectively

- $\hat{\Theta}$, $\dot{\hat{\Theta}}$ - the estimated trajectory in terms of angular position and velocity for the joints respectively

- $\hat{\mathbf{x}}$, $\dot{\hat{\mathbf{x}}}$ - the estimated trajectory in terms of hand position and velocity respectively

- $\mathbf{x}_m$, $\dot{\mathbf{x}}_m$ - the actual trajectory in terms of muscle position and velocity respectively

- Θ, $\dot{\Theta}$ - the actual trajectory in terms of angular position and velocity for the joints respectively

- $\mathbf{x}$, $\dot{\mathbf{x}}$ - the actual trajectory in terms of hand position and velocity respectively

- $\mathbf{T}_d$ - the desired joint torques

- $\mathbf{T}$ - the actual torque generated by the muscles

- $\mathbf{F}_x$ - the external force acting on the hand

- $\mathbf{N_C}$ - the descending motor command from the brain

- $\mathbf{N_R}$ - the additional motor command from the spinal reflex

- **N** - the motor command input to the muscles given by $\mathbf{N} = h_i * [\mathbf{N_C} + \mathbf{N_R}]$, where h_i is the activation filter.

- K_p, K_v - the gains of the supraspinal linear feedback controller that receives error signal between desired and estimated trajectory

- t - the current time in msec

- Δ - the delay in the neural paths

Note: Signals for the state of the arm ($\mathbf{x}, \mathbf{\Theta}$) are represented at certain places as only position signals but actually refer to both position and velocity signals. The activation filter h_i is not explicitly shown in the block diagrams for the controllers, but is used for computing $\mathbf{N}$.

2.4 Feedforward Control of the Human Arm

This refers to a control method by the brain that uses only the predetermined desired trajectory to generate control signals for movement of the arm. It is a feedforward control system and does not rely on feedback during the movement. Stability of the system is achieved by the spinal reflex loop and equilibrium properties of the muscle. An important distinction of this method to feedback methods discussed later is that desired trajectory directly drives the system without the use of intermediate variables like muscle activation or torque, although they are used in block diagrams for simplification. The brain does not have independent control over torque or muscle activation generated in the system and controls only the trajectory. It was established in Section 1.5 that the muscle can be used as a trajectory controller or as a torque generator. In the feedforward methods discussed here, the controller relies on trajectory control properties of the muscle.

2.4.1 Equilibrium Point Control

An important property of the system is the existence of a stable equilibrium state for the arm that can be programmed by muscle activations and spinal reflex set points. Any hand trajectory through space can be represented in terms of muscle lengths and velocities as a series of equilibrium states. Given the stable equilibrium properties of the human musculature shown in Sec.1.3.2, the arm will asymptotically track the desired the desired equilibrium trajectory. Exact tracking of a fast trajectory may not be possible because the system is only asymptotically stable, implying that it will go to equilibrium at infinite time. However it will approach equilibrium with a faster or slower time constant depending on the dynamics of the arm that depend on the inertia, stiffness and viscosity. Higher stiffness, for example, will cause closer tracking of the desired trajectory.
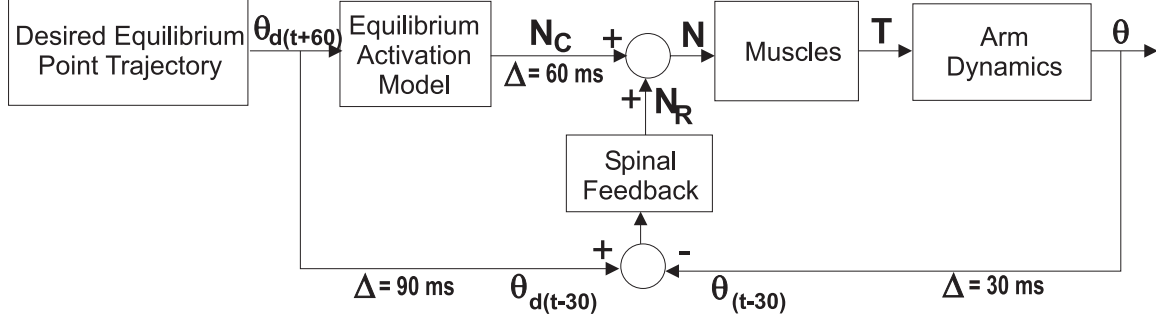
Figure 2.1: Block diagram illustrating the equilibrium point control method

This is a very simple form of control and requires programming of muscle activations and spinal reflex set point to the equilibrium values of muscle lengths and velocities. Let the desired hand trajectory be given by $\boldsymbol{\Theta_d}, \dot{\boldsymbol{\Theta}}_{\mathbf{d}}$. If the neural activation N_m (m = s,e,t) to each muscle pair is programmed such that $T_s = T_e = T_t = 0$ then it represents an equilibrium state for the arm because torque about the joints are zero. This was derived as the solution of the following equations for the linearized muscle model,

$$\alpha(\mathbf{N_{m1}} - \mathbf{N_{m2}})\mathbf{r} = K_\theta(\boldsymbol{\Theta_d} - \boldsymbol{\Theta_0}) + B_\theta\dot{\boldsymbol{\Theta}}_{\mathbf{d}}$$
$$\mathbf{N_{m1}} = \frac{\mathbf{N_{mc}}^2}{\mathbf{N_{m2}}}$$

which then gave,

$$\mathbf{T} = K_\theta(\boldsymbol{\Theta_d} - \boldsymbol{\Theta}) + B_\theta(\dot{\boldsymbol{\Theta}}_{\mathbf{d}} - \dot{\boldsymbol{\Theta}})$$

If now we additionally program the set point for the spinal reflex as the desired trajectory,

$$\mathbf{N_R} = K_s(\hat{\mathbf{x}}_{\mathbf{m}} - \mathbf{x_{m_d}}) + B_s(\dot{\hat{\mathbf{x}}}_{\mathbf{m}} - \dot{\mathbf{x}}_{\mathbf{m_d}})$$

then,

$$\mathbf{T} = K_\theta(\boldsymbol{\Theta_d} - \boldsymbol{\Theta}) + B_\theta(\dot{\boldsymbol{\Theta}}_{\mathbf{d}} - \dot{\boldsymbol{\Theta}}) + K_{\theta s}(\boldsymbol{\Theta_d} - \boldsymbol{\Theta}) + B_{\theta s}(\dot{\boldsymbol{\Theta}}_{\mathbf{d}} - \dot{\boldsymbol{\Theta}})$$

This is a feedback control loop acting on each joint and providing asymptotically stable control. For the nonlinear muscles, the muscle activation can be computed from the following equations and as already established in Sec. 1.3, retain the equilibrium control properties around the joint.

50
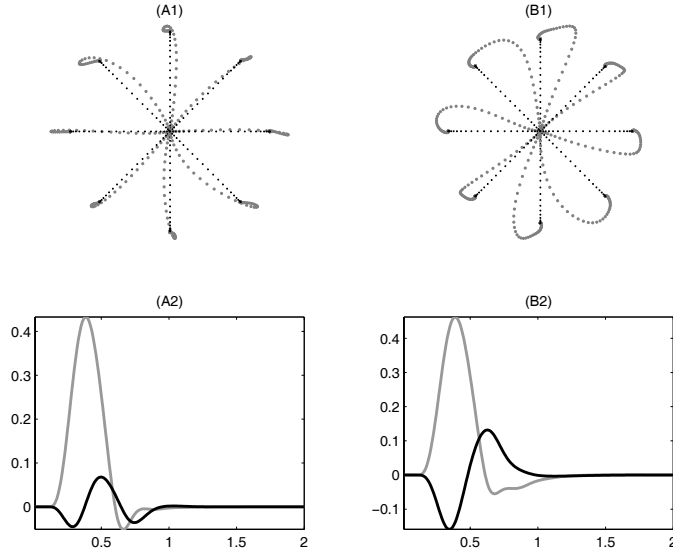
Figure 2.2: Simulated trajectories for equilibrium point control. (A) null field, (B) force field B_1. (1), hand paths for eight directions movement represented as dots (big gray dots- actual; small black dots- desired) at 20 ms intervals. (2), parallel (gray line) and perpendicular (black line) hand velocities for downward movement direction

$$
\begin{aligned}
\mathbf{F_{t_1}} &= \frac{F_b^2}{\mathbf{F_{t_2}}} \\
\mathbf{F_{t_1}} &= \mathbf{F_{t_2}} \\
\mathbf{N_C} &= \hat{f}_M^{-1}(\mathbf{F_t}, \mathbf{x_{m_d}}, \dot{\mathbf{x}}_{\mathbf{m_d}})
\end{aligned}
$$

The Equilibrium point hypothesis is very attractive not only because of its stability but also because the computation involved for generating arm movements is very simple. It is represented as a block diagram in Fig 2.1. The desired trajectory is the input to the equilibrium activation model, which is equivalent to an inverse model of the muscle dynamics, and is based on an estimate of the non linear muscle properties K_θ and B_θ. The output is the computed neural signals N_C. This is the only computation performed in this system. The desired trajectory has to precede the actual trajectory by 60 ms because of conduction pathway delays. The desired trajectory also acts as set-point to the spinal reflex and is delayed 30 ms to arrive in synchrony with the feedback signal.

Note: All simulations in this chapter are performed without the robot dynamics coupled to the arm. An unloaded arm refers to dynamics of just the human arm. In the following chapters where comparison is made with experimental data robot dynamics will be coupled to the arm and taken into account during the simulations.

A simulation using equilibrium point control shows the advantages and disadvantages of the
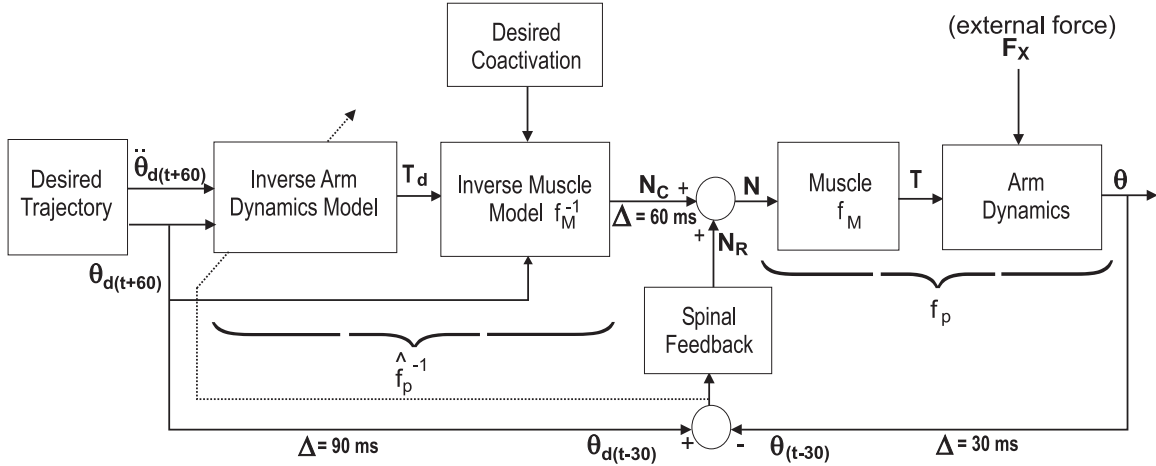
Figure 2.3: Block diagram illustrating inverse dynamics model control

method. Fig. 2.2 shows two movements (A) and (B). The desired trajectory for both movements is a minimum jerk trajectory from the center of the workspace directly outward to a point 10 cms away. (A) is a movement of the unloaded arm. For normal stiffness levels (based on data by (Gomi and Kawato, 1996)) during a movement, the actual hand path only approximately follows the desired straight line path showed in dotted line. Hence it is not possible to generate the desired movement with this method. Another disadvantage is in terms of adaptation to novel dynamics as presented by the curl force field. (B) shows a movement in the force field B_1 with 1.5 times the normal stiffness and shows a large deviation from the desired trajectory. Muscle coactivation is the only control parameter in this model and an increase in coactivation and stiffness does not seem to be an energy efficient or a very effective way to correct for forces due to the field. However the advantage to be noted here is that although the movement in the field is not as desired, the gross characteristics of movement are preserved and the system tracks the desired behavior in a *asymptotically stable* manner. Passive dynamics of the arm are completely ignored but stability is still maintained. Another advantage is that delays in the system can be ignored and do not affect the behavior of the plant.

2.4.2 Inverse Dynamics Model Control

A modification of the equilibrium point control that can overcome its drawbacks is the addition of an *inverse dynamics* model to the feedforward control. The muscles are not only programmed by the desired equilibrium trajectory but also by the torque required to move the arm along the trajectory. An inverse dynamics model of the arm is capable of generating the torques required to move along the desired trajectory. The motor commands sent to the muscles can then be programmed to produce these torques as well as maintain an equilibrium trajectory. The computations involved are based on the equations derived in previous sections:

The torque required to move along the desired trajectory expressed in terms of joint angle $\mathbf{\Theta_d}$, is given by,

$$\mathbf{T_d} = D(\mathbf{\Theta_d})\ddot{\mathbf{\Theta}}_\mathbf{d} + C(\mathbf{\Theta_d}, \dot{\mathbf{\Theta}}_\mathbf{d})\dot{\mathbf{\Theta}}_\mathbf{d} \tag{2.1}$$

The inverse dynamic model is an approximation of this relationship that computes the desired torque $\mathbf{T_d}$ required to move along the desired trajectory. $\mathbf{T_d}$ is then converted to desired forces in individual muscles $\mathbf{F_{t_d}}$, and then using the inverse muscle model, to give the motor commands $\mathbf{N}$,

$$\mathbf{N} = \hat{f}_M^{-1}(\mathbf{F_{t_d}}, \mathbf{x_{m_d}}, \dot{\mathbf{x}}_{\mathbf{m_d}})$$

To generate the correct torque and exactly track the desired trajectory, perfect knowledge of the dynamic relationships represented by D, C, f_M^{-1} is required. If T_d and N is computed by the brain and sent to the muscles, then for the linearized three muscle pair model one can derive the actual torque generated by the muscles as,

$$\mathbf{T} = \mathbf{T_d} + K_\theta(\mathbf{\Theta_d} - \mathbf{\Theta}) + B_\theta(\dot{\mathbf{\Theta}}_\mathbf{d} - \dot{\mathbf{\Theta}})$$

The torque is a sum of the desired torque and corrective terms derived for the equilibrium point control in the previous section. The system retains the equilibrium point characteristics and is able to compensate for known dynamics of the arm.

Fig. 2.3 shows the block diagram for this method of control. The main computational block in this system is the inverse dynamics model represented by $\hat{f}_D^{-1}$ which is an estimate of the inverse passive dynamics represented in Eq. 2.1. A perfect inverse muscle model $\hat{f}_M^{-1} = f_M^{-1}$ is assumed. Together they can be represented as the estimated inverse dynamics for the whole plant $\hat{f}_P^{-1}$.

When the inverse model perfectly models the dynamics of the arm $\hat{f}_P^{-1} f_P = 1$, there is exact tracking of the desired trajectory and $\mathbf{T} = \mathbf{T_d}$. and the equilibrium properties of the muscles and spinal reflex are not required. However when the model is not accurate and does not generate the correct torque values causing deviation from the desired trajectory, the equilibrium control takes over and controls the characteristics of movement just as in the previous section, thereby still maintaining the asymptotically stable behavior of the plant. This is illustrated in a simulation in the null (A) and force field (B) in Fig. 2.4. In both cases the inverse dynamics model is estimating only the dynamics of the unloaded arm with no external dynamics. The null field simulation is an unloaded arm movement when no external forces act on the arm. In this situation a near perfect movement is obtained. The reason that the movement is not exact is because the dynamics associated with the neural activation filter h_i cannot be inverted and
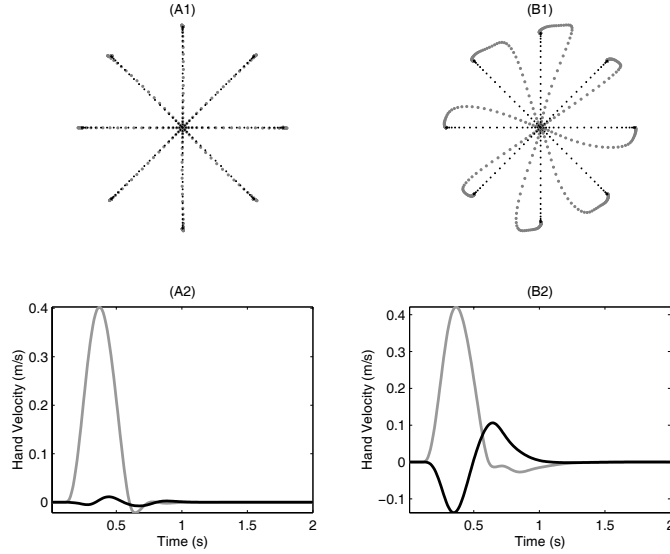
Figure 2.4: Simulated trajectories for inverse model feedforward control. (A) null field, (B) force field B_1. (1), hand paths for eight directions movement represented as dots (big gray dots-actual; small black dots- desired) at 20 ms intervals. (2), parallel (gray line) and perpendicular (black line) hand velocities for downward movement direction

is approximated here by a time delay of 20 ms. When the force field is turned on in (B) then the hand trajectory initially shows a clockwise deviation due to the force field but then returns to the desired end-point position in a stable manner due to the equilibrium properties of the arm.

In force field B_1, if the inverse dynamics model is altered so that it predicts the force field and accounts for the change in dynamics due to the field, then the hand can track the desired trajectory exactly and looks like a movement in the null field. An adaptive mechanism that modifies the inverse model can be based on the error signal derived from the difference in desired and actual trajectory as shown in Fig. 2.3 by the dotted line. The model adjusts itself to minimize this error. A problem associated with this type of learning due to a particular form of redundancy in nonlinear systems has been pointed out by (Jordan, 1995). This problem can be overcome by using a *Feedback Error Learning* approach developed by (Kawato et al., 1987) that makes use of a feedback controller to guide the learning of the inverse model. In the case of the human arm, such a feedback controller is present in the form of spinal reflex, and the output neural activation of the spinal controller N_R can be used for adapting the inverse model. Hence the inverse model based feedforward control method provides stable control when the arm dynamics are suddenly altered and also a mechanism for adaptation to changes in the arm dynamics.

2.5 Feedback Control of the Human Arm

Feedback control is a method where the brain uses sensory feedback information about the state of the arm from vision and proprioception to generate or modify the motor commands sent to the arm based on error in the measured state and the desired trajectory.

The feedback control of a system has the following advantages:

- It is robust to noise and changes in the plant

- With high feedback gains it is possible to emulate the inverse dynamics of the system with a simple linear controller and achieve close to exact tracking of the desired trajectory

Its disadvantages:

- Extremely sensitive to noise in feedback

- Affected greatly by time delays in the feedback loop

- The actual trajectory can never track the desired trajectory exactly

In the human motor system, feedback control is very attractive because of its advantages, specially because humans have to interact with different environments that continually alter the dynamics of the system they are trying to control. And, visual control of movement is a form of feedback control that is very useful. However the time delays in the feedback loop severely limit the scope of feedback control and do not allow simple feedback control of the system. The reason is that information about the outcome of a control action is not available instantly and has to go through a delay before reaching the controller. By the time the control action is taken it may no longer be appropriate for dealing with the current errors in the output of the system. To overcome delays in the feedback, what is required is a method to obtain the current state or output of the system without having to wait for it to feed back. For stable feedback control the brain has to compute the state of the arm at current time t from a delayed measurement of the state at time $t - t_0$, where t_0 is the feedback delay, and a history of motor commands sent out by the brain until the current time t. In control literature, a computational unit that estimates or predicts current state estimates is called an *observer*. Hence an observer has to be designed to solve the time-delay problem. In the context of arm movements, the concept of a *Forward Model* has been proposed by (Miall and Wolpert, 1996) to construct an observer and achieve feedback control in the presence of time delays in the system.

Forward Dynamics Model based Feedback Control

The *forward dynamics model* refers to a hypothetical computational network in the brain and has been defined by (Miall and Wolpert, 1996) as an internal model that mimics the causal flow of a process by predicting its next state given the current state and the motor commands. The forward model is a model of the input-output mapping of the human arm from muscle activation to arm movement. It can be represented as an estimate of the forward dynamics of the plant $\hat{f}_P$, that predicts hand acceleration $\hat{\ddot{\mathbf{x}}}$, from neural signal $\mathbf{N}$ and hand state $\mathbf{x}, \dot{\mathbf{x}}$. (Miall et al., 1993) proposed a control strategy based on the forward model known as a Smith predictor model for feedback control of fast movements. This method was initially developed by O.J.M. Smith for time-delayed single variable linear systems. Miall et al. tested the Smith predictor method for feedback control of a time-delayed single variable linear system and showed that it succeeded in doing so, but became unstable when the delay time or the plant was not accurately modeled. The main problem with the Smith predictor approach is that it cannot be used for nonlinear systems and results in unstable oscillatory behavior. To test this method for estimating the state of a two-joint human arm, let us formulate the problem in the framework of an observer. The actual plant can be expressed as:

$$
\begin{aligned}
\mathbf{\Sigma} : \qquad \ddot{\mathbf{x}}(t) &= f_p(\mathbf{N}(t),\, \mathbf{x}(t),\, \dot{\mathbf{x}}(t)) \\
\mathbf{y}(t) &= \mathbf{x}(t - t_0) \\
\dot{\mathbf{y}}(t) &= \dot{\mathbf{x}}(t - t_0)
\end{aligned}
$$

where, $\mathbf{N}$ is the motor command input to the system, $\mathbf{x}$ is the state of the system, and $\mathbf{y}$ is the output of the system being measured. We have to design an observer that can estimate the state $\mathbf{x}$ from the measurement $\mathbf{y}$ and input $\mathbf{N}$. The observer design based on a Smith predictor is as follows:

$$
\begin{aligned}
\mathbf{\Sigma}_0 : \qquad \ddot{\check{\mathbf{x}}}(T) &= \hat{f}_p(\mathbf{N}_C(T),\, \check{\mathbf{x}}(T),\, \dot{\check{\mathbf{x}}}(T)) \\
\check{\mathbf{x}}(0) &= \mathbf{x}(0) \\
\dot{\check{\mathbf{x}}}(0) &= \dot{\mathbf{x}}(0) \\
\dot{\check{\mathbf{x}}}(t + i\Delta) &= \dot{\check{\mathbf{x}}}(t + (i-1)\Delta) + \int_{t+(i-1)\Delta}^{t+i\Delta} \ddot{\check{\mathbf{x}}}(T)\, dT \\
\check{\mathbf{x}}(t + i\Delta) &= \check{\mathbf{x}}(t + (i-1)\Delta) + \int_{t+(i-1)\Delta}^{t+i\Delta} \dot{\check{\mathbf{x}}}(T)\, dT \\
\dot{\hat{\mathbf{x}}}(t) &= \dot{\check{\mathbf{x}}}(t) + [\dot{\mathbf{y}}(t) - \dot{\check{\mathbf{x}}}(t - t_0)] \\
\hat{\mathbf{x}}(t) &= \check{\mathbf{x}}(t) + [\mathbf{y}(t) - \check{\mathbf{x}}(t - t_0)] + \Delta\,[\dot{\mathbf{y}}(t) - \dot{\check{\mathbf{x}}}(t - t_0)] \\
i &= 0...\infty
\end{aligned}
$$

X, Ẋ$_{(t-t_0)}$ $\hat{f}_p$ x̆, x̆$_{(t-t_0+\Delta)}$ $\hat{f}_p$ x̆, x̆$_{(t-t_0+2\Delta)}$ ...... x̆, x̆$_{(t-\Delta)}$ $\hat{f}_p$ $\hat{x}, \hat{\dot{x}}_{(t)}$

$N_{c(t-t_0)}$ $N_{c(t-t_0+\Delta)}$ $N_{c(t-t_0+n\Delta)} = N_{c(t-\Delta)}$
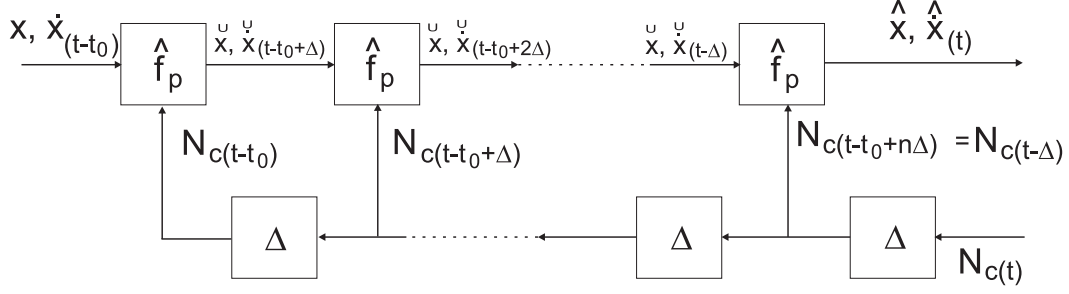
Δ ...... Δ Δ $N_{c(t)}$

Figure 2.5: Block diagram showing how a forward model $\hat{f}_p$ can be used to construct an observer for a time-delayed nonlinear system.

where, $\hat{\mathbf{x}}, \hat{\dot{\mathbf{x}}}$ are the feedback-updated state estimates output by the observer, and $\check{\mathbf{x}}, \check{\dot{\mathbf{x}}}$ are the non-updated state estimates. The observer is presented in Fig. F. Simulation of a movement based on this observer is presented in a later section in Fig. F and shows that this method is unstable in the presence of unmodeled dynamics when the forward model does not exactly mimic the plant.

The Smith method is based on the solution of a *linear* system at time t given the output of the plant at time $t - t_0$ and the inputs to the system in the interval $t - t_0$ to t. It uses a single forward model to compute the state estimates. However, it does not work for nonlinear systems because the solution to nonlinear systems cannot be found analytically and has to be computed iteratively. So an observer has to be designed that can solve a nonlinear system iteratively. A new observer that is capable of performing this iterative computation can be formulated as follows:

$$
\begin{aligned}
\mathbf{\Sigma}_0 : \qquad \check{\ddot{\mathbf{x}}}(T) &= \hat{f}_p(\mathbf{N}_C(T), \check{\mathbf{x}}(T), \check{\dot{\mathbf{x}}}(T)) \\
\check{\mathbf{x}}(t - t_0) &= \mathbf{y}(t) \\
\check{\dot{\mathbf{x}}}(t - t_0) &= \dot{\mathbf{y}}(t) \\
\check{\mathbf{x}}(t - t_0 + i\Delta) &= \check{\mathbf{x}}(t - t_0 + (i-1)\Delta) + \int_{t-t_0+(i-1)\Delta}^{t-t_0+i\Delta} \check{\dot{\mathbf{x}}}(T)\, dT \\
\check{\dot{\mathbf{x}}}(t - t_0 + i\Delta) &= \check{\dot{\mathbf{x}}}(t - t_0 + (i-1)\Delta) + \int_{t-t_0+(i-1)\Delta}^{t-t_0+i\Delta} \check{\ddot{\mathbf{x}}}(T)\, dT \\
\hat{\mathbf{x}}(t) &= \check{\mathbf{x}}(t) \\
\hat{\dot{\mathbf{x}}}(t) &= \check{\dot{\mathbf{x}}}(t) \\
i &= 0...\frac{t_0}{\Delta}(= n)
\end{aligned}
$$

where, $\hat{\mathbf{x}}, \hat{\dot{\mathbf{x}}}$ are state estimates output by the observer, and $\check{\mathbf{x}}, \check{\dot{\mathbf{x}}}$ are intermediate variables used by the observer. The above equations represent the iterative solution of a system $\hat{f}_p$ at time t, given the initial state of the system $\mathbf{y}, \dot{\mathbf{y}}$ and the input $\mathbf{N}_C$ during the time interval $t - t_0$ to

t. Δ is the discretized iteration time interval which should ideally be infinitely small. However for practical systems the value of Δ can be determined by the frequency response of the system and for simulations in the current study was chosen to be 0.004 sec. A network to implement the forward model based observer is presented in Fig. 2.5. It requires multiple copies of the forward model. The number of these copies n can be optimized by choosing the optimal Δ. The computation time for the observer to generate current state estimate depends on the number of forward models computations that have to be performed and hence is directly proportional to n. In the current study this computation time was modeled as 8 msec and was the time delay in the estimation process.

For the simulations, t_0 has a value of 210 msec, and is composed of 150 msec feedback delay and 60 msec descending neural path delay including the 20 msec muscle activation delay. The estimate represents the best knowledge of the current state of the hand and can then be used by the brain to issues neural commands to correct for error in the desired and estimated state. The forward model will give wrong estimates if the estimate of the plant $\hat{f}_p$ is not equal to f_p. This occurs when the dynamics of the arm are altered by unknown external perturbations to the arm. In the following sections the ability of the forward model to control arm movements, its robustness to unmodeled dynamics, and its adaptive capabilities are examined.

Three different modalities of feedback control based on three coordinate systems involved in the motor system are possible. The first one is based on the muscle coordinate system and uses linear feedback to directly modulate the activation of muscles. The second method is based on the joint coordinates and applies linear feedback to control the torque produced by the arm. And the third method based on cartesian coordinates uses linear feedback to change the desired acceleration of the hand. The estimates derived from the forward model can be expressed in either of these three coordinates and then used for appropriate control. These three methods are examined in the next three sections.

2.5.1 Neural Activation Feedback Control

The descending motor command $\mathbf{N_C}$ is directly controlled and is computed as:

$$\mathbf{N_C} = K_p(\hat{\mathbf{x}}_\mathbf{m} - \mathbf{x}_{\mathbf{m_d}}) + K_v(\dot{\hat{\mathbf{x}}}_\mathbf{m} - \dot{\mathbf{x}}_{\mathbf{m_d}}) \tag{2.2}$$

This is a very simple form of feedback control which requires computation of the muscle state through the forward model and then uses a linear controller to vary the neural activation to each muscle based on the error in muscle length and velocity. It is analogous to the way that spinal reflex works. The set-point to the spinal reflex loop is the estimated muscle postion and velocity, which gives,
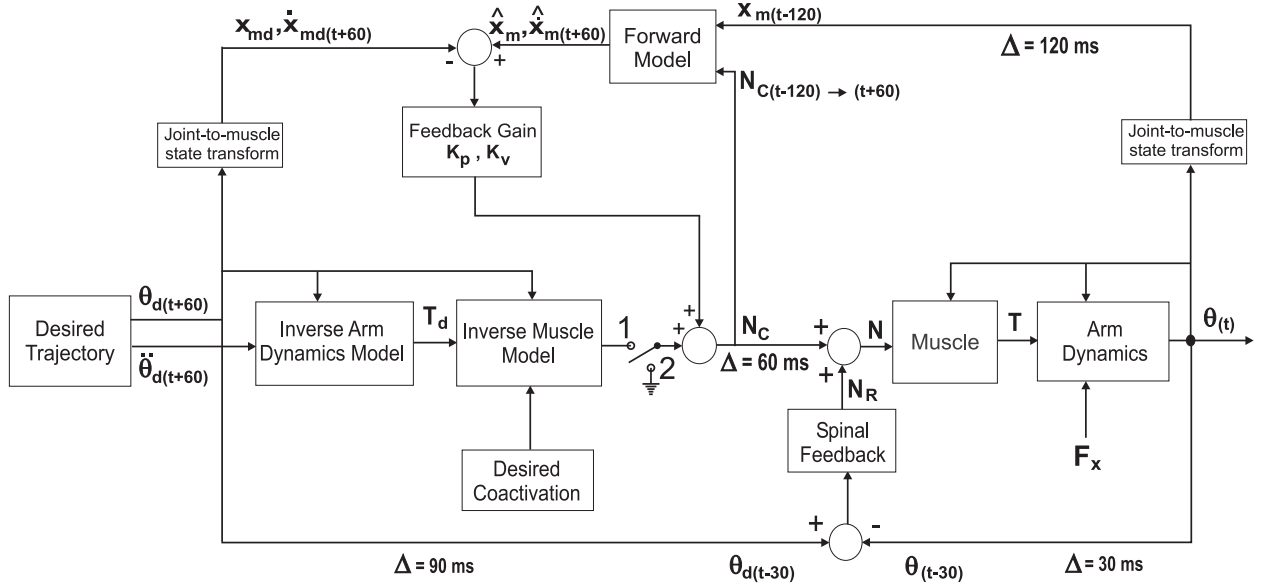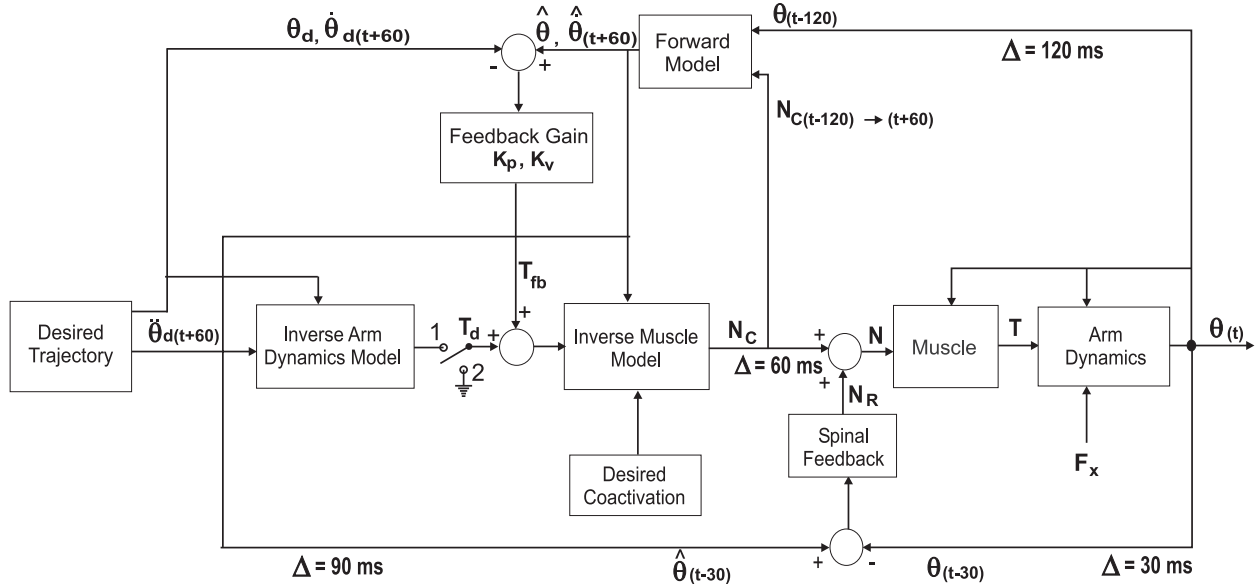
Figure 2.6: Block diagram illustrating the neural activation feedback control method. The switch is in position 2 for feedback only control and in position 1 for feedback+feedforward control

$$\mathbf{N_R} = K_s(\hat{\mathbf{x}}_\mathbf{m} - \mathbf{x}_\mathbf{m}) + B_s(\dot{\hat{\mathbf{x}}}_\mathbf{m} - \dot{\mathbf{x}}_\mathbf{m})$$

The block diagram for this control is shown in Fig. 2.6 with the switch connected to 2. The simulations using this control for arm movements in eight directions for the unloaded arm (null field) and in the presence of force field B_1 is shown in Fig. 2.7(A-B). The forward model in both cases, models the dynamics of the arm in the null field and therefore generates wrong estimates when the external force field is introduced. The gains of the feedback control used for the simulations are $k_p = 10$ and $k_v = 1$. The gains are fixed at half the value at which they cause unstable oscillations in the system in the force field. The ratio of k_p and k_v is optimized to give the maximum gain possible. The movements in the null field are not straight and do not track the desired trajectory exactly, although they converge to the target. This is because the feedback gains are not infinitely high. Simulations in the force field show that the system is oscillatory but damped so that stability is maintained. It is possible to change the forward model so that it models the force field B_1 and produces correct state estimates. A mechanism for this adaptation of forward model could be based on the error in estimated and actual state of the arm. Fig. 2.7(C) shows the simulation for the corrected forward model. There is great improvement in the performance of the system and the movement is closer to the desired trajectory. However it is still not able to track the deisred trajectory exactly in a straight line path. This shows that this method though effective for stable feedback control of movement, is not able to produce the desired behavior exactly. The reason for this inability
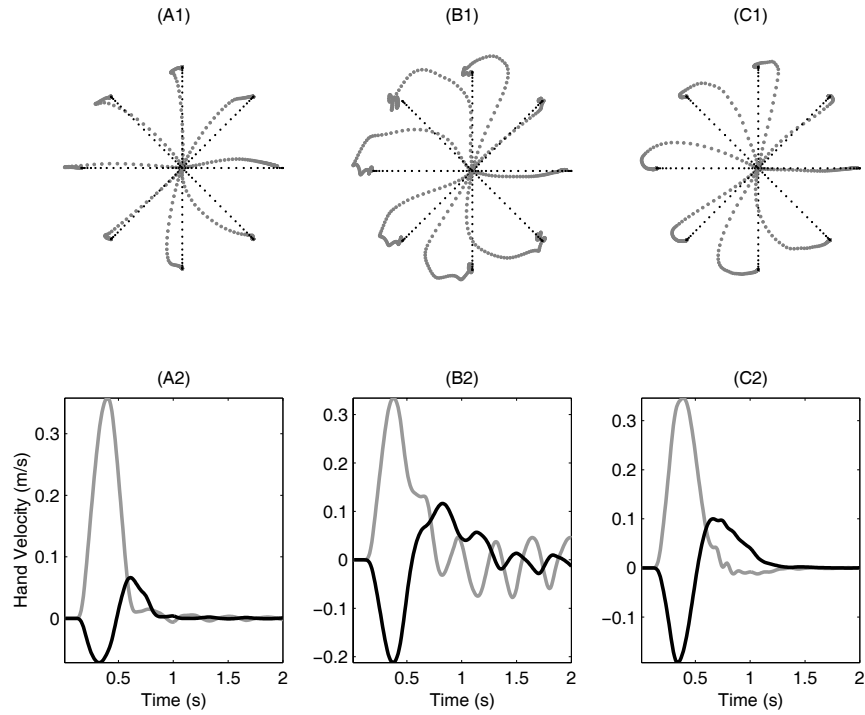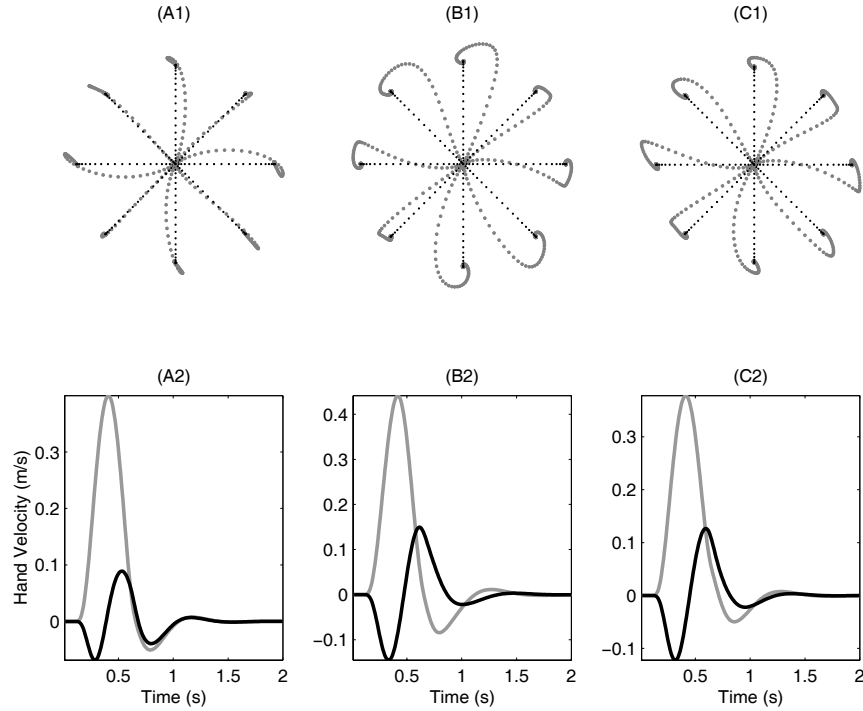
Figure 2.7: Simulated trajectories for neural activation feedback control. (A) null field, (B) force field B_1, (C) force field B_1 with the forward model adapted for the field. (1), hand paths for eight directions movement represented as dots (big gray dots- actual; small black dots- desired) at 20 ms intervals. (2), parallel (gray line) and perpendicular (black line) hand velocities for downward movement direction
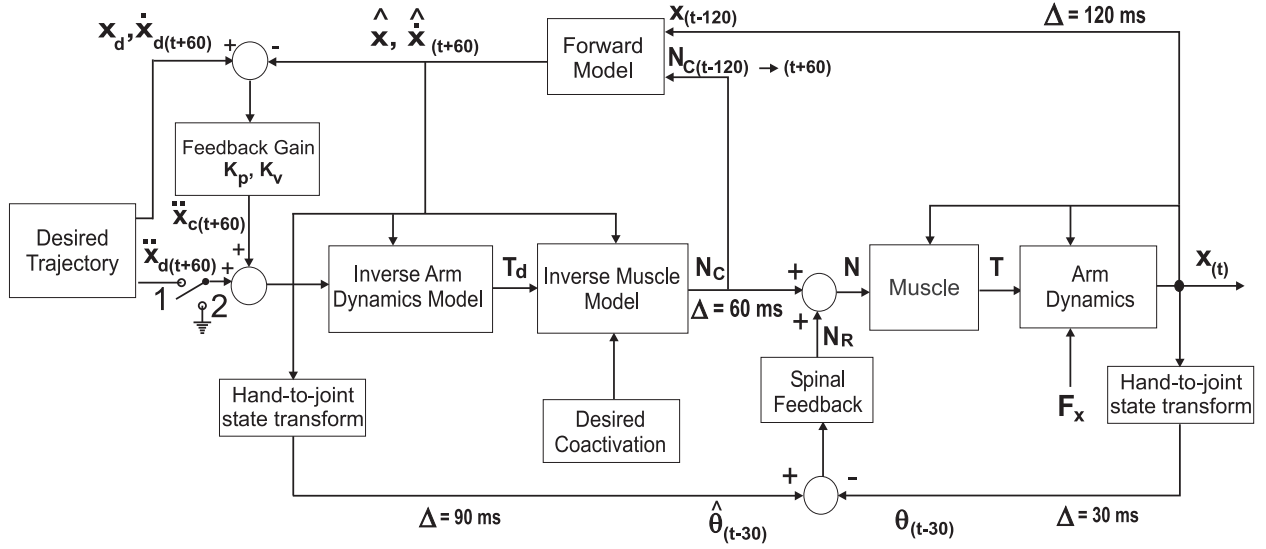
Figure 2.8: Block diagram illustrating the joint torque feedback control method. The switch is in position 2 for feedback only control and in position 1 for feedback+feedforward control

to produce the desired trajectory is that dynamics of the plant are completely ignored in the controller and the feedback gains are not infinitely high.

2.5.2 Joint Torque Feedback Control

This is a method of torque control based on the linear feedback error between estimated and desired joint state. The muscles are programmed to control the joint torque. The desired torque is computed as:

$$\mathbf{T_d} = K_p(\hat{\mathbf{\Theta}}_\mathbf{d} - \mathbf{\Theta}) + K_v(\dot{\hat{\mathbf{\Theta}}}_\mathbf{d} - \dot{\mathbf{\Theta}}) \tag{2.3}$$

The individual muscle forces $\mathbf{F_t}$ are determined from the desired torque, and then the motor commands are computed using the inverse muscle model f_M^{-1},

$$\mathbf{N_C} = f_M^{-1}(\mathbf{F_t}, \hat{\mathbf{x}}_\mathbf{m}, \dot{\hat{\mathbf{x}}}_\mathbf{m})$$

It is important to note that the inverse muscle model relies on estimated muscle state generated from the forward model to compute the activation. In order to produce the desired torque and muscle force one requires the current state of the muscle. The best knowledge of the current state for a time-delayed system is the estimate from the forward model.

The set-point to the spinal reflex loop is again,

Figure 2.9: Simulated trajectories for torque feedback control. (A) null field, (B) force field B_1, (C) force field B_1 with the forward model adapted for the field. (1), hand paths for eight directions movement represented as dots (big gray dots- actual; small black dots- desired) at 20 ms intervals. (2), parallel (gray line) and perpendicular (black line) hand velocities for downward movement direction

$$\mathbf{N_R} = K_s(\hat{\mathbf{x}}_\mathbf{m} - \mathbf{x}_\mathbf{m}) + B_s(\dot{\hat{\mathbf{x}}}_\mathbf{m} - \dot{\mathbf{x}}_\mathbf{m})$$

The block diagram representing this control method is given in Fig. 2.8 with the switch in position 2. Fig. 2.9 shows the simulations of arm movements with this method. The feedback gains are $k_p = 30$ and $k_v = 3$ and chosen with the same critireon as in the previous control method. In the null field the movements of the hand are not straight even though the estimates are correct. This is because dynamics of the arm are ignored in the computation of the torque and the gains are not infinitely high. If the feedback gains are kept limited by the uncertainties in the dyanmics of the arm, then this represents a drawback for this control. The simulations with the force field seem to be oscilatory but stable and converge to the target after the initial deviation. The performance is more stable than the neural feedback control because of added stability of inverse muscle dynamics, but it suffers from the same drawbacks. The same arguments as in the case of neural feedback system apply here. A change in the forward model so that it models the force field B_1 and produces correct state estimates, is simulated in Fig. 2.9(C) and shows that there is improvement in the performance of the system and the

Figure 2.10: Block diagram illustrating the hand acceleration feedback control method. The switch is in position 2 for feedback only control and in position 1 for feedback+feedforward control

movement is closer to the desired trajectory. However it is still not able to track the deisred trajectory exactly in a straight line path. This method like the activation control is effective for stable feedback control of movement, but is not able to produce the desired behavior exactly.

2.5.3 Hand Acceleration Feedback Control

In this method, the brain controls the acceleration of the hand based on the error in estimated and desired hand position and velocity. The acceleration is computed as:

$$\ddot{\mathbf{x}}_{\mathbf{d}} = K_p(\mathbf{x}_{\mathbf{d}} - \hat{\mathbf{x}}) + K_v(\dot{\mathbf{x}}_{\mathbf{d}} - \dot{\hat{\mathbf{x}}}) \tag{2.4}$$

To produce the desired acceleration, the controller relies on the inverse plant model $\hat{f}_P^{-1}$, that consists of the inverse dynamics model $\hat{f}_D^{-1}$ and the inverse muscle model f_M^{-1}, to generate the motor commands.

$$\mathbf{N}_{\mathbf{C}} = \hat{f}_P^{-1}(\ddot{\mathbf{x}}_{\mathbf{d}}, \hat{\mathbf{x}}, \dot{\hat{\mathbf{x}}})$$

It is important to note that the inverse plant model also relies on estimated muscle state generated from the forward model to compute the activation.

The set-point to the spinal reflex loop is again,

$$\mathbf{N}_{\mathbf{R}} = K_s(\hat{\mathbf{x}}_{\mathbf{m}} - \mathbf{x}_{\mathbf{m}}) + B_s(\dot{\hat{\mathbf{x}}}_{\mathbf{m}} - \dot{\mathbf{x}}_{\mathbf{m}})$$
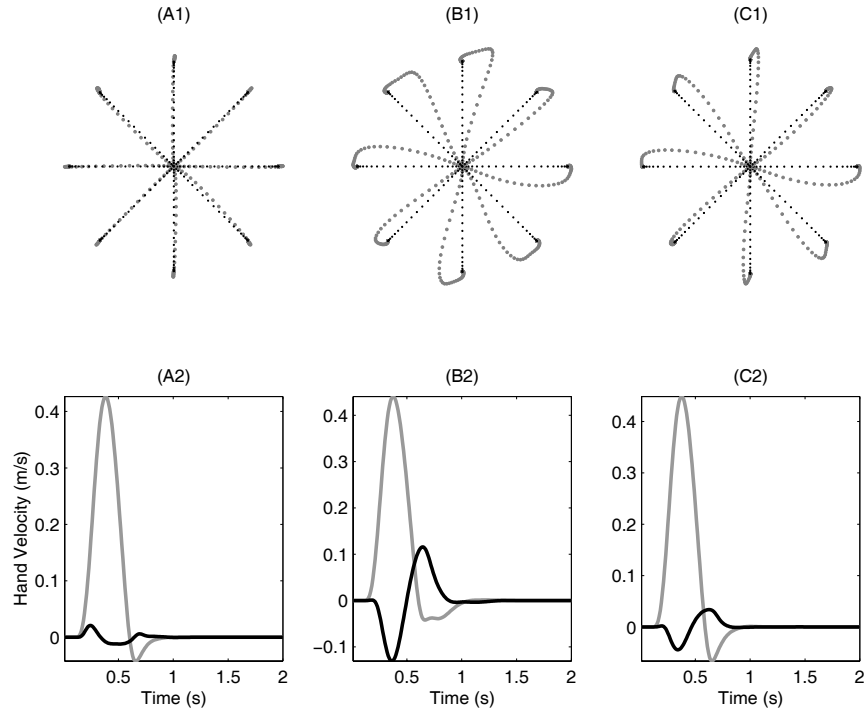
Figure 2.11: Simulated trajectories for hand acceleration feedback control. (A) null field with IM=FM=0, (B) force field B_1 with IM=FM=0, (C) force field B_1 with the forward model adapted for the field, IM=0, FM=B_1. (1), hand paths for eight directions of movement represented as dots (big gray dots- actual; small black dots- desired) at 20 ms intervals. (2), parallel (gray line) and perpendicular (black line) hand velocities for downward movement direction

The block diagram representing this control method is given in Fig. 2.10 with the switch in position 2. Fig. 2.11 shows the simulations of arm movements with this method. The feedback gains are $k_p = 500$ and $k_v = 50$ and chosen with the same critireon as in the previous control method. In the null field the movements of the hand are straight and almost exactly track the desired trajectory. This had not been possible with the previous two methods. The reason that performance is much better for feedback in hand space is the incorporation of an inverse dynamic model of the arm in the controller. The simulations with the force field B_1 seem to be oscillatory but stable and converge to the target after the initial deviation. Fig. 2.11(C) shows that if the forward model is changed so that it now models the altered dynamics with the force field B_1, then the performance of the system is greatly improved. Performance identical to that in the null field can be obtained if a change is also made in the inverse dynamics model to include the force field. Hence with this method it is possible to not only provide stable feedback control but to also to adapt to altered dynamics of the arm and converge to the straight path desired movement.

2.6   A Method using both Feedforward and Feedback Control

One of the problems associated with feedback control is that of tracking the desired trajectory exactly. With feedback gains that are not sufficiently high, the actual trajectory only approximates the desired trajectory as was seen with only feedback control of movement for neural activation and torque control methods. The other disadvantage with these methods was that of adapting to altered dynamics by changing the forward model, which improved performance but still caused errors in tracking the desired trajectory. One way to overcome this drawback is to combine inverse model feedforward control with feedback control. In the new configuration, the feedforward signal controls the system and the feedback signal corrects for unmodeled disturbances to the system, hence this method integrates the advantages of both the feedforward and feedback techniques. New block diagrams for the three feedback schemes considered earlier are obtained by connecting the switch to position 1, which adds feedforward signals to the controller. The results of simulations for the null field and force field B_1 movements are provided in Figs. 2.12-14(A-C) for the three control methods. There is great improvement in behavior for the first two methods with neural activation and torque feedback control. For the neural activation feedback (Fig. 2.12(A)), there is great improvement in stability of the system. This is expected because a muscle inverse model that provides equilibrium point control is added to the system. An inverse plant model generates the feedforward activation for the null field case from the desired trajectory. For the torque feedback (Fig. 2.13(A)), the improvement occurs in the null field case because of addition of the inverse dynamics model that generates the correct torque for the movement. This allows for exact tracking of the desired trajectory. There is almost no change in the hand acceleration feedback case. Figs. 2.12-14(B) show the trajecto-
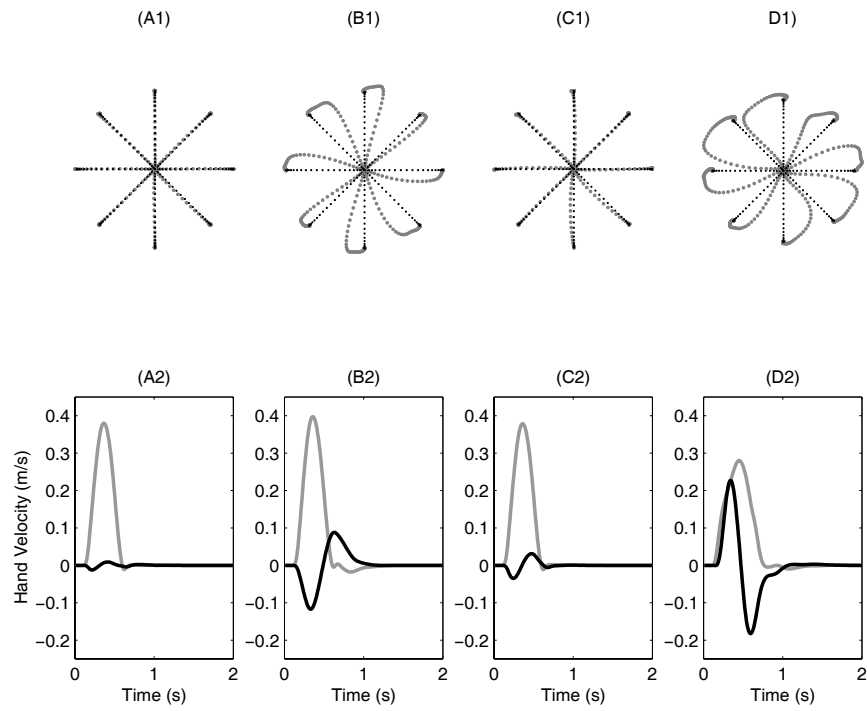
Figure 2.12: Simulated hand paths for feedback+feedforward neural activation control shown in Fig. 2.6 with switch in position 1. (A) null field with IM=FM=0, (B) force field B_1 with IM=FM=0, (C) force field B_1 with IM=FM=B_1, (D) force field B_2 with IM=FM=B_1
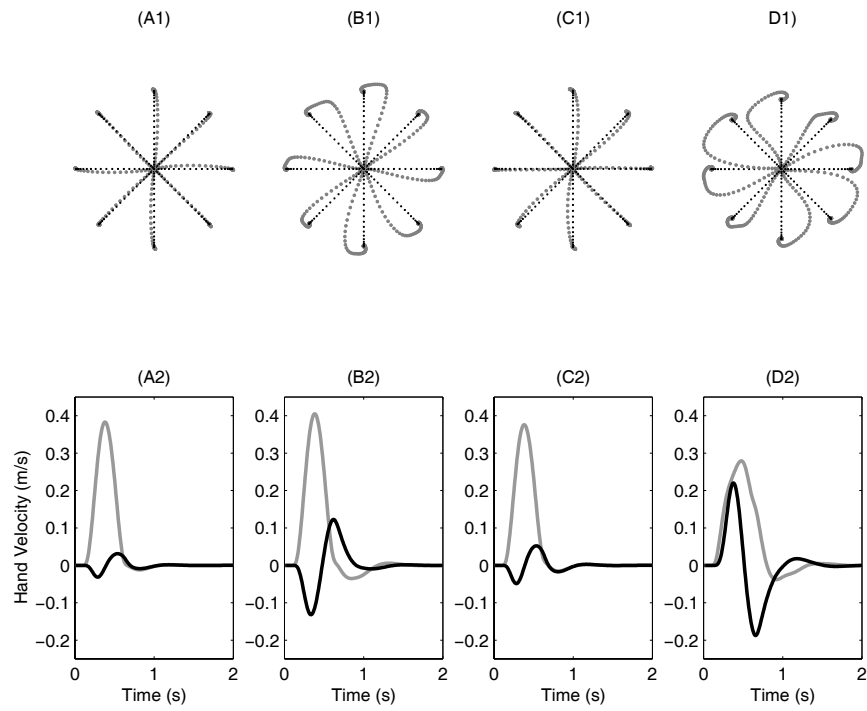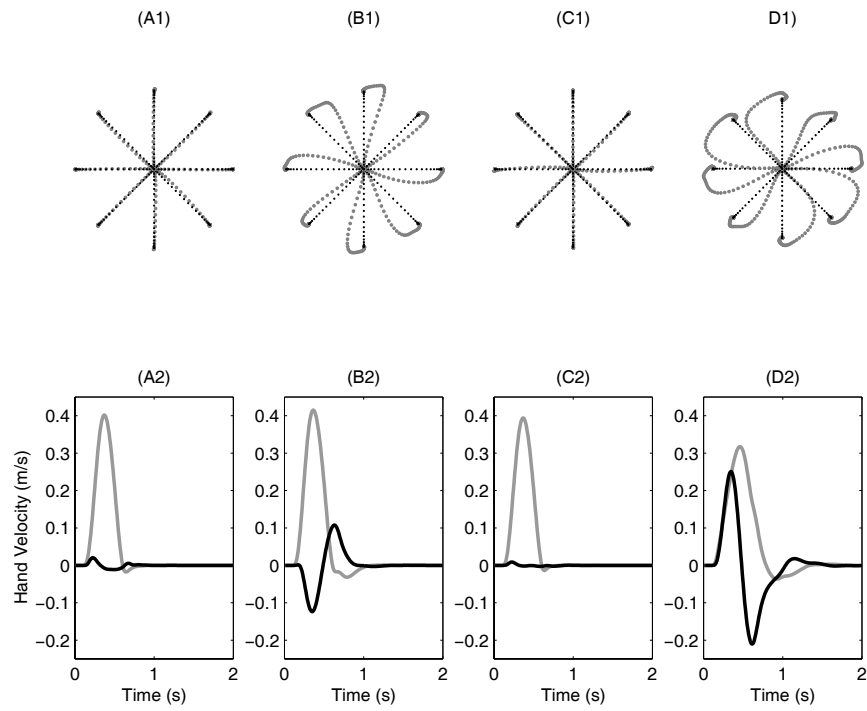
Figure 2.13: Simulated hand paths for feedback+feedforward torque controlshown in Fig. 2.8 with switch in position 1. (A) null field with IM=FM=0, (B) force field B_1 with IM=FM=0, (C) force field B_1 with IM=FM=B_1, (D) force field B_2 with IM=FM=B_1

Figure 2.14: Simulated hand paths for feedback+feedforward hand acceleration control shown in Fig. 2.10 with switch in position 1. (A) null field with IM=FM=0, (B) force field B_1 with IM=FM=0, (C) force field B_1 with IM=FM=B_1, (D) force field B_2 with IM=FM=B_1.

ries for the three controllers in unmodeled force field B_1. Figs. 2.12-14(C) show the change in behavior once both the inverse and forward models adapt to field B_1. All three controllers are capable of adapting fully to altered dynamics. A fourth simulation in Figs. 2.12-14(D) where both the forward and inverse models have changed to adapt to force field B_1 but are made to perform in the opposite field B_2, is done to test the stability and robustness of the three methods to a larger error in modeled dynamics. Comparison of the simulations for the three cases where both feedforward and feedback control is used, with each other, reveals that they are almost identical in behavior and stability properties. This suggests that all three methods of control are almost equivalent although their feedback structure is in different coordinates.

The common properties of these three methods are:

1. Use of an inverse model to generate the feedforward signals, and a forward model to generate the estimates for feedback control. Hence the control relies on both the forward and inverse plant models.

2. Exact tracking of the desired trajectory can be achieved.

3. Stable control of the arm in the presence of external force fields

4. Adaptation to the altered dynamic environments through changes in the forward and inverse models.

5. Greater sensitivity of performance of the system to changes or errors in the forward model than to the inverse model

Chapter 3

Experimental Results for Reaching Movements of the Arm

This chapter examines experimental data collected from human subjects for point-to-point reaching movements in order to assess the properties of the controller used by the brain when novel external dynamic conditions are introduced. The task given to the subjects is to move a robotic manipulandum (see Fig 1.6) in a horizontal plane at the shoulder level from one point to another. The position of the hand and the target to move to, are presented on a vertical screen in front of the subjects. They are instructed to move their hand from its current position to a target (a 1 cm^2 box) placed 10 cms away in one of eight equally spaced directions. They have to get to the target within 0.5 ± 0.05 s to successfully complete the movement. The target explodes if the movement is performed succesfully, otherwise it provides a visual cue to the subject to move faster if the movement is slow, or move slower if the movement is too fast. The robot can be programmed to apply a force on the hand when the movement is being made.

3.1   Terms used to describe Hand path and Trajectory

- Parallel velocity - the component of hand velocity in the direction of the target

- Perpendicular velocity - the component of hand velocity perpendicular to direction of the target

- Jerk - the third order derivative of hand position or the rate at which acceleration changes

3.2   Key Parameters for Characterization of the Movement

In order to quantify and charaterize the movement the following general parameters are defined:

70

1. Movement time (t_m) - the time required to complete the movement, defined as the time from when the speed increases beyond 10% of its maximum value to the time when it drops below 5% of its maximum value and then stays below it.

2. Movement distance (d_m) - the path length for the movement

3. Peak speed - a measure of how fast the movement is, defined as the first peak in the speed profile after the speed crosses 10

4. Jerk ratio - the ratio of the cumulative squared jerk for the movement and the cumulative squared jerk for a minimum jerk movement of the same peak speed. It measures the smoothness of the acceleration profile for a movement with respect to that of a minimum jerk movement.

5. Movement Area - the area between the hand path and the straight line connecting the starting point to the target. It is a measure of the deviation from the straight line path.

6. Movement Correlation - the correlation coefficient of hand velocity of a movement with that of a minimum jerk movement. The method for computation of the correlation coefficient is provided in (Shadmehr and Mussa-Ivaldi, 1994)

7. Perpendicular displacement - the perpendicular displacement of the hand path from the straight line path, 150 or 250 ms into the movement. It measures deviation from the desired trajectory

8. Perpendicular power - the power in the frequency spectrum of perpendicular velocity.

9. Mean Error Energy - the mean of a Lyapunov like energy function for the movement defined as $E = (\dot{\mathbf{\Theta}}_\mathbf{d} - \dot{\mathbf{\Theta}})^T D (\dot{\mathbf{\Theta}}_\mathbf{d} - \dot{\mathbf{\Theta}}) + (\mathbf{\Theta}_\mathbf{d} - \mathbf{\Theta})^T K (\mathbf{\Theta}_\mathbf{d} - \mathbf{\Theta})$, where D is the inertia matrix and K is the stiffness matrix associated with the plant dynamics.

As will be shown later, the movements to the target in the presence of force fields exhibit *near-discontinuous* behavior in the hand path during the corrective phase of the movement. These near-discontinuities cause the hand path to look segmented. Hence the near-discontinuities are termed as *segmentation points*. The near-discontinuities occurs where there is a sharp change in the direction of movement and in the derivative of speed of the movement. Hence a segmentation point is defined as a point in the movement that exhibits a sharp change in movement direction and speed derivative. The segments also exhibit curious kinematic patterns. In order to quantify this kinematic pattern, the following segmentation parameters are defined:

1. t_1 - the time required to move from the start point to the first segmentation point

2. d_1 - the distance covered in the first segment

3. λ_1 - the angle between the line joining start point to the target and the first segment

4. t_2 - the time required to move from the first segmentation point to the second segmentation point

5. d_2 - the distance covered from the first segmentation point to the second segmentation point

6. λ_2 - the angle between the line joining first segmentation point to the target and the second segment

7. t_3 - the time required to move from second segmentation point to the third segmentation point

8. d_3 - the distance covered during the third segment

9. λ_3 - the angle between the second segment and the third segment

10. N_S - the number of segmentation points in a movement

11. $|v|_{SP1}$ - the hand speed at the first segmentation point

The significance of these segmentation parameters will be established in the next chapter. Fig. 4.1 in the next chapter shows the segmentation process and the segmentation parameters.

3.3 Movements in the Null Field

The subjects are initially trained to make reaching movements with the robotic manipulandum for four sets of 192 movements each. The robot does not produce any active force on the hand. This is called the Null field. This is to train the subjects thoroughly with the experimental paradigm, the visuomotor transformation from the horizontal plane hand coordinates to the vertical plane visual coordinates, and the passive dynamics of the robotic manipulandum. The averaged movement and the maximum correlated movement for eight movement directions at the end of training for a group of 16 subjects is shown in Fig. 3.1-3.2. The last three movements in each direction for the last set of 192 movements is taken for each subject (and hence a total of 48 movements for each direction). The movements are normalized to a peak velocity of 0.4 m/s by scaling the time axis and the hand velocity by the ratio of peak velocity for the movement and the normalization velocity of 0.4 m/s. The normalized trajectories are subsequently averaged to obtain the mean trajectory. For each movement direction, the correlation between velocity profiles of the 48 movements is computed, and the movement with the maximum correlation
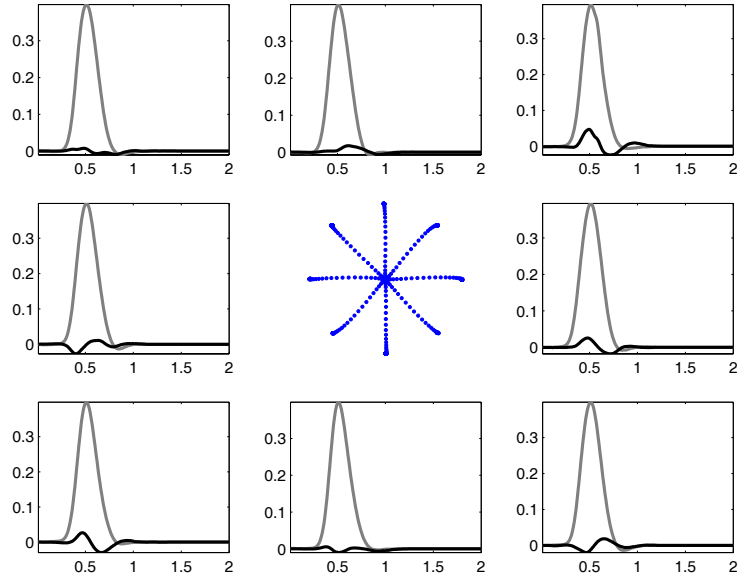
Figure 3.1: Average Trajectories of final three movements in Null Field. Center subplot- average hand paths for 8 movement directions. Dots represents hand position at 20 ms interval. Surrounding subplots - parallel (gray line) and perpendicular (black line) velocities for corresponding movement directions (units for y-axis are in m/sec and x-axis in sec).
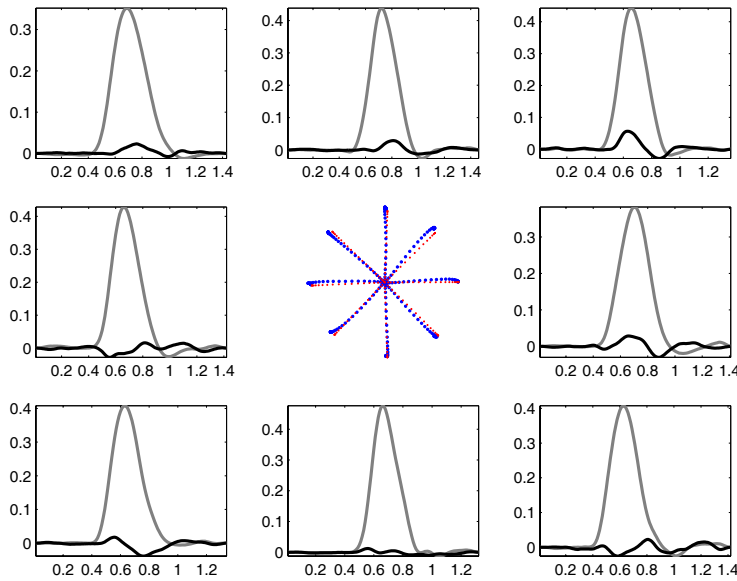
Figure 3.2: Maximum correlated typical trajectories for late null field training. Center subplot- typical hand paths (big dots) minimum jerk hand path (small dots). Surrounding subplots- parallel (gray line) and perpendicular (black line) velocities (units for y-axis are in m/sec and x-axis in sec).
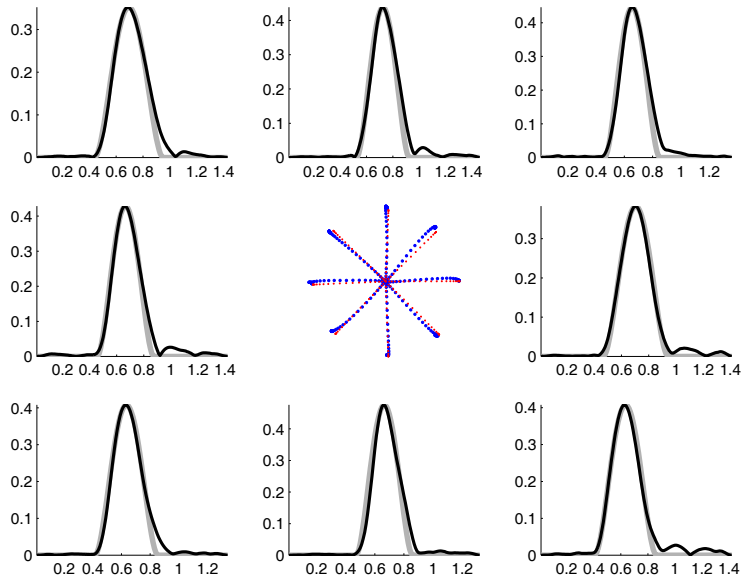
Figure 3.3: Typical and desired speed profile for late training in null field. Center subplot- hand paths. Surrounding subplots- minimum jerk desired speed (gray line) and typical movement speed (black line). Units for y-axis are in m/sec and x-axis in sec.

to all other movements found. This is defined as the typical movement for all the subjects. In Fig. 3.3 the speed profile for the typical movements is compared to the minimum jerk speed profile. From these figures, the following can be concluded about hand trajectory formation at the end of training:

1. The subjects are able to complete the movement successfully in 0.5 s

2. The hand paths are straight line movements to the target

3. The speed profiles are bell-shaped and symmetric about the center of movement where peak in speed also occurs and correspond very closely to the minimum jerk speed profile

4. The subjects are able to adapt completely to the visuomotor transform and the dynamics of the robot

It has been shown previously by (Flash and Hogan, 1985) that humans plan reaching movements in order to follow a minimum jerk trajectory. The results here are consistent with the previous findings. The minimum jerk trajectory seems to represent the desired behavior for subjects when making reaching movements. In other words, it is their kinematic plan for moving from one point to another.
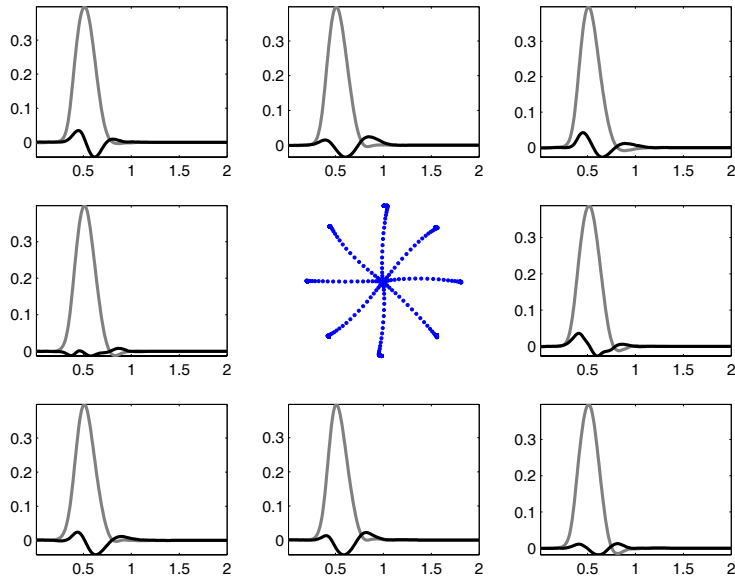
74
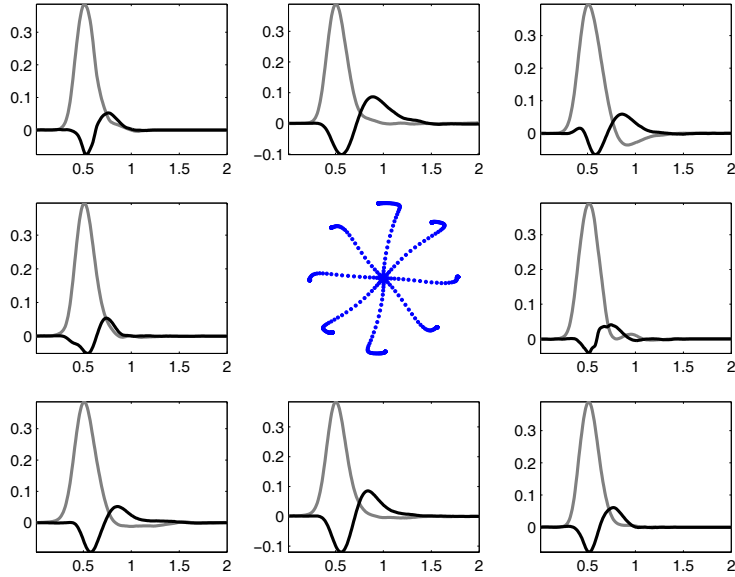
Figure 3.4: Average Trajectories in Early Training of Force Field B_1. Center subplot- hand paths. Surrounding subplots- parallel (gray line) and perpendicular (black line) velocities (units for y-axis are in m/sec and x-axis in sec).

3.4 Movements in Force Field B_1

After the initial training in the null field, the robot is programmed to generate active forces on the hand while a movement is being made. The forces produced by the robot simulate the force field B_1 introduced in Sec. 2.1. This alters the dynamics of the system that the subjects are trying to control as presented previously. The subjects perform three sets of 192 movements in this force field. The behavior of 16 human subjects is summarized in Fig. 3.4-3.6. Figs. 3.4-3.5 shows the average and typical hand paths and velocity profiles when the subjects are initially exposed to field B_1. There is an initial deviation from the straight line desired path as the force field pushes the hand in a clockwise direction, followed by a quick corrective movement to the target. The typical trajectories show that there is some oscillatory and unstable behavior as the subject tries to correct for deviation due to the force field.

As the subject trains in the force field the performance shows a gradual improvement until it converges back to the desired minimum jerk trajectory. Figs. 3.7-3.8 show the average and maximally correlated movements late in the training of field B_1 and one can see that the hand paths are almost straight lines to the target with smooth bell shaped speed profiles. This shows that some change has taken place in the controller used by the brain, that allows one to counteract the forces due to the force field and adapt to the altered arm dynamics. To understand how the behavior of the controller progresses over time, certain key movement parameters are studied over the duration of the three sets of training. Fig. 3.10 shows how the
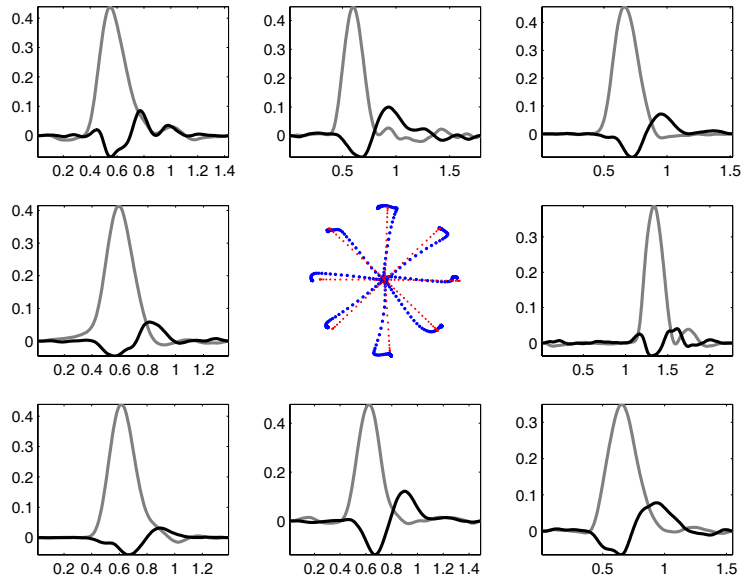
Figure 3.5: Typical Trajectories in Early Training of Force Field B_1. Center subplot- typical hand paths (big dots) minimum jerk hand path (small dots). Surrounding subplots- parallel (gray line) and perpendicular (black line) velocities (units for y-axis are in m/sec and x-axis in sec).
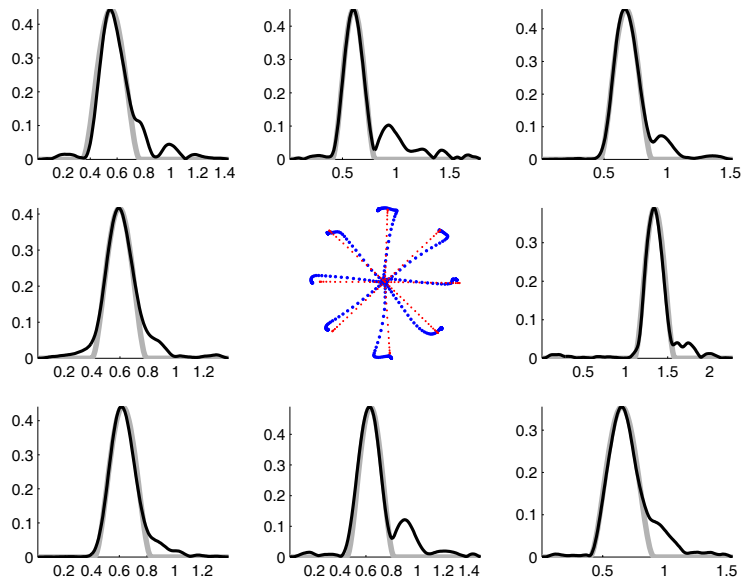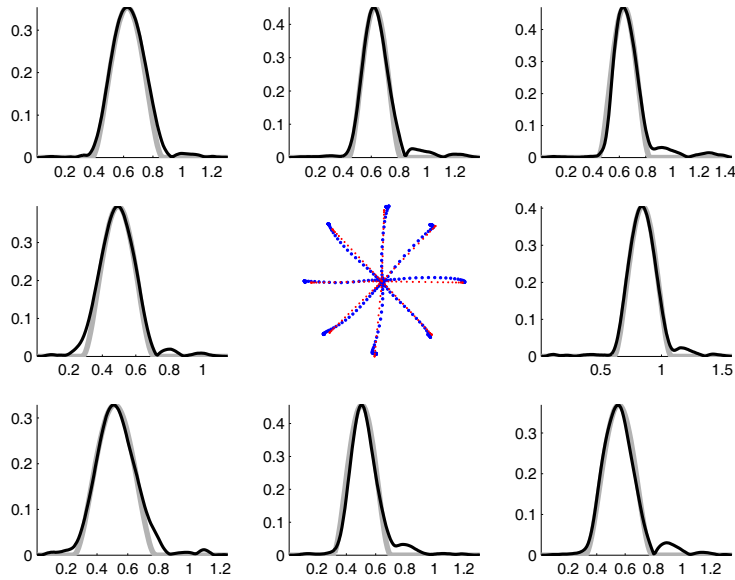

Figure 3.6: Typical Speed Profiles in Early Training of Force Field B_1. Center subplot- hand paths. Surrounding subplots- minimum jerk speed profile (gray line) and movement speed (black line). Units for y-axis are in m/sec and x-axis in sec.
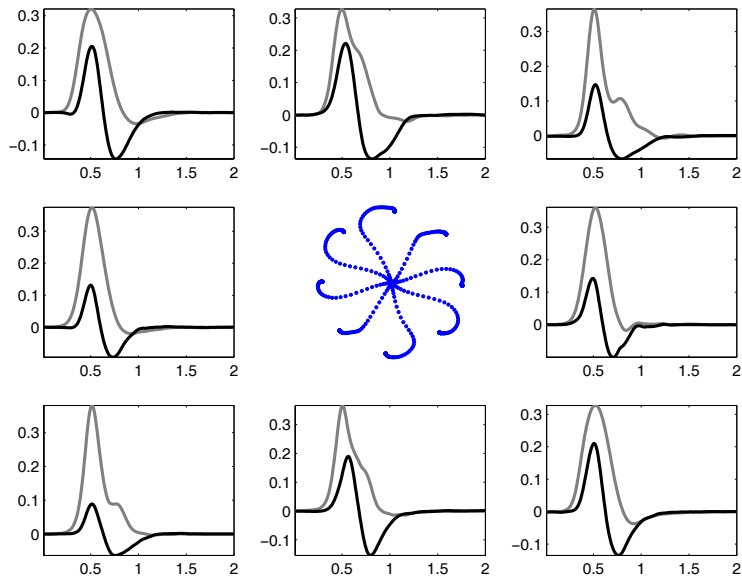
Figure 3.7: Average Trajectories in Late Training of Force Field B_1. Center subplot- hand paths. Surrounding subplots- parallel (gray line) and perpendicular (black line) velocities (units for y-axis are in m/sec and x-axis in sec).
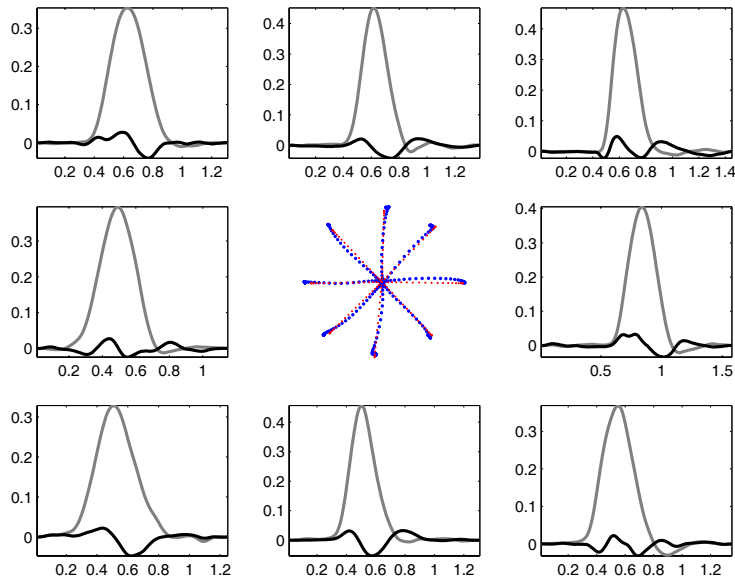
Figure 3.8: Typical Trajectories in Late Training of Force Field B_1. Center subplot- typical hand paths (big dots) minimum jerk hand path (small dots). Surrounding subplots- parallel (gray line) and perpendicular (black line) velocities (units for y-axis are in m/sec and x-axis in sec).
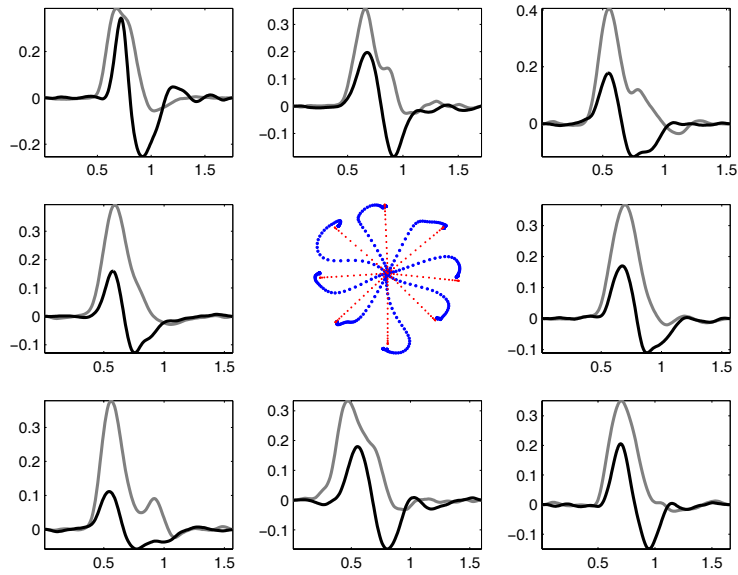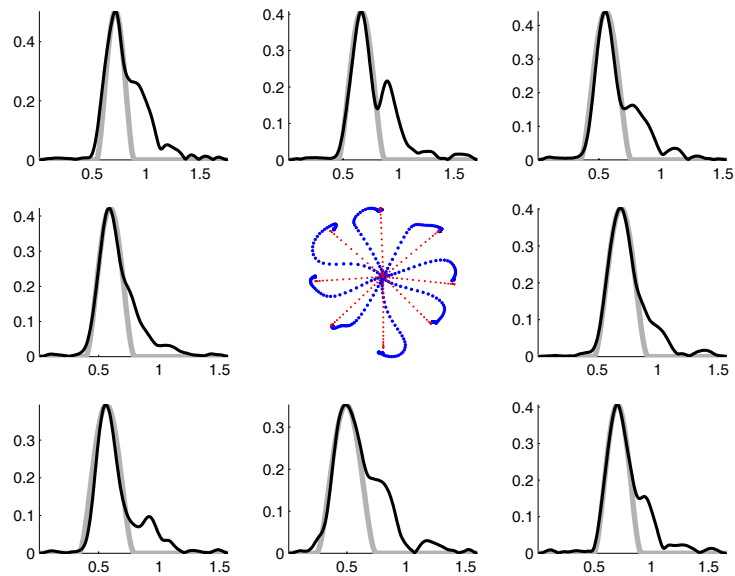
Figure 3.9: Typical Speed Profiles in Late Training of Force Field B_1. Center subplot- hand paths. Surrounding subplots- minimum jerk speed profile (gray line) and movement speed (black line). Units for y-axis are in m/sec and x-axis in sec.

key movement parameters, averaged for groups of 32 movements and for all 16 subjects, progress with training in the field. The exponential change in the parameters supports the hypothesis that there is a gradual transition in the controller that causes improvement in performance with training.

In another set of experiments, 16 other subjects are trained in the null field and then in the force field. However, for 32 movements in each set of 192 movements in the force field, the force field is turned off so that the movement is made in the null field. The subject is not told of this sudden change. The behavior of the subject in the null field is termed an after-effect as it reflects the effect of training in the force field. After-effect movements and late in training of the force field are compared with early fielded movements in Fig. 3.11. The after-effect movements appear to be a mirror image of the fielded movements. Previous results similar to this one, had prompted (Shadmehr and Mussa-Ivaldi, 1994) to suggest the gradual formation of an internal model in the controller that predicted the force field and produced signals to overcome the force field.

3.5 Movements in Force Field B_2

After training for three sets in force field B_1 a subset of the first group of 16 subjects was made to perform two sets of reaching movements in force field B_2. Figs. 3.12-3.17 show averaged and typical movements for early and late training periods in field B_2. B_2 being opposite in effect

78
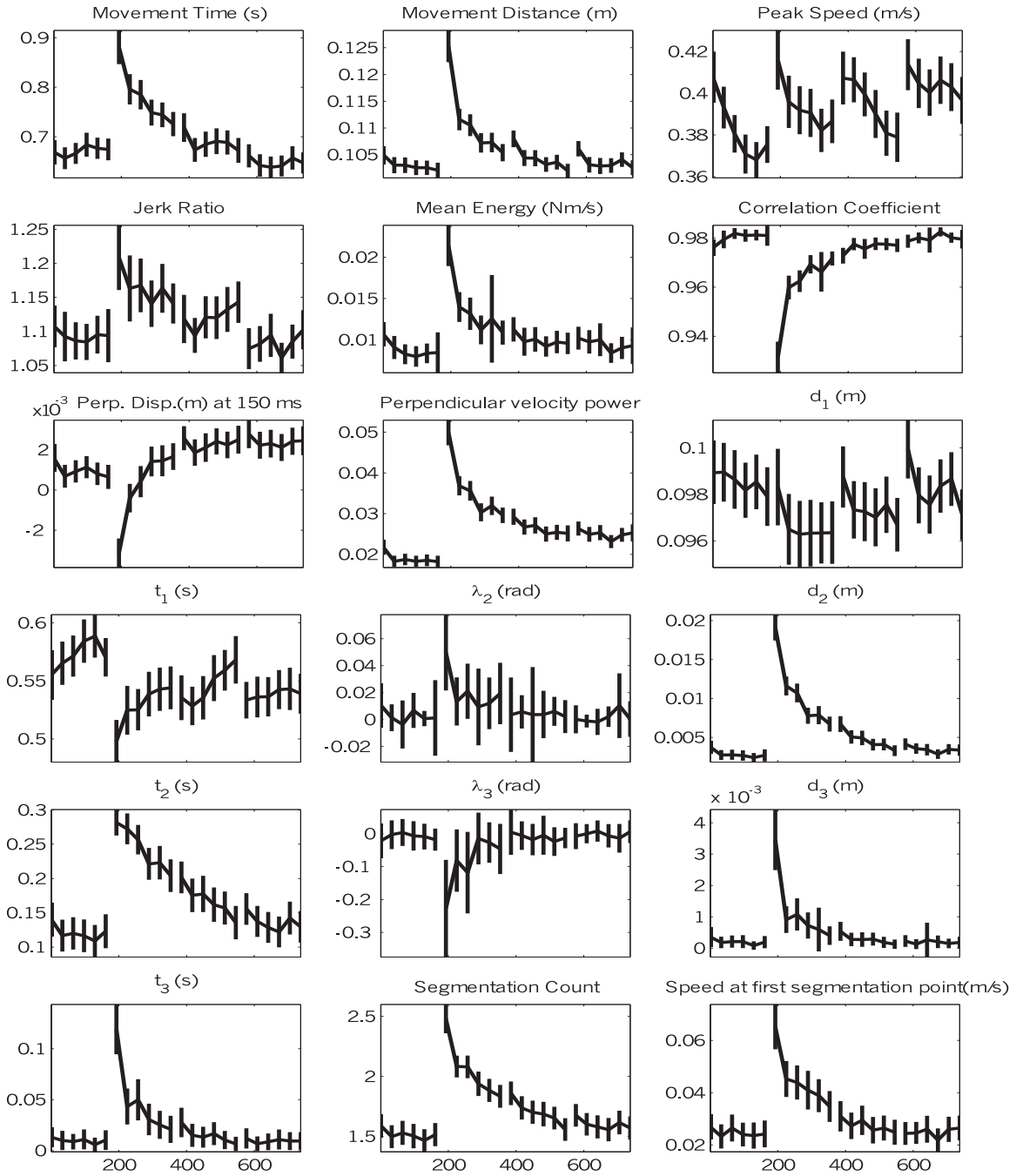
Figure 3.10: Changes in key movement parameters for the three sets of training in field B_1. Plot of average of 32 movement groups with standard deviation for 16 subjects.
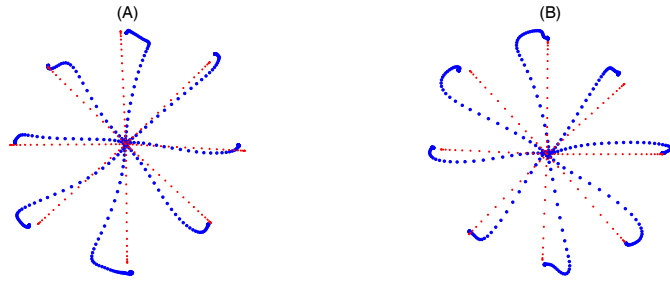
Figure 3.11: Comparison of hand paths for early fielded movements (A) with late after-effect trajectories (B) in force field B_1.

Figure 3.12: Average Trajectories in Early Training of Force Field B_2. Center subplot- hand paths. Surrounding subplots- parallel (gray line) and perpendicular (black line) velocities (units for y-axis are in m/sec and x-axis in sec).
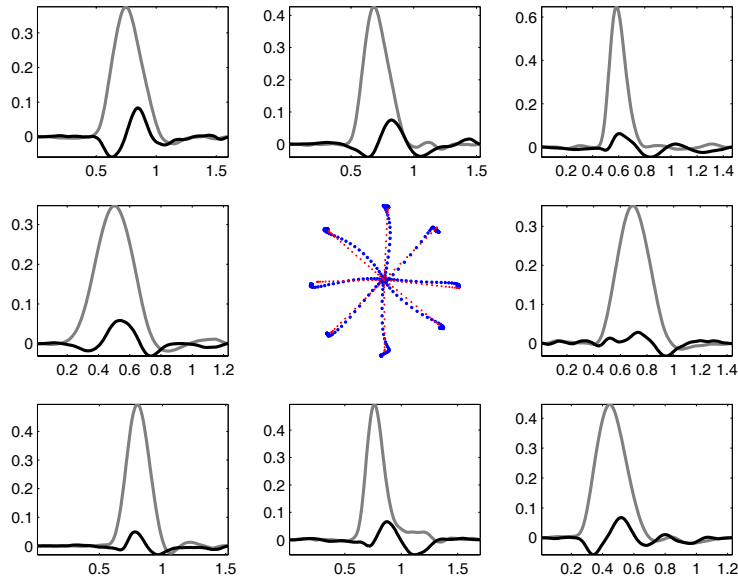
Figure 3.13: Typical Trajectories in Early Training of Force Field B_2. Center subplot- typical hand paths (big dots) minimum jerk hand path (small dots). Surrounding subplots- parallel (gray line) and perpendicular (black line) velocities (units for y-axis are in m/sec and x-axis in sec).

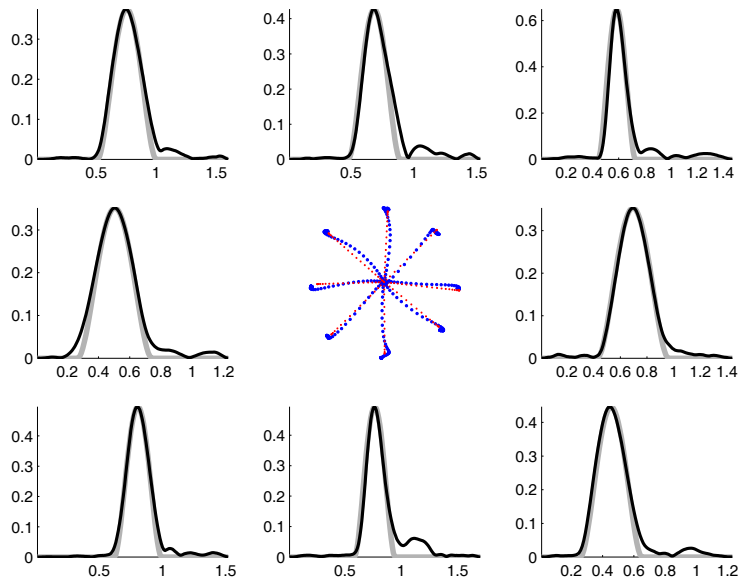
Figure 3.14: Typical Speed Profiles in Early Training of Force Field B_2. Center subplot- hand paths. Surrounding subplots- minimum jerk speed profile (gray line) and movement speed (black line). Units for y-axis are in m/sec and x-axis in sec.
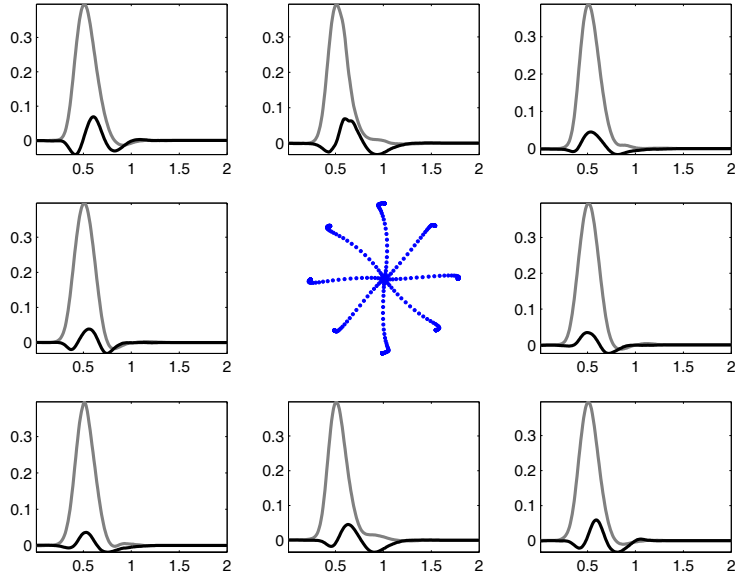
Figure 3.15: Average Trajectories in Late Training of Force Field B_2. Center subplot- hand paths. Surrounding subplots- parallel (gray line) and perpendicular (black line) velocities (units for y-axis are in m/sec and x-axis in sec).

to B_1, pushes the arm in an anticlockwise direction. The deviations are much greater early in B_2 than they are in B_1 because in addition to field B_2, the subjects expecting clockwise force field B_1 push in the anticlockwise direction. There is also a greater difference in the expected and actual dynamics of the arm, which leads to greater instability and increased oscillatory behaviour. Late in B_2, the performance improves greatly, showing convergence to the minimum jerk trajectory.

The remaining subjects from the group of 16 come back after 6 hours to perform in force field B_2. The idea is to determine the changes that take place in the controller during a period of rest. A comparison of the changes in key movement parameters during training in B_2 for the 0 and 6 hour groups is shown in Fig. 3.18. The performance for the 6 hour group is definitely better than the 0 hour group for most movement parameters. This represents a reduced interference from the previously learned field B_1. In a recent work by (Shadmehr and Holcomb, 1997), it was found that 6 hours seemed to be a critical period for memory consolidation for field B_1. Is it possible that the reduced interference from memory of field B_1 and the consolidation of B_1 are due to related changes in the controller occuring during the period of rest? This will be discussed in detail in a later section.

Figure 3.16: Typical Trajectories in Late Training of Force Field B_2. Center subplot- typical hand paths (big dots) minimum jerk hand path (small dots). Surrounding subplots- parallel (gray line) and perpendicular (black line) velocities (units for y-axis are in m/sec and x-axis in sec).

Figure 3.17: Typical Speed Profiles in Late Training of Force Field B_2. Center subplot- hand paths. Surrounding subplots- minimum jerk speed profile (gray line) and movement speed (black line). Units for y-axis are in m/sec and x-axis in sec.
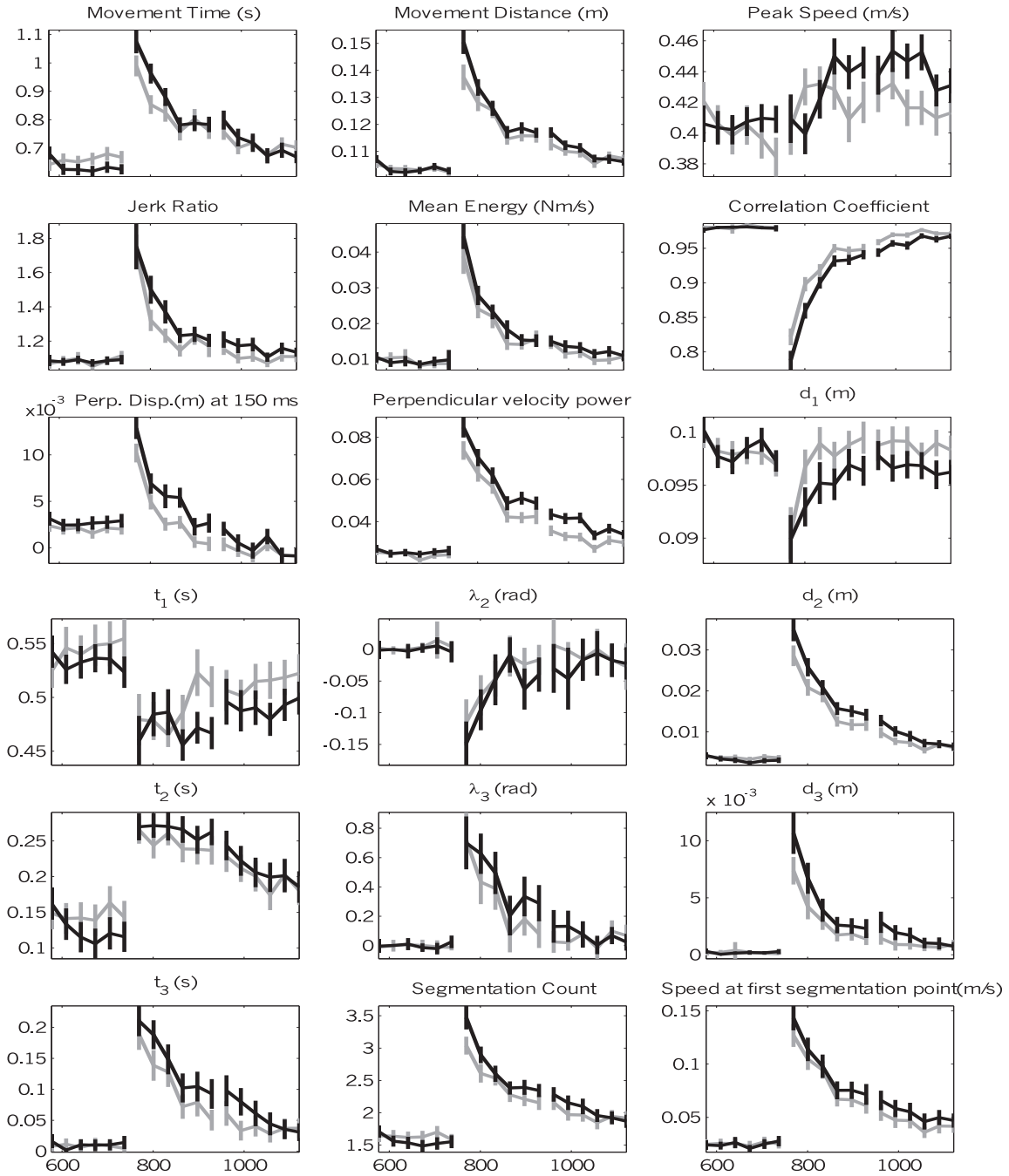
Figure 3.18: Changes in key movement parameters for the two sets of training in field B_2. Zero hour group (black line) Six hour group (gray line). Plot of average of 32 movement groups with standard deviation.

Chapter 4

Methods for Adaptive Motor Control using Internal Models

The experimental results from the last chapter establish that learning of the force field takes place gradually over time. It has been proposed by (Shadmehr and Mussa-Ivaldi, 1994) that this process of learning occurs by adaptation of Internal Models that predict the dynamics of the force field. After-effect movements provide evidence in support of this theory. Of the various methods for human motor control described in Chapter 2, there are only two methods that support gradual and perfect adaptation to external dynamics. One is the inverse model feedforward control where the inverse model gradually adapts to the external dynamics. The other is the combination of forward model feedback and inverse model feedforward control, where both the inverse and forward model exist and gradually adapt to the altered dynamics. The behavior of the three different modalities for the feedforward + feedback control was nearly the same as shown in chapter 2. Hence we look at only one of them in greater detail here. This is the hand acceleration linear feedback method with both the forward and inverse models being a part of the feedback loop. It is intuitively the most appropriate form of control for a visually guided task that directly controls the acceleration of the hand. Therefore two types of control and adaptive models are examined in this chapter:

    1) Adaptive Inverse Model based Feedforward Control

    2) Adaptive Forward-Inverse Model based Cartesian Feedback Control

4.1   Near-discontinuities and segmentation patterns in hand paths

An attempt is made to distinguish between the two cases based on their stability properties. Then the two cases are compared to experimental results to determine if any of them can reasonably explain the adaptation data collected from human experiments. For the purpose of
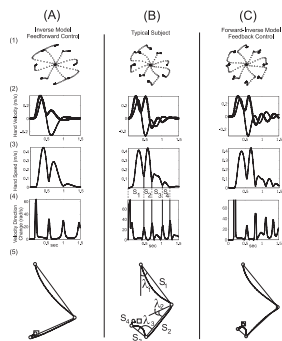
Figure 4.1: Hand trajectories for two simulations using inverse model feedforward control (A, left column) and forward-inverse model feedback control (C, right column), and for a typical subject (B, middle column). (1) hand paths for 8 movement directions, (2) parallel (gray line) and perpendicular (black line) hand velocity, (3) hand speed, (4) derivative of velocity direction, (5) segmented hand path, for the downward movement direction. $S_1 - S_4$ represent the movement segments
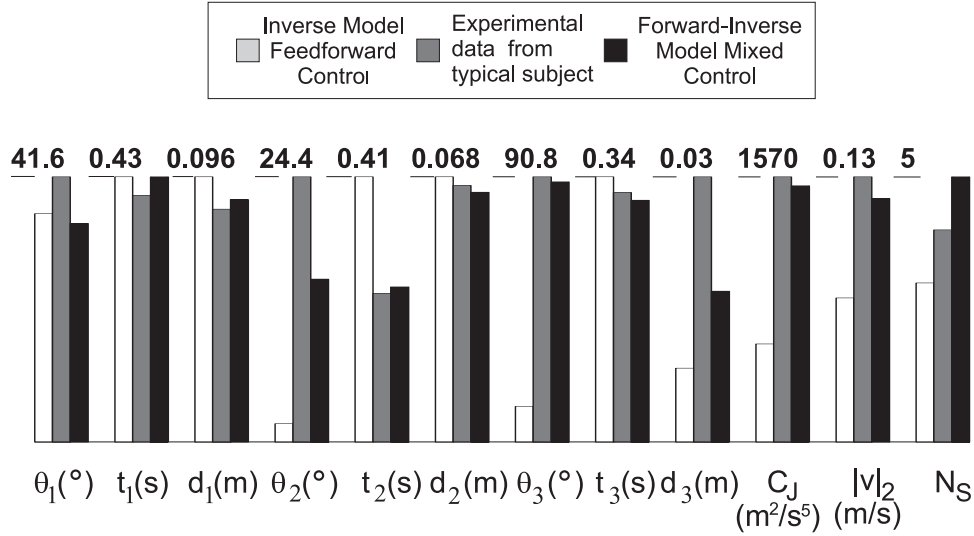
Figure 4.2: Segmentation parameters for the two simulation methods and the typical subject. The values are represented by three bars- inverse model feedforward control (white, left side), forward-inverse feedback control model (black, right side), typical subject (dark gray, middle). The value of the highest bar is given at the top and the others are scaled proportionately

distinguishing between the two, the movement in force field B_2 when the forward and inverse model are expecting field B_1 is examined. Since the two force fields are anti-correlated, the greatest error between the plant and the dynamics model occurs in this situation, and causes the system to be maximally unstable. The simulations for 8 directions of movement are shown for the inverse model feedforward control in Fig 4.1(A) and for the forward-inverse mixed control in Fig 4.1(C). There are clear differences in the stability and corrective behavior of the system. The first method using only feedforward control is more stable and converges to the target along a straight line after the initial deviation for directions 3,4,7,8. The feedback method on the other hand is more unstable and shows oscillatory behavior around the end-point. It also produces curious kinematic patterns marked by near-discontinuities in the hand path during the corrective phase of the movement. The first corrective movement does not point in the direction of movement which constitutes a clear difference from the feedforward only case. This is especially marked for the downward movement direction.

To compare the simulations with actual human behavior, arm trajectories generated by the group of 16 normal subjects are studied, when they make reaching movements under the same force field condition. This is achieved by training the subjects in field B_1 until they have converged to the desired behavior and have, presumably, perfectly adapted their internal model to this field (including both inverse and forward model if it exist). This is because atleast within the framework of the two methods discussed here, desired behavior can be achieved only when both the inverse and forward models have adapted to the dynamics of the plant. The
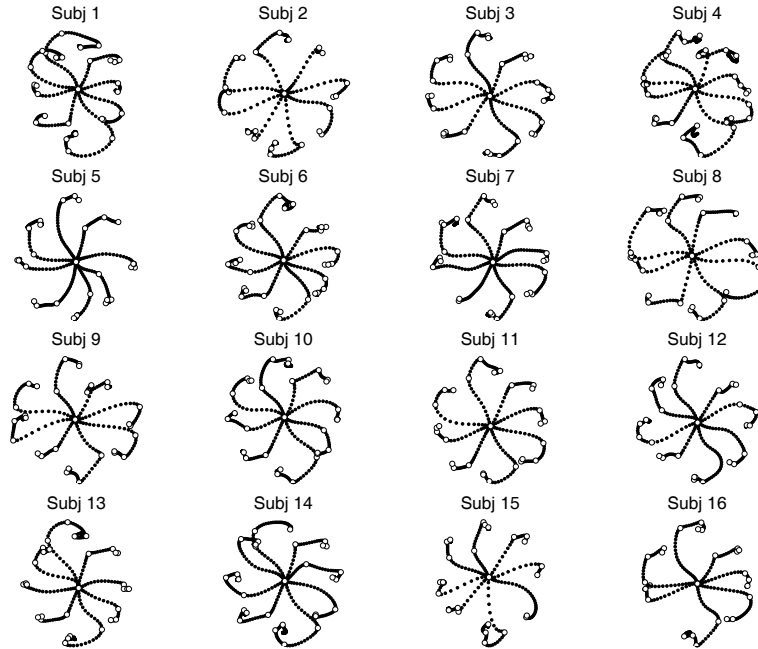
Figure 4.3: Hand paths for 16 subjects for first movement in each direction in the force field B_2. Circular dots represent segmentation points
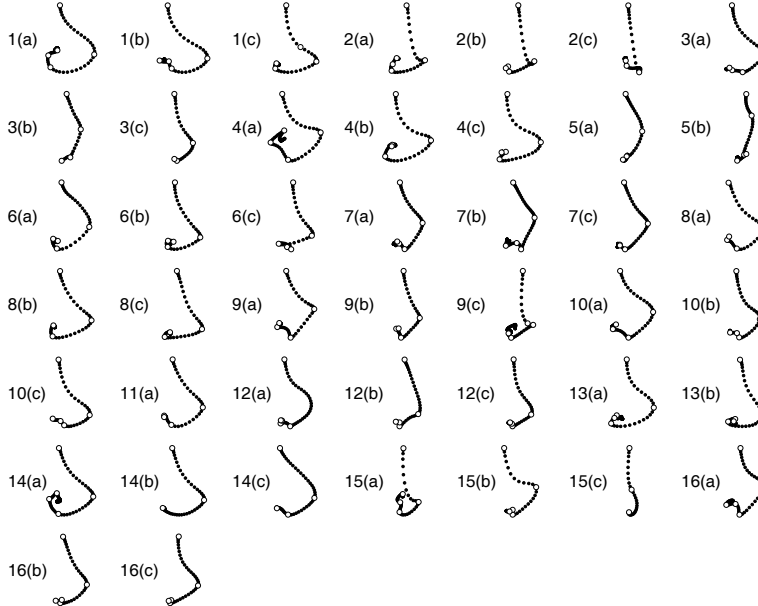

Figure 4.4: Hand paths for 16 subjects for first three movements in -90° downward direction in field B_2. Circular dots represent segmentation points. The number on the side of the movement represents subject number and the alphabet the movement number, eg. 5(b) is the second movement in the field for subject 5

subjects are subsequently tested in field B_2, and their first three movements in each direction compared to the simulations. The trajectories for a typical subject are shown in Fig. 4.1(B). The subject has great difficulty in stabilizing the arm and stopping the hand at the target. The subject's trajectory shows qualitatively the same kinematic pattern of near discontinuities and segmentation of movement as the forward-inverse mixed control.

Note: The experimental data presented in this chapter is from a group of 16 subjects composed of two subgroups - 8 subjects that performed in field B_2 immediately after training in field B_1 and 8 other subjects that performed in field B_2 six hours after B_1 training. The segmentation behavior of the two groups did not show a significant difference in kinematic pattern of discontinuities and hence are treated together as one group in this chapter.

The "near path-discontinuities or segmentation points" were defined in the previous chapter as points on the trajectory where there is a sudden change in both the derivative of hand speed and the direction of hand velocity, are used to quantify this kinematic pattern. The segmentation points represent the start of corrections to the ongoing movement and relate directly to feedback and equilibrium properties of the control model that cause corrections to external perturbations. The two different control methods differ in their feedback and equilibrium properties and hence these points are very appropriate to describe the trajectory and segment the movement to define its kinematic behavior. Most of the movements studied have atleast three segments. The first segment is a result of feedforward neural signal and external force field, while the second and third segments are mainly due to feedback correction to the deviation. Based on these three segments the following parameters were defined in the previous chapter: θ_1, angle between the first segment and the straight path to the target; d_1, the distance covered during the first segment; θ_2, angle between the second segment and straight path to the target from the first segmentation point; t_2, time duration of the second segment; θ_3, angle between the second and third segments; N_S, the number of segmentation points in the movement. We also calculate the cumulative jerk C_J in the movements to get a measure of the instability in the system. Fig. 4.1(B(2-4)) shows how the segmentation points are defined based on speed profile and direction of hand velocity profile, and characterize the kinematic pattern in the hand path for the downward direction movement for the typical subject.

Fig. 4.2 plots the values of various segmentation parameters obtained for the three downward direction movements in Fig. 4.1. They are represented as bars whose height is a factorized value for the parameter. The inverse model feedforward control (light gray, left side) and the forward-inverse feedback control model (black, right side) when compared to the typical subject (dark gray, middle), clearly establish that only the feedback control method can explain the experimental data.

To show that this kinematic pattern of segmentation is present across most of the subjects, the first movement in each direction in force field B_2 is presented in Fig. 4.3 for the 16 subjects.
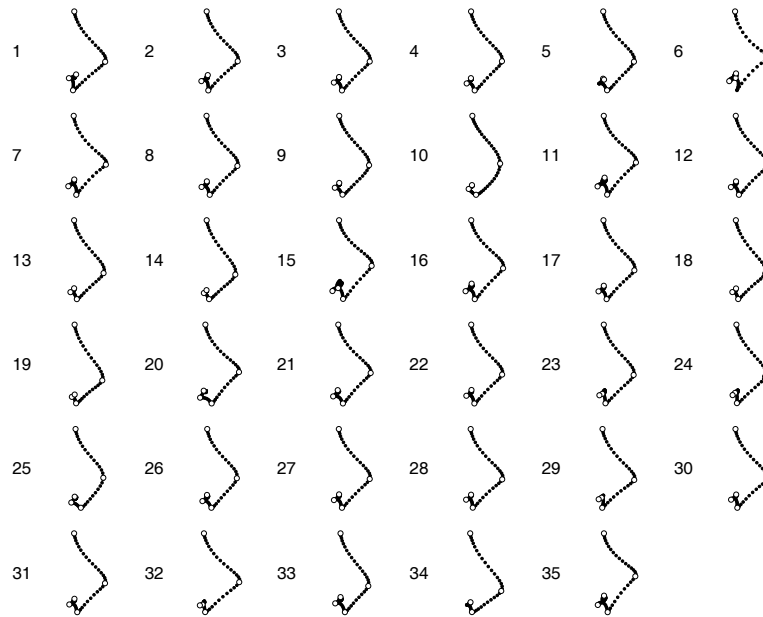
Figure 4.5: Segmented hand paths for 35 simulations of the forward-inverse model feedback control in -90° downward direction in field B_2. Inverse and Forward model expect field B_1. Movement control parameters varied for the 35 simulations
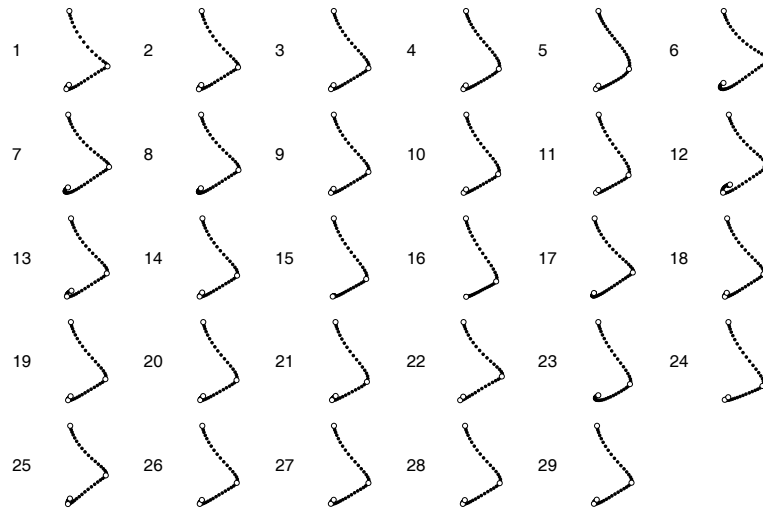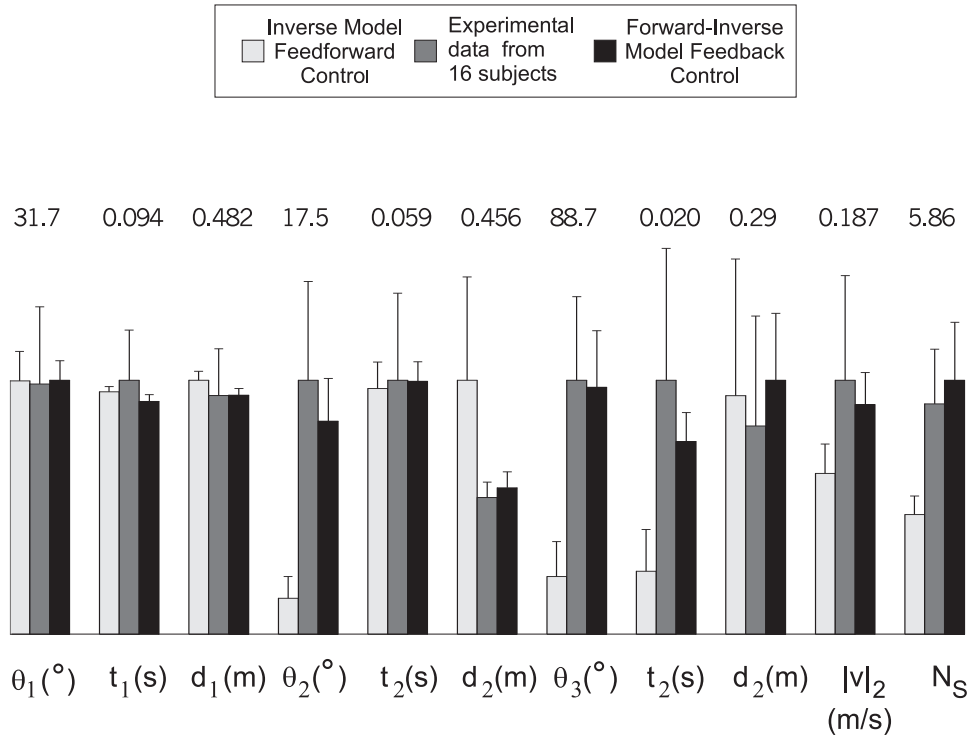

Figure 4.6: Segmented hand paths for 29 simulations of the inverse model feedforward control in -90° downward direction in field B_2. Inverse model expects field B_1. Movement control parameters varied for the 29 simulations

Figure 4.7: Bar plot of average segmentation parameters with standard deviation for the first fielded movement for 16 subjects (dark gray, middle), 29 simulations of inverse model feedforward control (light gray, left side) and 35 simulations of forward-inverse model feedback control (black, right side) for the -90° downward movement

Fig. 4.4 shows the subjects first three movements (a-c) in the downward direction and is the data used primarily for distinguishing between feedforward and feedback control. The hand paths show the segmentation points as circular dots and establish that the characterization of the discontinuities is achieved well by the segmentation points. One can clearly see from Figs. 4.3 and 4.4 that the kinematic pattern is present in the first movement of all subjects and to a lesser extent in their later movements. In order to have a substantial number of movements for quantitative analysis, the first three movements in each direction are considered, and it is assumed that no adaptation of internal models takes place during this time. This group of 48 (16 subjects x 3) movements is compared to 35 simulations of the forward-inverse model feedback control and 29 simulations of the inverse model feedforward control. The different simulations of the two control methods is obtained by varying the control parameters in the two methods- feedback gains, desired movement time or peak speed, stiffness or cocontraction level, muscle viscosity, inertia and link lengths of the arm. These parameters are expected to vary from one subject to another and also within a subject from one movement to another. A $\pm 15\%$ change is considered in muscle viscosity, inertia and link lengths - parameters that vary only across subjects. A $\pm 50\%$ change is considered in feedback gains and stiffness because exact knowledge of these parameters or how they can change across movements and subjects is not known. A $\pm 10\%$ is considered in the movement time based on peak speed measurements for subjects. The movement in downward direction for the 29 simulations of inverse model feedforward control is given in Fig. 4.5, and for the 35 simulations of forward-inverse feedback control in Fig. 4.6.

The average values with standard deviation of the segmentation parameters for the simulations and the experimental data are presented in Fig. 4.8. for three directions of movement that show greatest differences in the two methods of control: (a) -90° downward,(b) 90° upward and (c) 135° upward. It is interesting to observe that the performance of the three groups in the first segment, as represented by θ_1 and d_1, is nearly the same as expected. Only in the parameters of the second and third segment, as represented by θ_2, t_2, θ_3, and t_3 does feedback control perform very differently from feedforward control. The behavior of human subjects is very well predicted by the forward-inverse model feedback control.

4.2 Modified control method based on an Estimate Reliance Factor

There are some subjects (1,3,6,8,12,13,14,15,16) whose second (b) or third (c) movements in Fig. 4.4 do not show the kinematic pattern at all and cannot be explained by variation of control parameters for the feedback control method. These movements appear very similar to that predicted by the inverse model feedforward control and have similar stability properties.
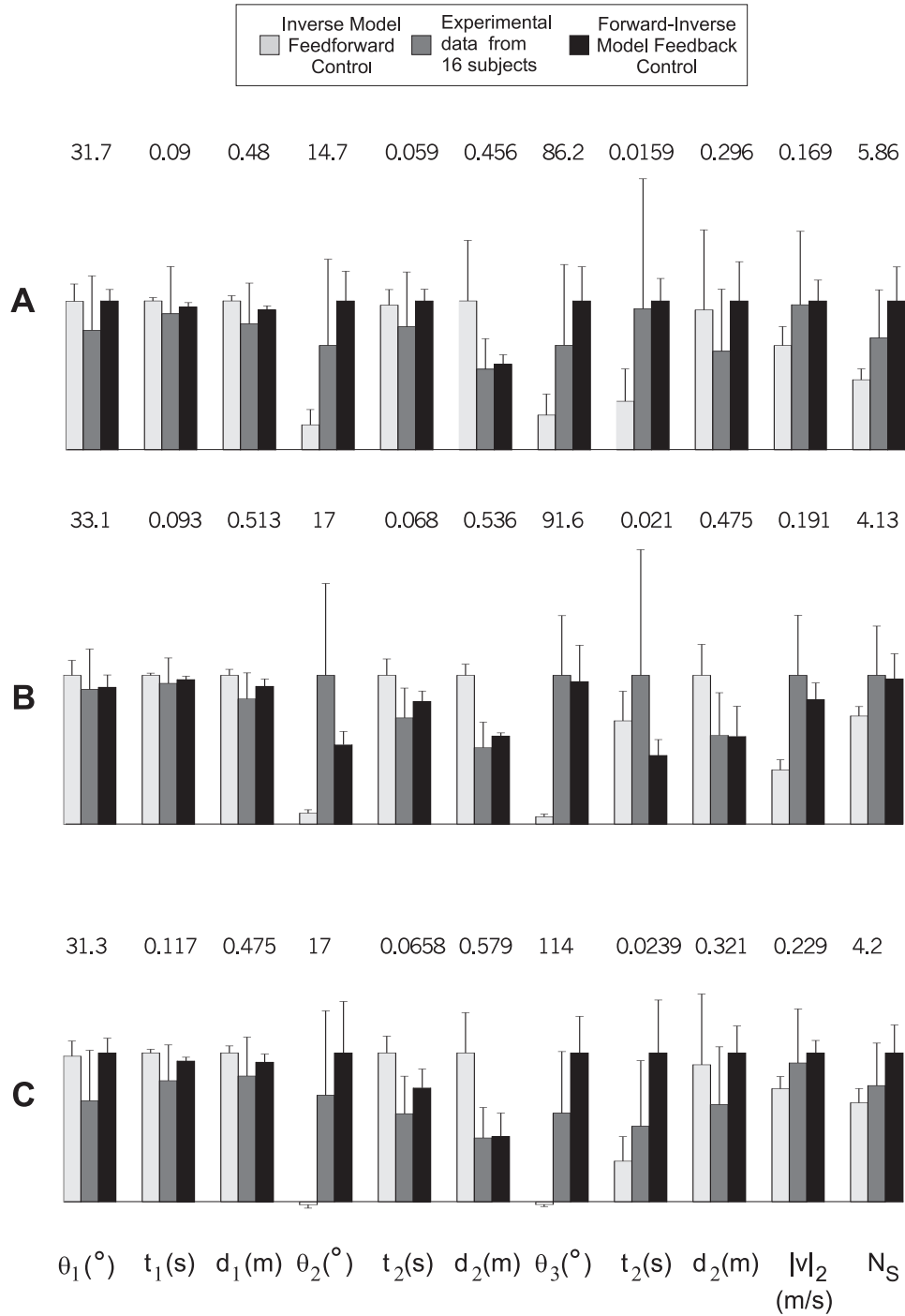
Figure 4.8: Bar plot of average segmentation parameters with standard deviation for first three field B_2 movements in each direction for 16 subjects (dark gray, middle), 29 simulations of inverse model feedforward control (light gray, left side) and 35 simulations of forward-inverse model feedback control (black, right side). Three movement directions are shown (a) -90° downward, (b) 90° upward and (c) 135° upward.
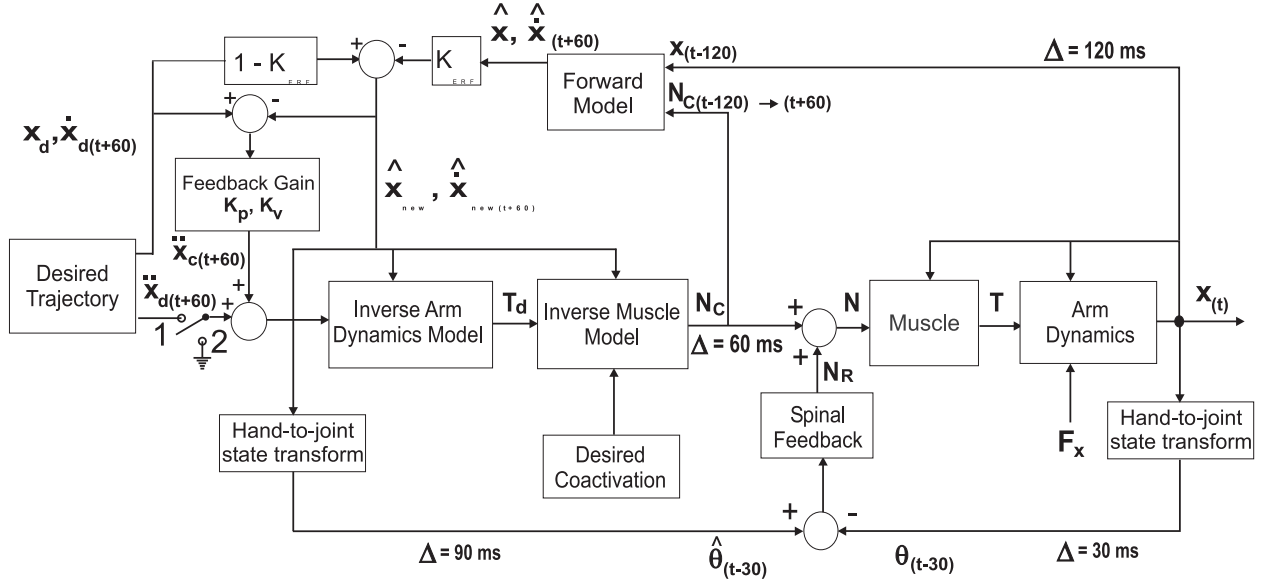
Figure 4.9: The new control configuration that includes a 'Estimate Reliance Factor' K_{ERF}. The value of K_{ERF} can vary between 0 and 1.

It is unlikely that the subject generates the first fielded movement with the forward-inverse feedback control and hence causes the segmentation pattern, and then switches to a different control method, the inverse feedforward control, for subsequent methods. There is a way, however, of explaining this behaviour within the framework of one control method, by making a smooth transition in an additional control variable. Consider a new control method outlined in Fig 4.9. The scheme is broadly the same as the forward-inverse feedback control. A new variable called the 'Estimate Reliance Factor' is introduced that determines the reliance on feedback information and the forward model. This reliance factor K_{ERF} determines a new estimated state of the arm $\hat{\mathbf{x}}_{\mathbf{new}}, \dot{\hat{\mathbf{x}}}_{\mathbf{new}}$ as a combination of the estimates from the forward model and the desired trajectory as follows:

$$\hat{\mathbf{x}}_{\mathbf{new}} = K_{ERF}\hat{\mathbf{x}} + (1 - K_{ERF})\mathbf{x_d} \tag{4.1}$$

$$\dot{\hat{\mathbf{x}}}_{\mathbf{new}} = K_{ERF}\dot{\hat{\mathbf{x}}} + (1 - K_{ERF})\dot{\mathbf{x}}_{\mathbf{d}} \tag{4.2}$$

The feedback gain is effectively K_{ERF} times the original gain:

$$\ddot{\mathbf{x}}_{\mathbf{d}} = K_p(\mathbf{x_d} - \hat{\mathbf{x}}_{\mathbf{new}}) + K_v(\dot{\mathbf{x}}_{\mathbf{d}} - \dot{\hat{\mathbf{x}}}_{\mathbf{new}}) \tag{4.3}$$

$$= K_p[\mathbf{x_d} - K_{ERF}\hat{\mathbf{x}} - (1 - K_{ERF})\mathbf{x_d}] + K_v[\dot{\mathbf{x}}_{\mathbf{d}} - K_{ERF}\dot{\hat{\mathbf{x}}} - (1 - K_{ERF})\dot{\mathbf{x}}_{\mathbf{d}}] \tag{4.4}$$

$$= K_{ERF}[K_p(\mathbf{x_d} - \hat{\mathbf{x}}) + K_v(\dot{\mathbf{x}}_{\mathbf{d}} - \dot{\hat{\mathbf{x}}})] \tag{4.5}$$

94

When $K_{ERF} = 1$, the new state estimates are equal to the forward model estimates and there is maximum reliance on the state estimates of the forward model. The control is exactly the same as forward-inverse feedback control. When $K_{ERF} = 0$, on the other hand, the new estimates are equal to the desired trajectory and there is no reliance on state feedback or the forward model. The feedback corrective acceleration is zero and the desired states govern the action of the inverse plant model, which is precisely the same as the inverse model feedforward control. The first reason behind it is that if the forward model is not updated by sensory feedback and integrates only the motor commands, then it generates estimates that are equal to the desired trajectory. This is a good method to overcome erraneous or noisy feedback, where you stop paying attention to the feedback and rely only on the desired trajectory. The second reason, and one that is more relevant in this case, is that if the forward model is erraneouss and is generating wrong estimates, then for stabilizing the arm, it is much better to stop listening to the forward model and rely only on the desired trajectory and the stable feedforward control.

4.3   Explanation for segmentation of movement based on forward-inverse model feedback control

The results in this chapter are based on the unique pattern of near-discontinuities observed in movements of subjects in field B_2 and the ability of only the forward-inverse model based feedback method to mimic that behavior. We are able to rule out the inverse model feedforward control due to lack of this kinematic pattern. It is important to discuss here how the segmentation pattern occurs in adaptive forward-inverse model based feedback control when a movement is made in field B_2 and the expected field is B_1, in order to establish that it is only the presence of feedback and state estimation through an adaptive forward model that causes this segmentation behavior. For the feedforward control method the explanation for lack of deviations during the corrective movements is that muscles are programmed with the desired trajectory. This sets the equilibrium position for the muscles at the end of first 0.5 sec as the target location and the straight corrective movement is a result of the equilibrium target position pulling the hand directly towards it.

In the case of forward-inverse model feedback control the muscles are programmed with the estimated trajectory instead of the desired trajectory and there is additional corrective feedback. In this situation, there are three main causes for the deviation of the hand path from the straight line to the target, during the corrective phase that could give rise to the segmentation pattern:

1. The external force field B_2 that pushes the hand in an anticlockwise direction

2. The wrong forward model that anticipates a clockwise field B_1 and generates estimates
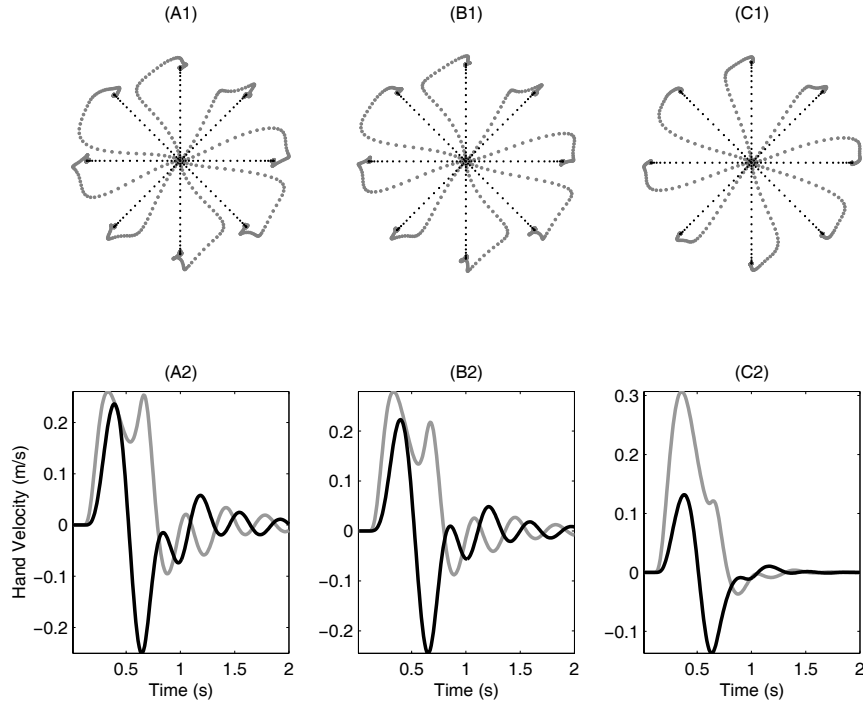
Figure 4.10: Simulated trajectories for forward-inverse model control for movements in field B_2 for three different states of adapatation of the inverse model (IM) and the forward model (FM). (A) IM=FM=B_1 (B) IM=0, FM=B_1, (C) IM=B_1, FM=0. (1), hand paths for eight movement directions represented as dots (big gray dots- actual; small black dots- desired) at 20 ms intervals. (2), parallel (gray line) and perpendicular (black line) hand velocities for downward movement direction

accordingly. The estimates might be shifted clockwise from the straight path to the target and generate corrections that will further push the arm in anticlockwise direction

3. The wrong inverse model that generates additional torques in the anti-clockwise direction to counteract the clockwise field B_1.

To assess the relative role of forward and inverse models, simulations in force field B_2 after training in field B_1 for two cases; one, where only the forward model has adapted to field B_1 (inverse model = null), and the other, where only the inverse model has adapated to field B_1 (forward model = null) are shown in Fig. 4.10. The movement in the first case with adaptation of only the forward model (Fig. 4.10-B) shows the segmentation pattern, whereas, the movement with adaptation of only the inverse model (Fig. 4.10-C) does not show a significant segmentation pattern. The pattern is observed only when the forward model is expecting field B_1 and producing incorrect estimates for the state of the hand. This establishes that the segmentation behavior is a result of adaptation of forward model to force field B_1 and is not significantly affected by the state of the inverse model.
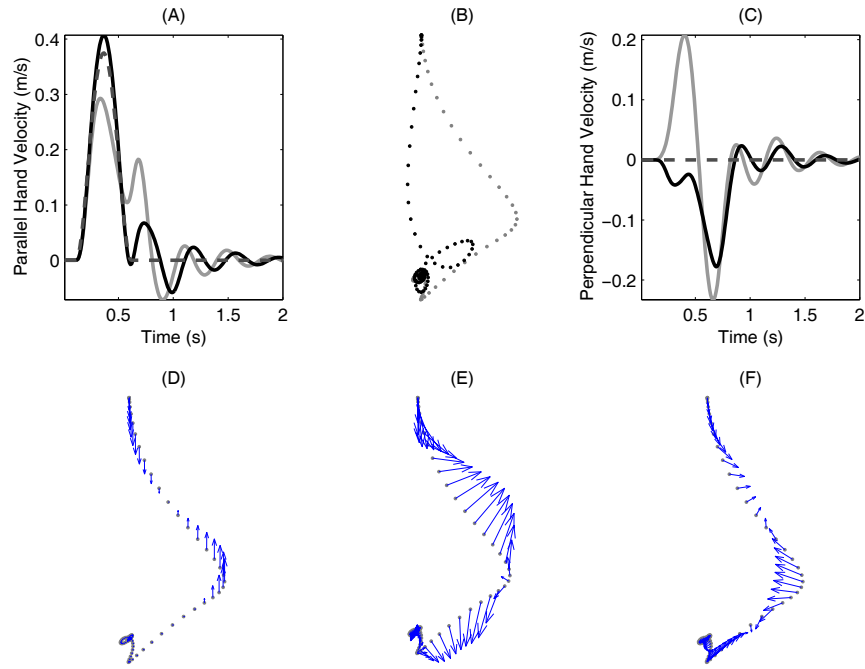
96

Figure 4.11: Simulation for forward-inverse model control for movements in field B_2 in downward direction. The inverse model correctly expects B_2 while the forward model expects B_1. (A),(C) parallel and perpendicular hand velocities for actual trajectory (gray line), estimated trajectory (black line), and desired trajectory (dotted line). (B) hand paths for actual trajectory (gray dots) and estimated trajectory (black dots). (D)-(F) desired, estimated and actual acceleration signals plotted as vectors at 20 ms time points on the actual hand trajectory. The largest acceleration vector in the three plots has a magnitude of 4.58 m/s^2 and all other vectors are scaled relative to that.

It is now a question of how the wrong state estimates are causing the segmentation pattern? The state estimates are used as input to (1) the feedback controller and (2) the inverse plant model. To test the influence of only the forward model and wrong estimates, we simulated the behavior of the system in field B_2 with the forward model expecting field B_1 and the inverse model correctly modeling field B_2. The results of the simulation are plotted in Fig. 4.11. The estimated trajectories are shown along with the desired and actual trajectories in figures (A)-(C). It is difficult to visualize the control process through only these estimates, therefore in plots (D)-(F), the desired, corrective and actual acceleration signals are plotted as vectors. It is immediately apparent from (E) that the cause of the kinematic pattern is incorrect feedback correction that tries to accelerate the hand in an anticlockwise direction away from the target direction. The feedback correction is a linear combination of difference in estimated and desired position and velocity, and depends on incorrect estimates. We also note that there is remarkable similarity in the acceleration vectors for the first and second segments of movement, and therefore the corrective phase of the movement i.e the second segment, is almost an independent submovement. This establishes that a wrong forward model that generates incorrect estimates causes the unique pattern of near-discontinuities through incorrect feedback action.

4.4 Conclusions

- The inverse model based feedforward control is found to be inadequte to explain the unique segmentation pattern observed during arm movements in field B_2.

- A forward-inverse model based feedback control is able to produce a kinematic pattern which is very similar to the one observed in movements of subjects.

- This constitutes evidence for feedback control through a forward model for rapid reaching movements.

- The adaptation of forward model to field B_1 and wrong state estimation is required to produce the segmentation pattern. This proves the existence and adaptation of a forward model based estimation process in learning control of arm movements.

Chapter 5

Forward-Inverse Model Hand Acceleration Feedback Controller

In the previous chapter it was shown how the inverse model feedforward control was unable to explain the segmentation data. On the other hand, the forward-inverse model feedback control was, on average, able to simulate the experimental segmentation results. This chapter looks at the forward-inverse model control in greater detail and tries to establish the important properties and characteristics of this control method. An attempt is also made to distinguish between the forward and inverse model used in the control.

5.1 Sensitivity Analysis and Robustness of the Control Method

The forward-inverse model hand acceleration feedback control provides stable feedback control of a time-delayed nonlinear system like the human arm and an adaptive control strategy that is capable of learning novel dynamic interactions. In this section we try to identify and characterize the control parameters in the model and test the behavior of the controller in the presence of feedback noise in sensory measurements.

5.1.1 Sensitivity Analysis of Control Parmeters

The controller is shown as a block diagram in Fig. 4.9. There are a number of control parameters that have to be specified in the controller in order for it to function. The values of some of these parameters are physiologically constant, while others can be modified by the brain during a movement or from one movement to another. It is useful to identify the parameters that the brain has direct control over and can vary over a reasonable range, and then test the sensitivity of movement behavior on these control parameters. This will give the extent to which the
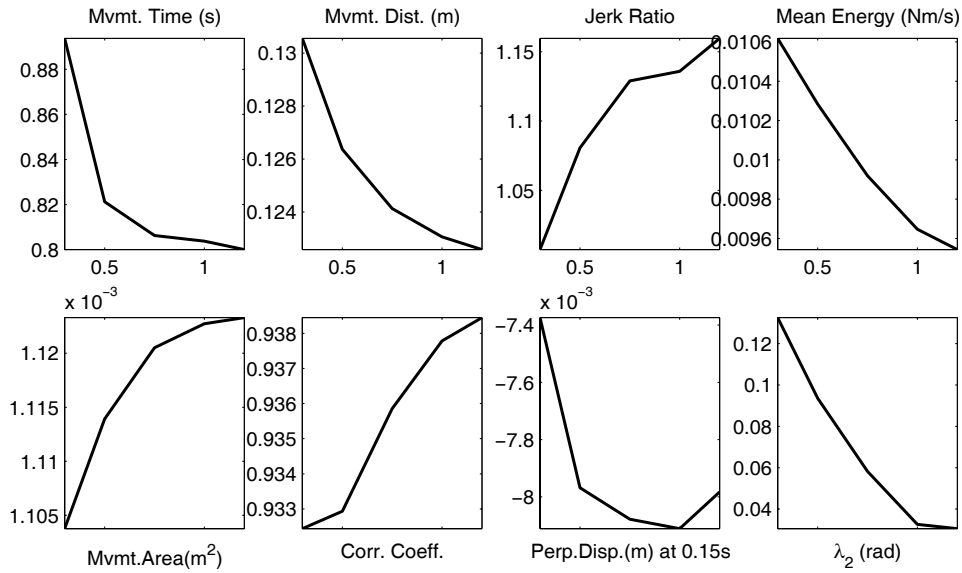
Figure 5.1: Change in key movement parameters for five different supraspinal feedback gains. Factor = [0.3, 0.5, 0.75, 1.0, 1.2]. Data averaged for the eight movement directions.
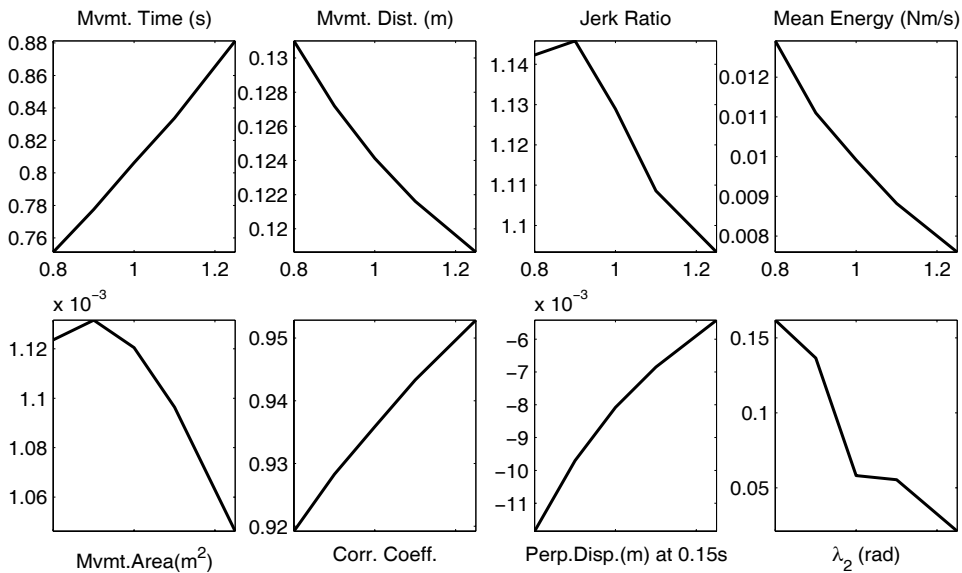

Figure 5.2: Change in key movement parameters for five different desired movement times. Factor = [0.8, 0.9, 1.0, 1.1, 1.25]. Data averaged for the eight movement directions.
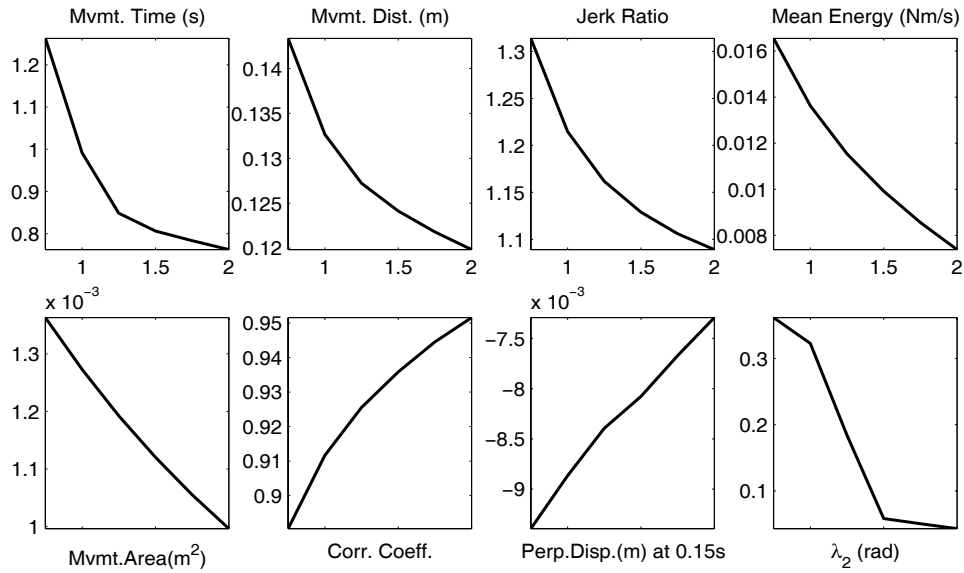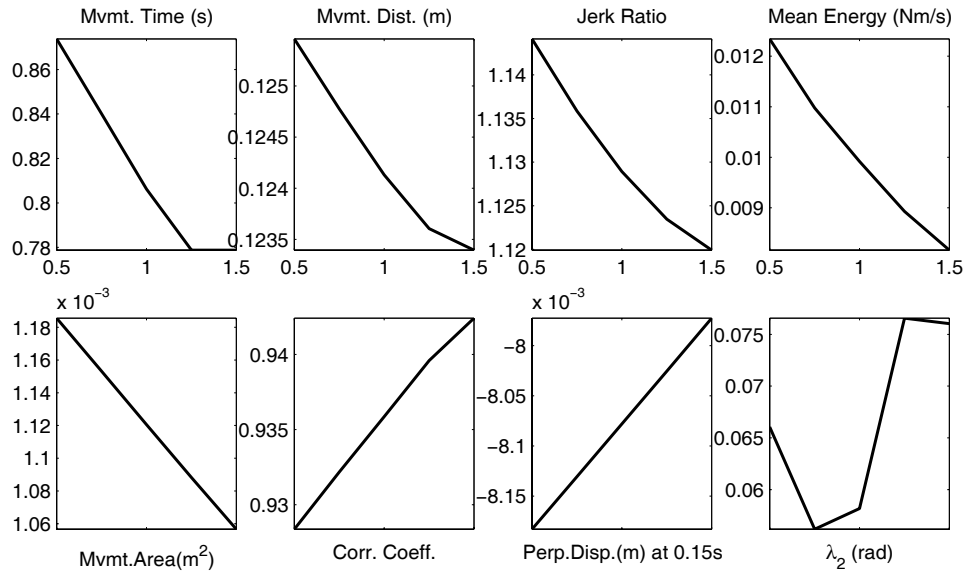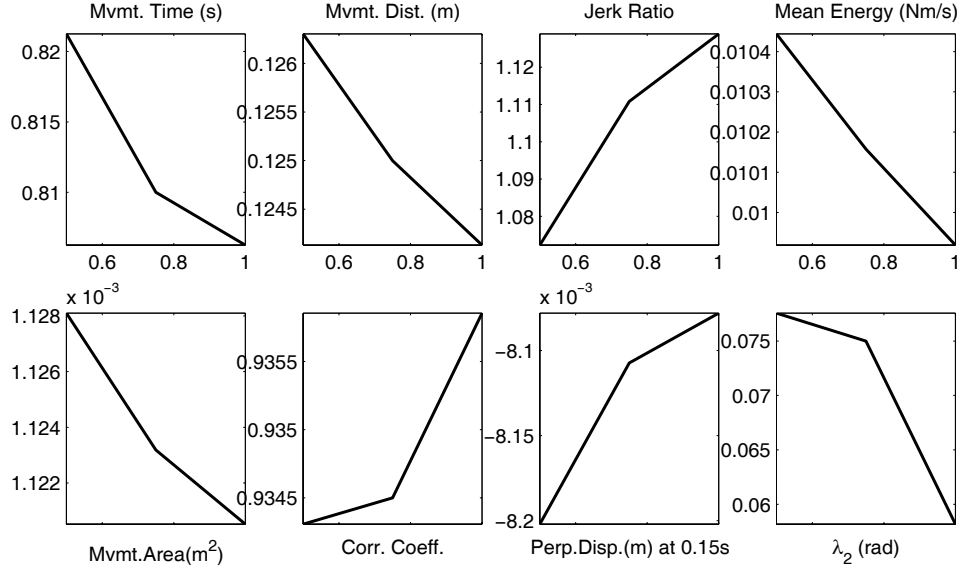
Figure 5.3: Change in key movement parameters for six different cocontraction levels. Factor = [0.75, 1.0, 1.25, 1.5, 1.75, 2.0]. Data averaged for the eight movement directions.

Figure 5.4: Change in key movement parameters for five spinal feedback gains. Factor = [0.5, 0.75, 1.0, 1.25, 1.5]. Data averaged for the eight movement directions.

Figure 5.5: Change in key movement parameters for three different estimate reliance factors. Factor = [0.5, 0.75, 1]. Data averaged for the eight movement directions.

brain can effectively vary the behavior of the system in a given control situation. The control parameters are:

1. Feedback gains of the Supraspinal Controller K_p, K_v

2. Preplanned Movement Time or Peak Speed for the movement

3. Baseline activation or Cocontraction Force for muscles $N_b.F_c$

4. Feedback gains of the Spinal Reflex loop K_s, B_s

5. Estimate Reliance Factor K_{ERF}

6. Contents of the Forward and Inverse Models and their parameters based on the level of adapatation to plant dynamics

The movement parameters considered for analyzing movement characteristics are: movement time, movement distance, jerk ratio, mean energy, movement area, correlation coefficient, perpendicular displacement and segmentation parameter λ_2. The simulations are performed in force field B_1 when the forward and inverse models are expecting the null field, so that the effect of control parameters can be tested in the presence of unknown disturbances. Figs. 5.1-5.5 show the sensitivity of these movement parameters to the first five control parameters listed above. The values for the movement parameters are averaged for all 8 movement directions. The different values of control parameters considered are specified as a factor of the value used
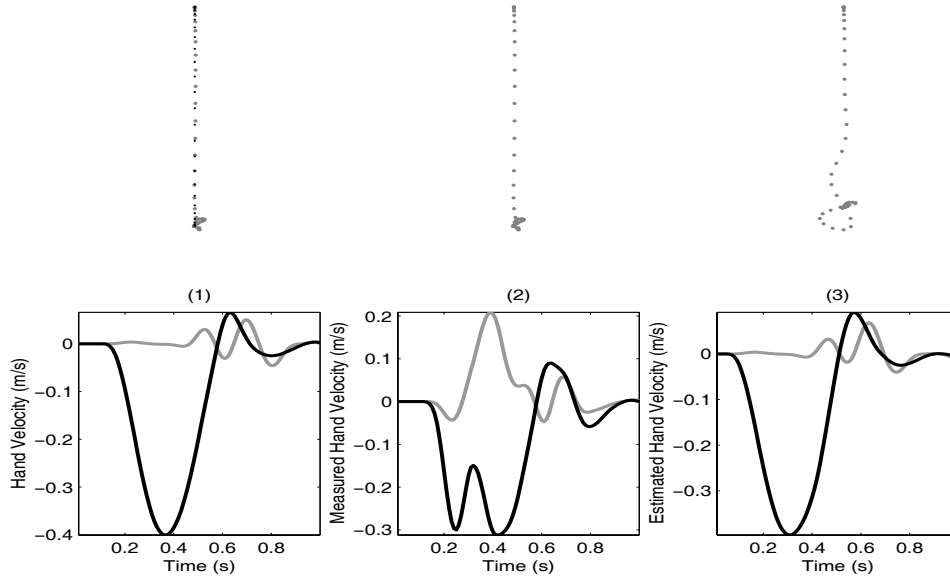
Figure 5.6: Simulated downward direction movement for a case with 5 Hz noise added to velocity measurement. (1) actual hand path and velocity along x-axis(gray) and y-axis(black) (2) measured hand path and velocity with noise added to actual velocity signal (3) estimated hand path and velocity (output of the forward model)

for normal simulations. To obtain a better performance, the controller would want to reduce jerk, increase the correlation coefficient, reduce the movement area and reduce λ_2. The jerk for the movement in the force field can be reduced by lowering supraspinal feedback gain, increasing preplanned movement time, increasing cocontraction, increasing spinal reflex gain, and lowering K_{ERF}. The correlation coeffecient can be improved by increasing preplanned movement time, increasing cocontraction and increasing spinal reflex gain. Similar trends can be observed for other control parameters. In summary, a good strategy to reduce the effect of perturbing force field is to increase movement time, increase cocontraction, increase spinal feedback gain, and reduce K_{ERF}.

5.1.2 Robustness to Measurement Noise

An important control issue for any controller is its robustness to system noise. The response of the controller to an unexpected force field as shown earlier, is equivalent to noise from the external environment. The controller has already been shown to be stable in that situation. Through further simulations, several sources of noise, not only in the measurement system but also in the controller are tested. It is found that the system is robust to noise in the feedforward path of the controller because of the feedback loop that corrects for any errors in the feedforward path. The major source of noise having the greatest influence on control of most systems is feedback measurement noise because it directly affects the feedback loop and
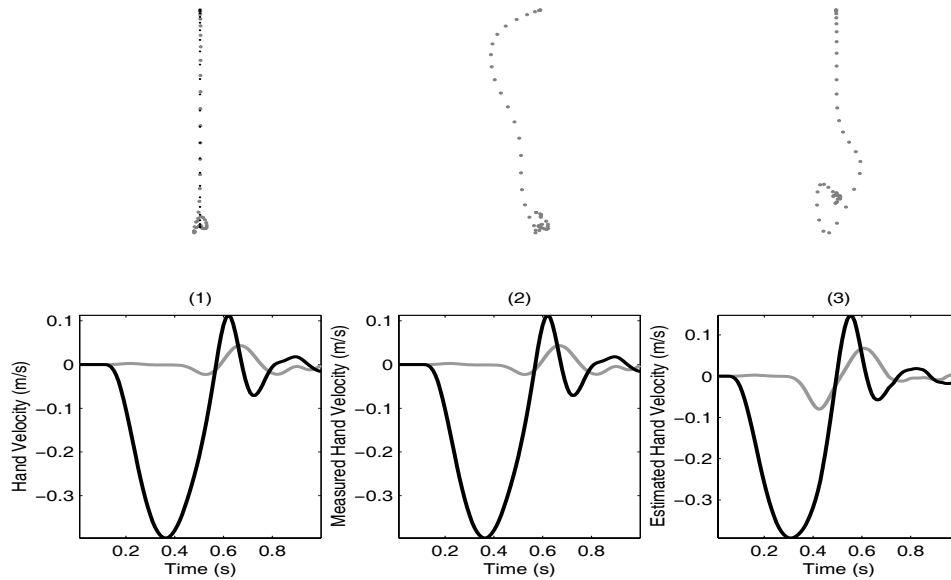
Figure 5.7: Simulated downward direction movement for a case with 5 Hz noise added to position measurement. (1) actual hand path and velocity along x-axis(gray) and y-axis(black) (2) measured hand path and velocity with noise added to actual position signal (3) estimated hand path and velocity

can cause instability in the system. Recent research work in robotics has focussed on design of observers that are robust to measurment noise ((Lohmiller and Slotine, 1996)). It is shown here that the forward model is extremely robust to noise in velocity feedback from the periphery, whereas it is robust to a lesser extent on position feedback. Two cases are considered in Fig. 5.6-5.7 - (1) random 5 Hz noise is injected into the velocity signal measured by the brain, that can have a magnitude as large as the velocity signal itself, and (2) random 5 Hz noise in the position signal that is proportional to the velocity and has a range of $\pm 10^o$ in joint angle coordinates. The hand paths and hand velocity signals are plotted for the actual movement trajectory, the measured movement trajectory and the estimated movement trajectory. In both cases the movement is along a straight line to the target and stable except at the very end of movement. In the case of velocity noise, the estimated velocity profile is almost exactly the same as the actual one, even though the measured velocity is greatly distorted by the noise. In the case of position noise, the estimated position is effected and the system shows greater instability.

The reason for robustness of the system to measurement noise is that the human arm is primarily a visco-elastic system, the neural input to which specifies not only a desired torque but also an equilibrium state for the arm. The forward model integrates the neural signals over a 200 ms period, so even when the initial states are incorrect due to noise, the output from the forward model tends towards the actual estimate because of equilibrium properties of the
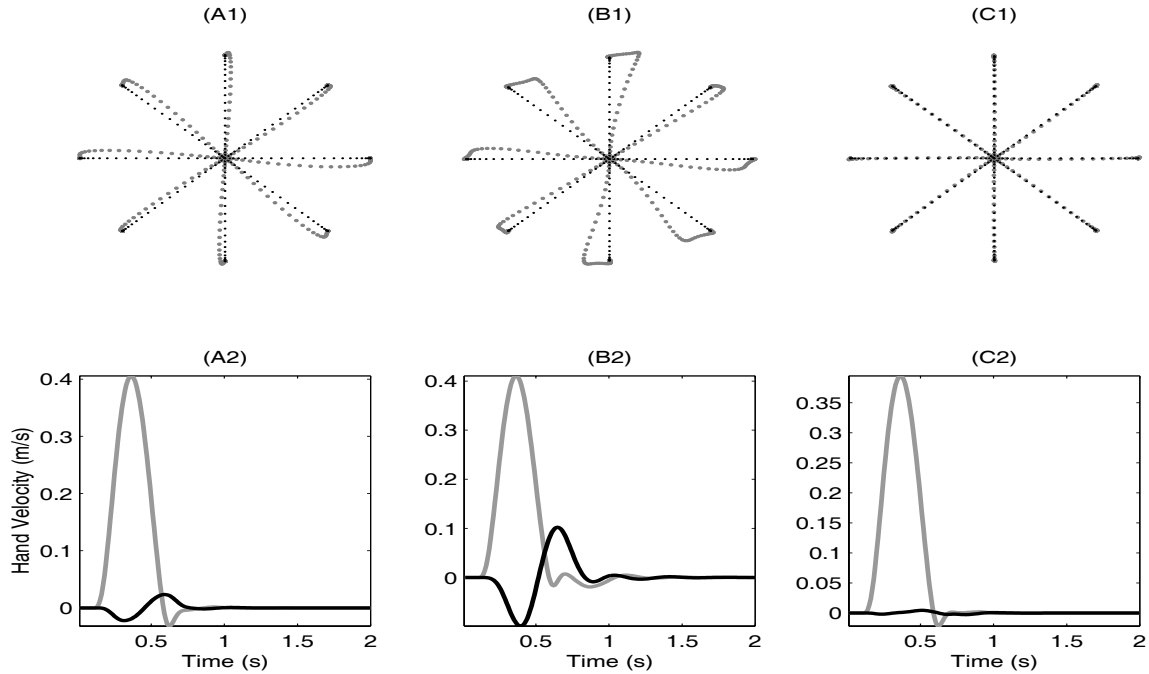
Figure 5.8: Movement trajectories in field B_1 - (1) hand paths and (2) parallel and perpendicular velocity for downward movement direction, for three cases of adaptation of forward (FM) and inverse (IM) models - (A) FM = B_1, IM = 0, (B) FM = 0, IM = B_1, (C) FM = B_1, IM = B_1

system that pull it towards the actual estimate.

5.2 The Role of Forward and Inverse Models

The forward-inverse feedback control method relies on both the inverse and forward model to generate arm movements. What is the relative role of the two models in the control and is there a way to distinguish between them in the brain? Is it possible that the two models are represented in different regions of the brain? The forward model generates the current state estimates from the measured state information and the motor commands. These state estimates are then used to compute the desired hand acceleration that drives the system. The inverse model acts as a controller that inverts plant dynamics to generate motor commands appropriate for achieving the desired acceleration. In a feedback control mothod, for high feedback gains, the properties of the overall system are governed mainly by the transfer function of the feedback pathway, and are insensitive to the transfer function of the feedforward path. Hence one would expect the forward model to dominate the behavior of the system and the inverse model to play a small role. However, the gains of the feedback pathway are limited due to unmodeled changes in plant dynamics that can make the system unstable. Hence it is expected that both the forward and inverse models play an important role in movement control.

105

To assess the relative role of the two, simulations in force field B_1 for two cases are performed. First one is with only the inverse model adapted to the force field, and the second one with only the forward model adapted to the force field. The simulations for the movements are shown in Fig. 5.8. It can be seen from the simulations that adaptation of the forward model Fig. 5.8(A), causes a great improvement in the performance and the hand path is almost the desired straight line path. On the other hand, the adaptation of only the inverse model in Fig. 5.8(B) does not effect the performance greatly. The hand path shows the same initial deviation from the straight line path and then a corrective movement to the target. There is also oscillation in the velocity profile. The performance does not improve with change in only the inverse model because the forward model is erraneous and computes wrong state estimate that drives the feedback action although none is desired. Fig. 5.8(C) shows that exact tracking of the desired trajectory is achieved only when both inverse and forward models adapt to the force field. This seems to indicate that although the forward model controls the movement behavior to a greater extent and its adaptation is crucial for improving performance in the field, the changes in the inverse model cannot be neglected and play a role in the process of adaptation.

When subjects are trained in field B_1, they show a gradual improvement in their performance that converges to the null field behavior towards the end of training. This data was presented in chapter 3. The exact convergence is only possible due to adaptation of both the inverse and forward models. It may be possible to distinguish between the two models if they have different time course of adaptation to the force field. For example, if the inverse model takes much longer to adapt than the forward model, then it may be possible to observe differential brain activity that persists for different periods of time. To determine the time course of adaptation of the two models, simulations with different levels of adaptation of the models are performed, and then compared to experimental movement data. Fig. 5.9 shows some important movement parameters for simulated movements in force field B_1 with different levels of adaptation of the forward and inverse model. The parameter values are averaged for the 8 movement directions. 6 different levels of adapatation of the two models are considered for a total of 36 combinations. The level of adaptation is defined as the amount of the force field learnt by the two models. It is assumed that the two models linearly adapt to the external force field as they change from expecting null field to force field B_1. The six levels correspond to modeling 0, 0.2, 0.4, 0.6, 0.8 and 1.0 fraction of the force field. The movement parameters for these 36 movements are computed and interpolated in 2-D to obtain values of these parameters for any combination of forward and inverse model adaptation.

There are two ways of determining the time course of adaptation of the two models using the simulation results. The first and easiest method is to find movement parameters that are influenced by adapatation of only one of the models, or to find the movement characteristics that depend almost exclusively on state of adaptation of one or the other model. When mapped with the experimental data, this will directly give the rate of adaptation of the two models. The
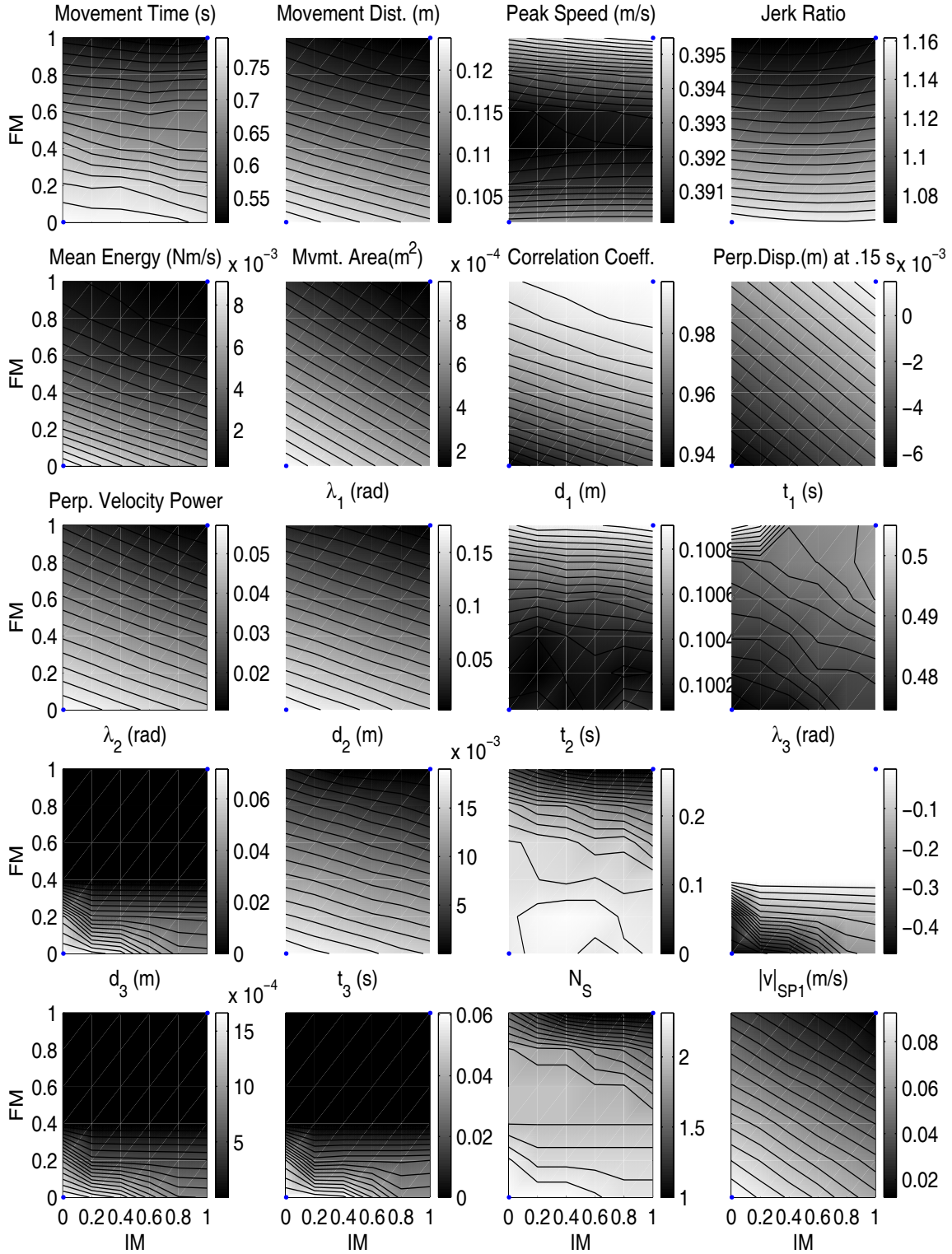
Figure 5.9: 2-D conotur plot of key movement parameters represented by a gray scale value for six different levels of adaptation of the forward and inverse models (FM,IM = 0, 0.2, 0.4, 0.6, 0.8, 1.0 B_1)

second method is to best fit adaptation curves of movement characteristics for different rates of adaptation of the two models with experimental data. In Fig. 5.9, none of the movement parameters show dependence on only the inverse model. Most of the parameters clearly have a greater dependence on the forward model. The relative pattern of dependence on the two models is also similar across parameters. Therefore the first method for distinguishing between the rates of the two models is not effective.

A second method is illustrated in Fig. 5.10 and shows the discrimination power of this method by considering two extreme cases. Two adapatation curves for each movement parameter are generated. The first one corresponds to a decaying exponential change in only the forward model that initially expects null field and gradually adapts to B_1 (black line), while there is no change in the state of the inverse model. The second curve corresponds to a change in only the inverse model from null to B_1 (gray line). Both the exponentials have a decay constant of 0.02 per movement, which implies that the by the 50th movement the models have adapted to 69% of the force field. The two cases predict different adaptation curves for most movement parameters. The first case where only the forward model adapts, shows significant improvement in movement parameters and looks much closer to reality (Fig 3.F) than the second case where only the inverse model adapts. Quite clearly, the adaptation of the forward model is necessary for improvement in performance, as occurs when subjects practice in the force field. This method seems to be capable of distinguishing between different rates of adaptation of the inverse and forward model.

Now consider a case where both the inverse and forward models are adapting exponentially with different decay rates given by r_{FM} and r_{IM}.

$$FM(n) = FM(0) + \Delta\{FM\}(1 - e^{-nr_{FM}})$$

$$IM(n) = IM(0) + \Delta\{IM\}(1 - e^{-nr_{IM}})$$

FM(n) and IM(n) are the adaptation states of the two models at movement number n in the force field and represent the time course of adaptation for the two models. FM(0) and IM(0) are the initial states of the forward and inverse models at the beginning of the force field training. $\Delta\{FM\}, \Delta\{IM\}$ are the difference in the initial state of the models and the force field being learnt. The equations are obtained by considering a rate of learning of the models that is proportional to the difference in the model and the field at any instant of time. When subjects begin the training in field B_1, they initially expect the null field. Hence the initial states of both the forward and inverse models are set to 0, $FM(0) = IM(0) = 0$. Also $\Delta\{FM\} = \Delta\{IM\} = B_1$. Six values for $r_{IM} = 0.0003, 0.003, 0.01, 0.03, 0.1, 0.3$, and five values for $r_{FM} = 0.003, 0.01, 0.03, 0.1, 0.3$, are considered for a total of 30 combinations.

To exactly simulate experimental conditions, we used the same set structure of movement directions that was experienced by our subjects. Therefore in field B_1 training, a total of 192x3
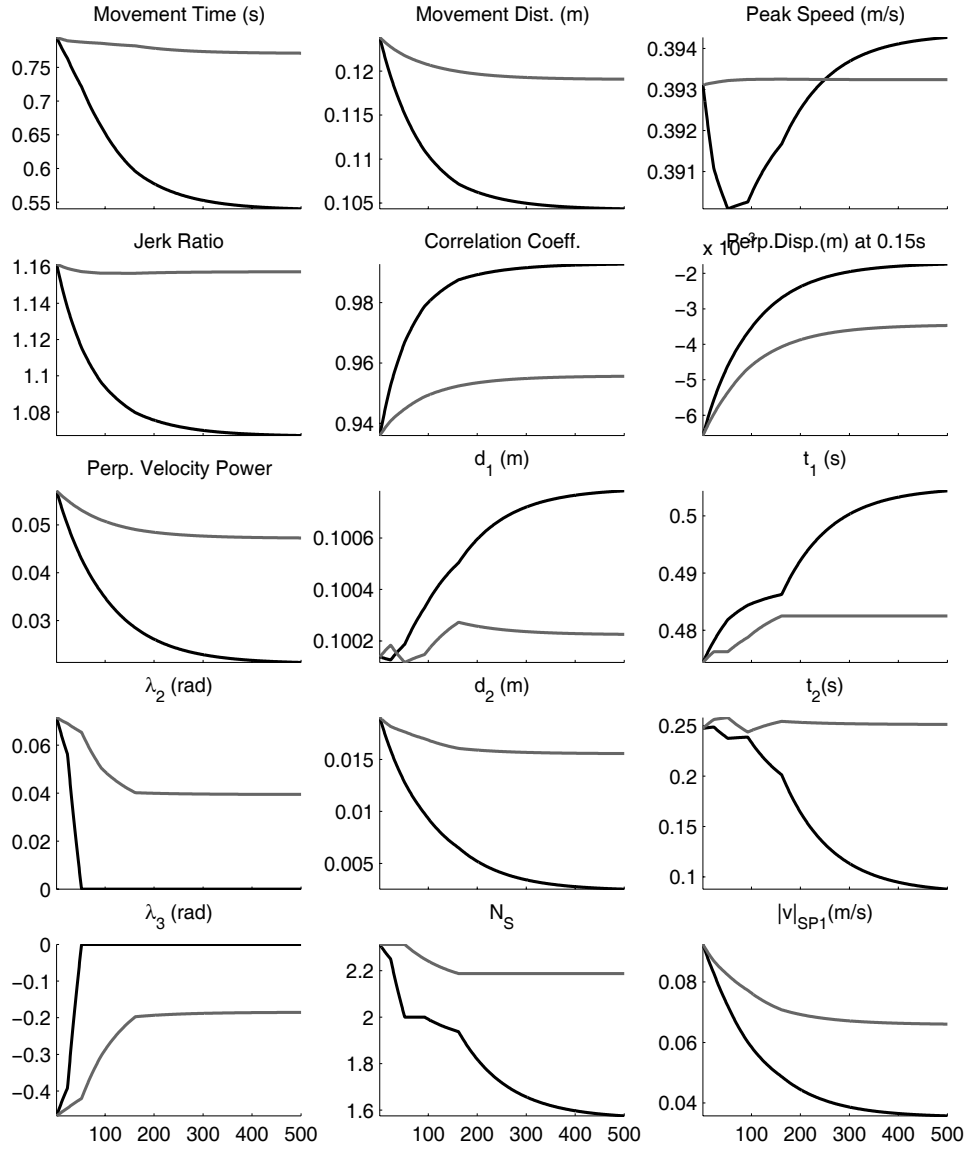
Figure 5.10: Adaptation curves for 15 movement parameters for simulated movements in field B_1 for two cases - (1) gray, only the inverse model adapts exponentially to B_1 and $r_{IM} = 0.02, r_{FM} = 0$, (2) black, only the forward model adapts to B_1 and $r_{IM} = 0, r_{FM} = 0.02$. The x-axis is the movement number from 1 to 576
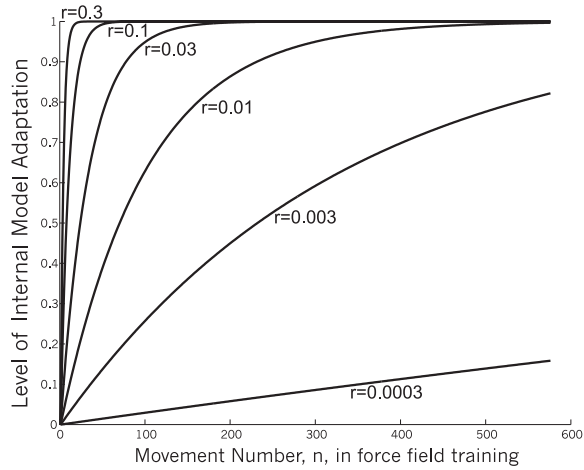
Figure 5.11: Learning curves for inverse and forward models for six different rate constants of adaptation ($r = 0.0003, 0.003, 0.01, 0.03, 0.1, 0.3$) plotted against movement number. The curves with higher r shift leftward indicating faster adaptation.
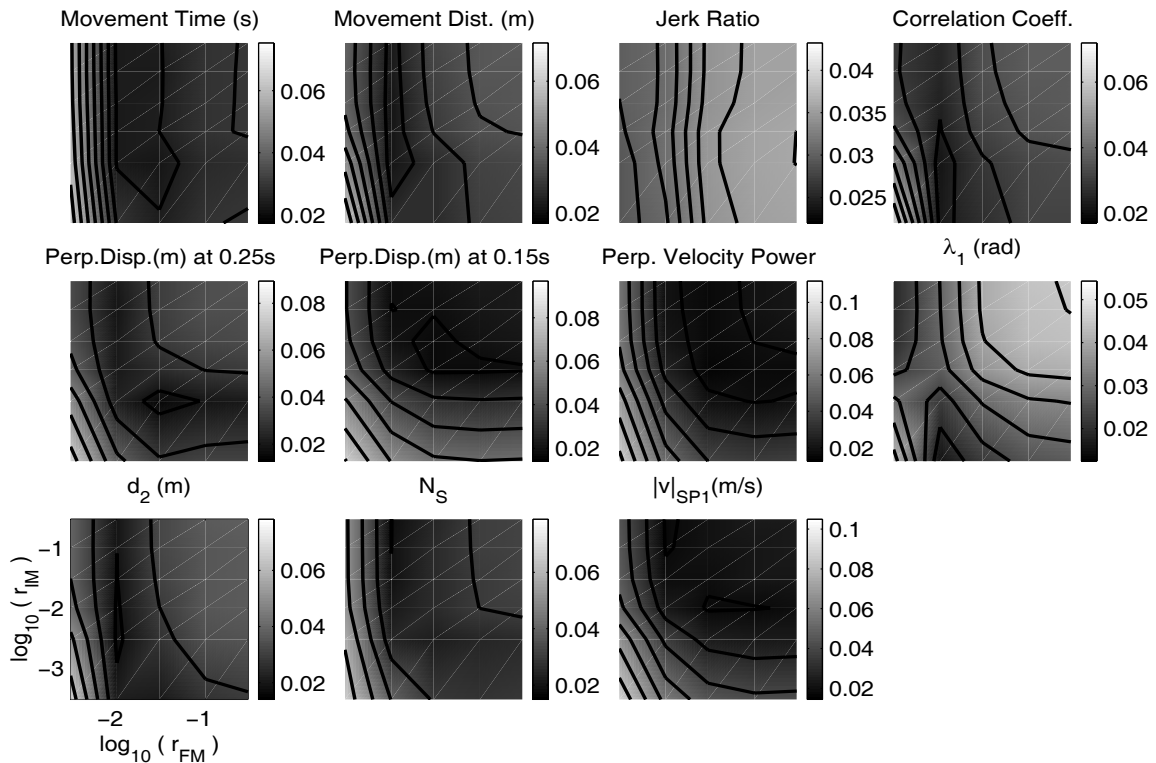
Figure 5.12: 2-D contour plot of normalized errors e_p in movement parameters represented by a gray scale value for five different rates of adaptation of the forward model ($r_{FM} = 0.003, 0.01, 0.03, 0.1, 0.3$) and six rates of inverse model ($r_{IM} = 0.0003, 0.003, 0.01, 0.03, 0.1, 0.3$)

= 576 movements is taken with one-eight of the movements in each direction in the exact sequence as they occured in the experiments. The value of movement number n goes from 1 to 576 and this gives the levels of FM and IM adaptation for each movement from Eqn. E. The level of adaptation of the internal model is plotted agaist movement number for 6 different adaptation rate constants $r = 0.0003, 0.003, 0.01, 0.03, 0.1, 0.3$ in Fig. 5.11. The 2-D map of movement parameter values for different adaptation levels of IM and FM, as shown in Fig. 5.9, is then used for the approriate movement direction and for the given adaptation levels of the two models, to give the value of each parameter for the nth movement. Since we are interested in the change in parameters from null field, the parameter values of a simulation in the null field for this direction are subtracted from the value obtained from the map. An adaptation or learning curve for movement parameters is obtained with n varying from 1 to 576 for each combination of r_{IM} and r_{FM}. The next step is to find the adaptation curve that best fits the data. The corresponding r_{IM} and r_{FM} will give the time course of adapataion of the two models. An error measure e is defined for each parameter p and all 30 adaptation curves $q = 1..30$,

$$e_{p_q} = \frac{\sum n = 1576(|y_{p_{qn}} - \mu_{p_n}| + \sigma_{p_n})}{\sum q = 130 \sum n = 1576(|y_{p_{qn}} - \mu_{p_n}| + \sigma_{p_n})}$$

where, $y_{p_{qn}}$ is the value of the simulated movement parameter p at the n_{th} movement in the adapataion curve for FM and IM adaptation rate q. μ_{p_n} is the mean of the parameter value for 16 subjects at movement n and σ_{p_n} is the corresponding standard deviation. The numerator in the equation is almost equal to the average area between the simulated and experimental adaptation curves. This error is normalized by the denominator that is the sum of the errors for the 30 different rates of IM and FM adaptation to make it independent of parameter units and values. The errors are plotted in Fig. 5.12 for all movement parameters. A low value of the error implies a better fit for that particular r_{IM} and r_{FM} compared to other rates. To combine the information from the different parameters, the errors are summed together to give a net error E,

$$E_q = \frac{\sum p = 1 p_n e_{p_q}}{p_n}$$

This net error is plotted as a function of r_{FM} and r_{IM} in Fig 5.13. The region surrounded by the thick line outlines the minima. Two regions are obtained. The error is clearly at its lowest for values of the forward model in the range, $r_{FM} = 0.01$. For the inverse model the rate of adaptation can lie within a much broader range of values and is not significantly different for $0.03 < r_{IM} < 0.003$. The reason for lower sensitivity to r_{IM} is the much weaker dependence of movement parameters on inverse model. So there is definite evidence for a fast learning forward and inverse model, although it cannot be determined whether the rate of learning of the inverse model is greater or lesser than that of the forward model. For a particular combination of
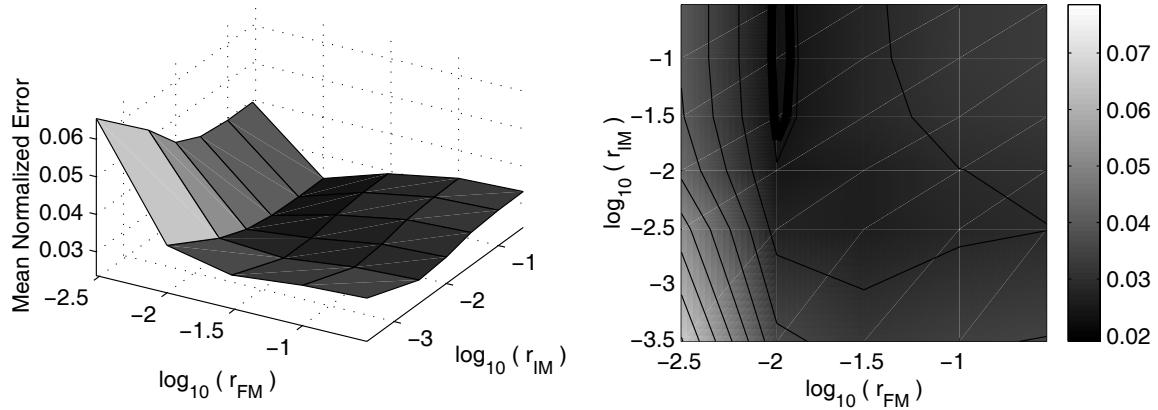
Figure 5.13: Net normalized error E represented by a gray scale value plotted as a 3-D surface and 2-D contour image, for five different rates of adaptation of the forward model ($r_{FM} = 0.003, 0.01, 0.03, 0.1, 0.3$) and six rates of inverse model ($r_{IM} = 0.0003, 0.003, 0.01, 0.03, 0.1, 0.3$). The region of minimum error value is highlighted by the thick black line.

adaptation rates in the minimum error region, $r_{FM} = 0.01, r_{IM} = 0.01$, the adapatation curves for 20 parameters are plotted in Fig. 5.14. We find an excellent fit with values of all movement parameters for the experimental data. The simulated curves even mimic the set structure due to the sequence of movement directions for experimental data. This indicates a great deal of confidence in the simulations using this control method and in the adapatation rates obtained for changes in forward and inverse models.

A similar procedure can be independently adopted for determining adaptation of the two models in field B_2 after having trained in field B_1. We assume that at the end of training in B_1 both forward and inverse models have adapted to field B_1. As training proceeds in field B_2, the models gradually change to B_2. 11 states for each of the forward and inverse model are considered as they make a transition from field B_1 to B_2. These are -1.0, -0.8, -0.6, -0.4, -0.2, 0, 0.2, 0.4, 0.6, 0.8 and 1.0 times B_2. Since the two fields are opposite each other, -1.0 B_2 is actually equal to B_1, so that the 11 states go from expecting B_1 to B_2. The map of movement parameters for these different levels of adaptation to field B_2 are shown in Fig 5.15. Again, most of the parameters show a strong dependence on the forward model. Adaptation curves based on the same principle as devised for training in B_1 are considered here for six values of r_{IM} and 5 values of r_{FM}. Initial states for the learning curves are $FM(0) = IM(0) = B_1$, and the change is $\Delta\{FM\} = \Delta\{IM\} = B_2 - B_1$. For comparison, data from the experimental group of 8 subjects who performed in field B_2 immediately after B_1 (zero hour group) is taken. Since they performed two sets of 192 movements each, the value of n goes from 1 to 384.

The error measure E is again determined for the 30 adaptation curves, by finding the summed normalized error for 16 movement parameters. To visually describe the goodness of fit
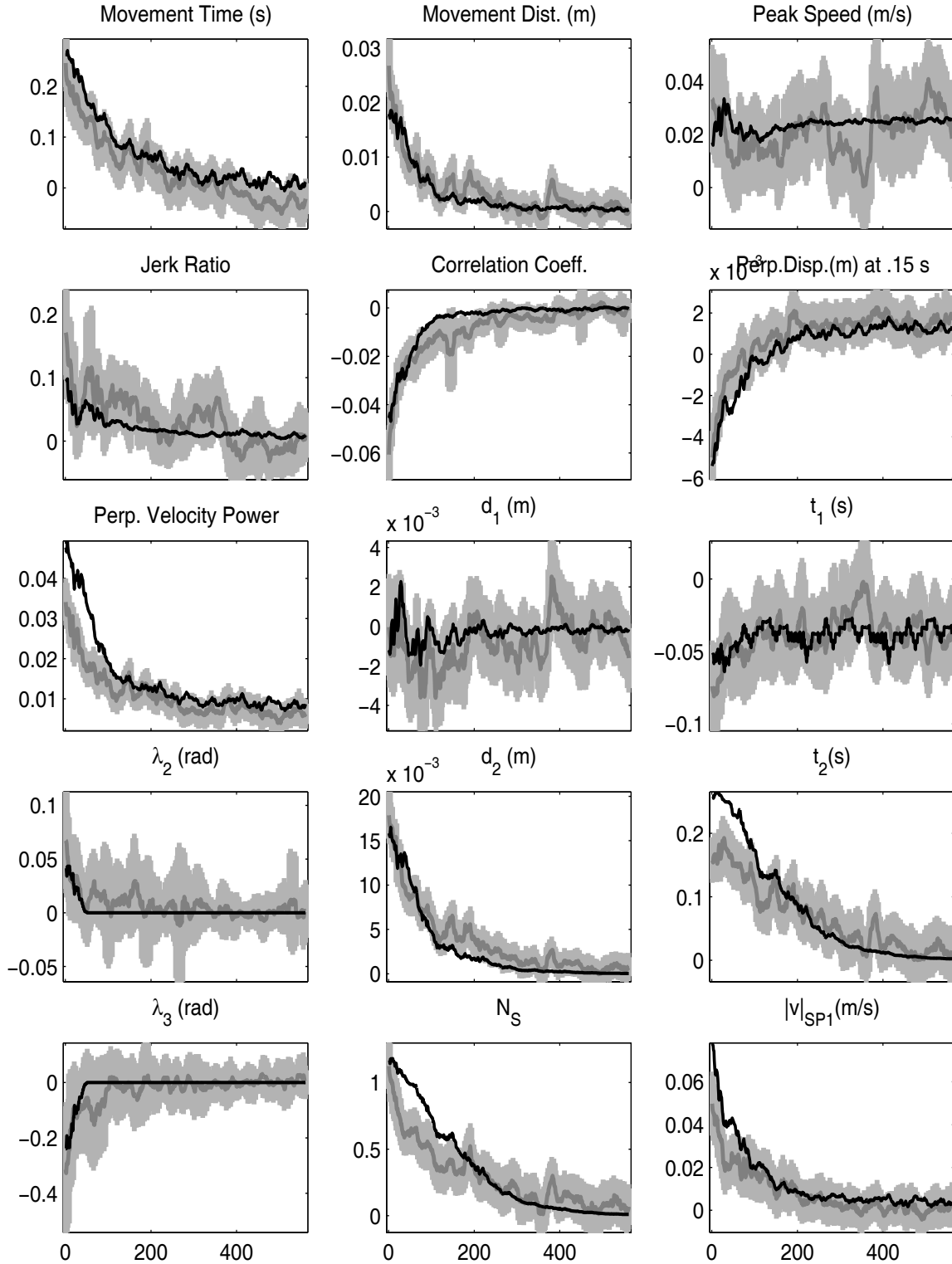
Figure 5.14: Adaptation curve for movement parameters in field B_1 for simulated movements (black) with adaptation constants $r_{FM} = 0.01, r_{IM} = 0.01$, compared to experimental data (gray) plotted as the mean and standard deviation.
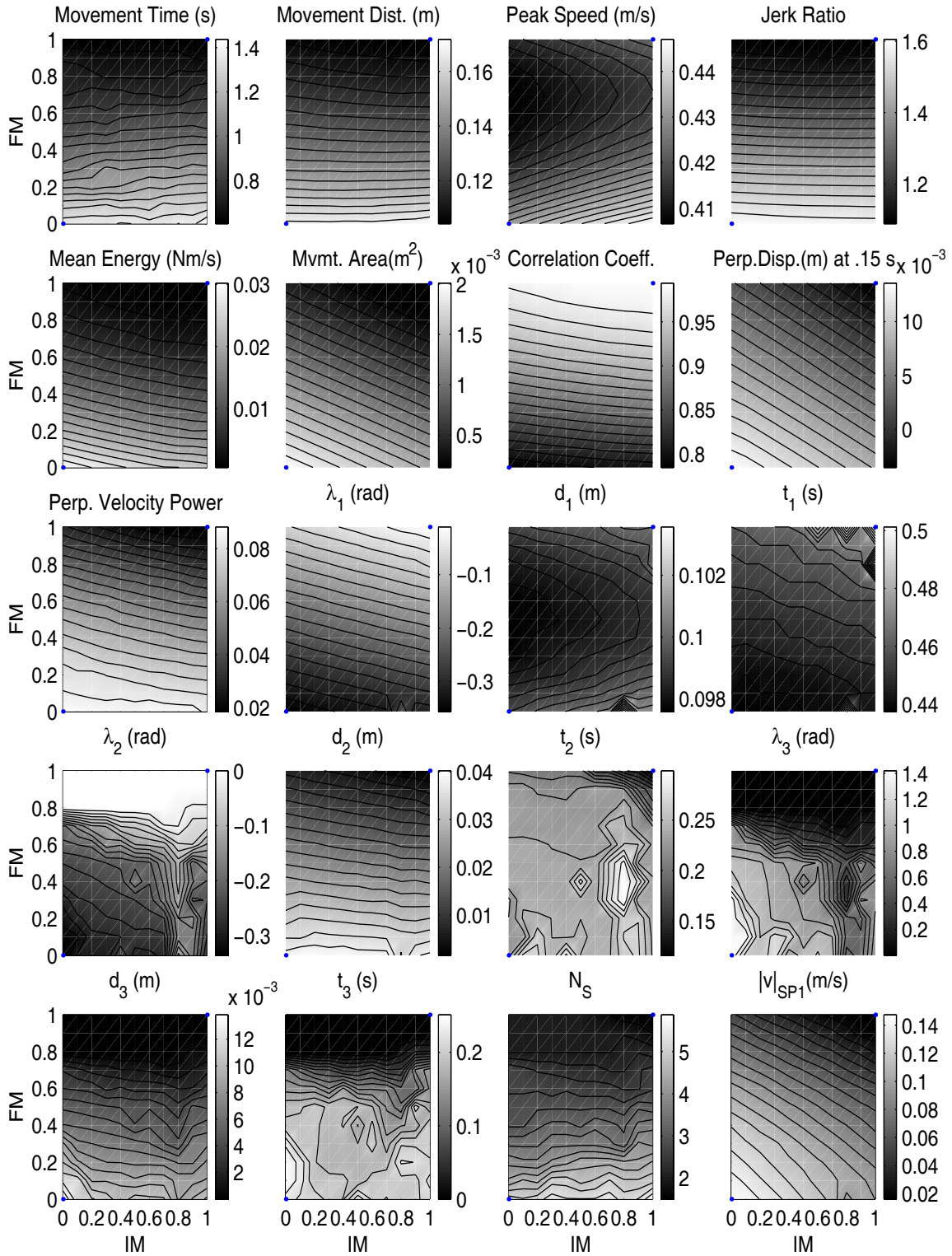
Figure 5.15: 2-D conotur plot of key movement parameters represented by a gray scale value for eleven different levels of adaptation of the forward and inverse models (FM,IM = -1.0, -0.8, -0.6, -0.4, -0.2, 0, 0.2, 0.4, 0.6, 0.8, 1.0 B_2) while movements are made in field B_2.
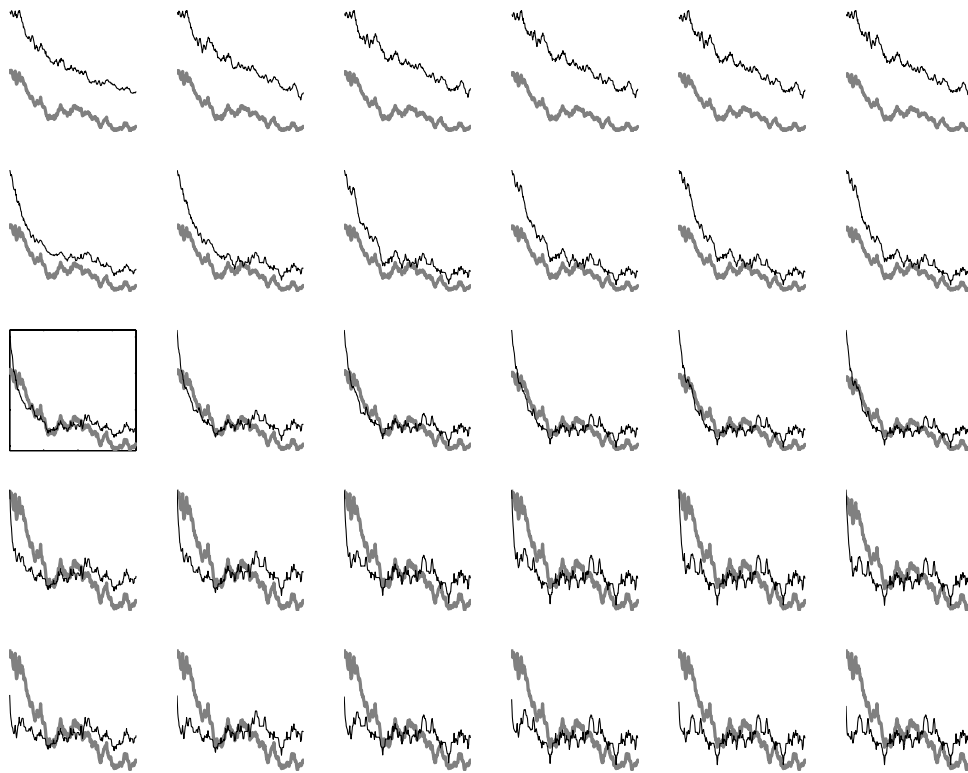
114

Figure 5.16: Adaptation curves for movement time for five different rates of adaptation of the forward model ($r_{FM} = 0.003, 0.01, 0.03, 0.1, 0.3$) represented by rows and six rates of inverse model ($r_{IM} = 0.0003, 0.003, 0.01, 0.03, 0.1, 0.3$) represented as columns, compared to mean experimental movement time in field B_2. The simulated curve is in black and the experimental data in gray. The box indicates the curves with closest match. In this case, $r_{FM} = 0.03, r_{IM} = 0.003$
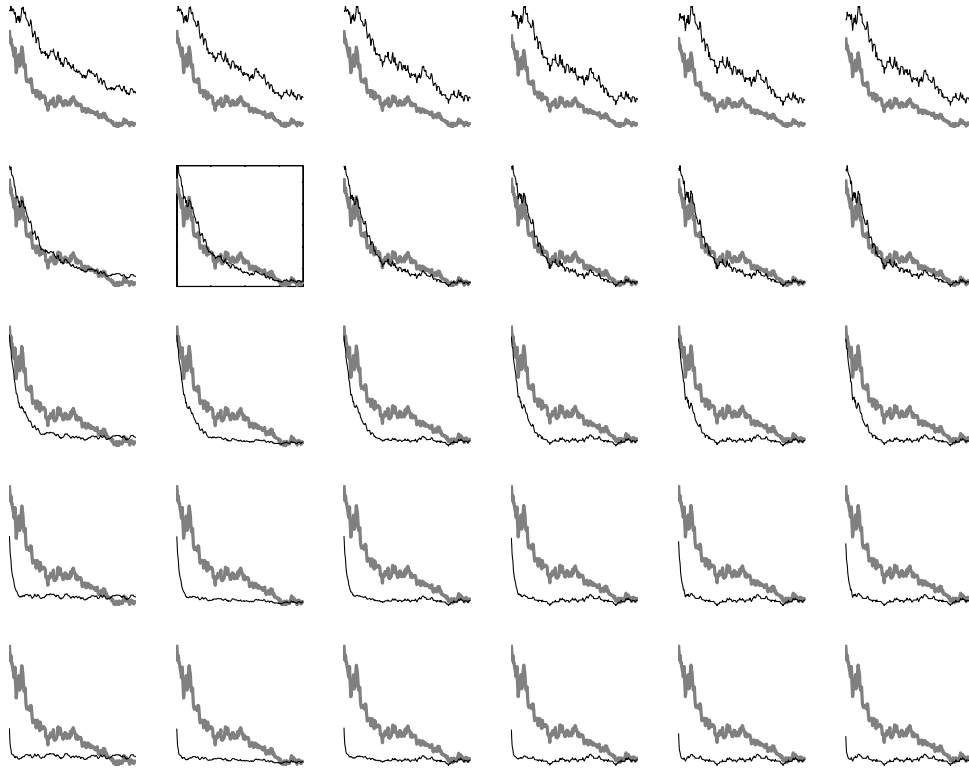
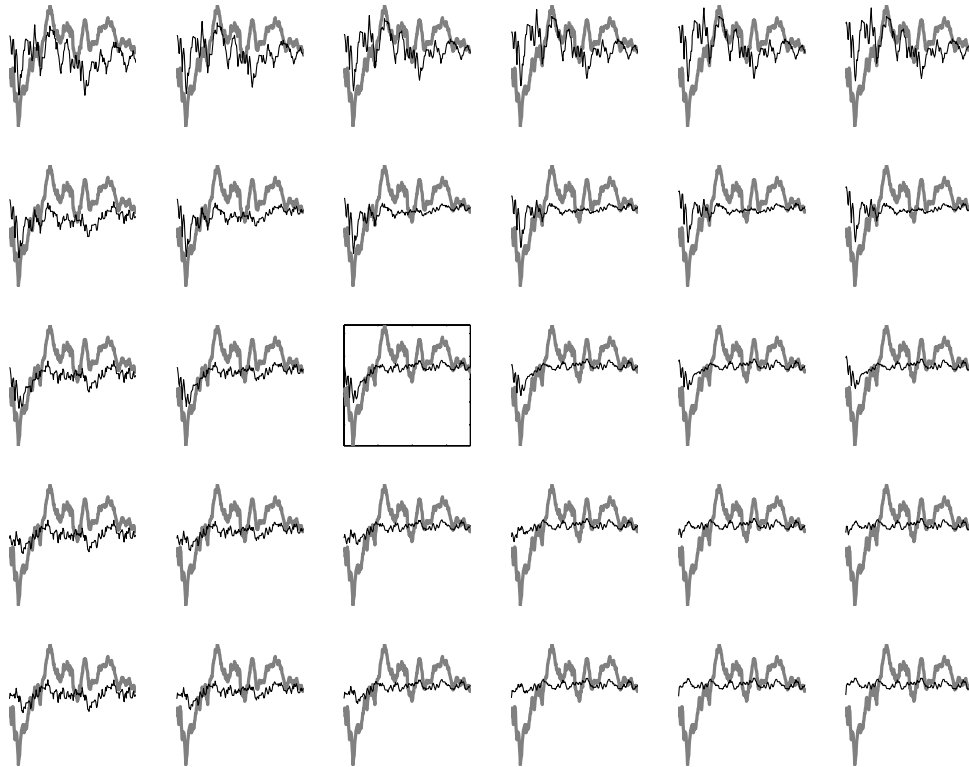Figure 5.17: Adaptation curves for movement distance
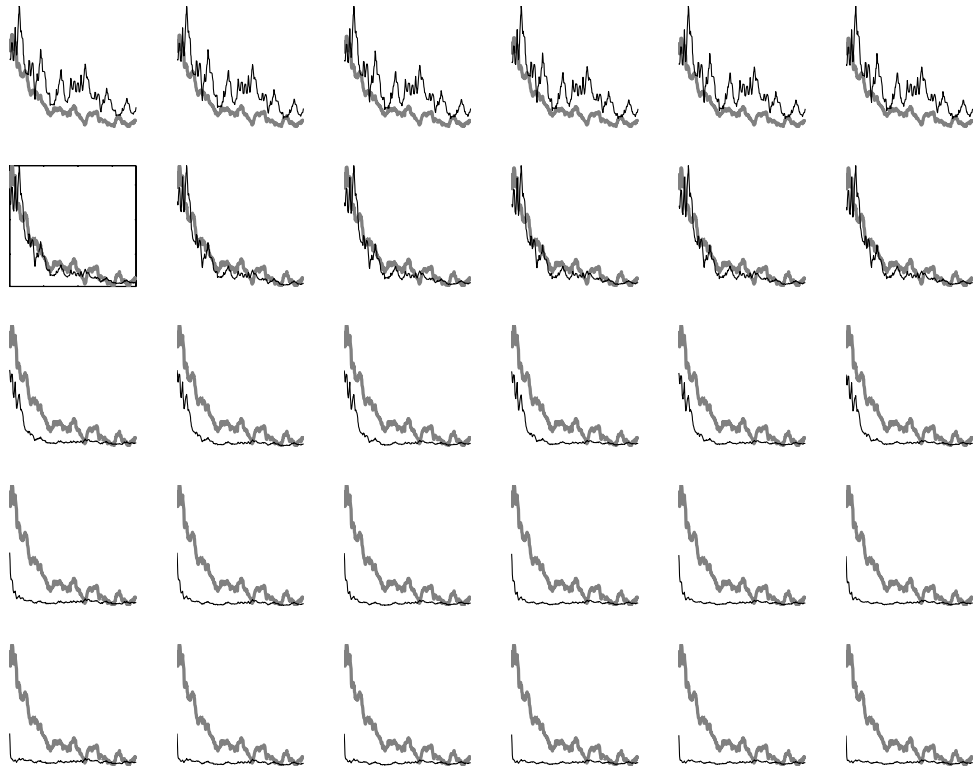

Figure 5.18: Adaptation curves for peak speed

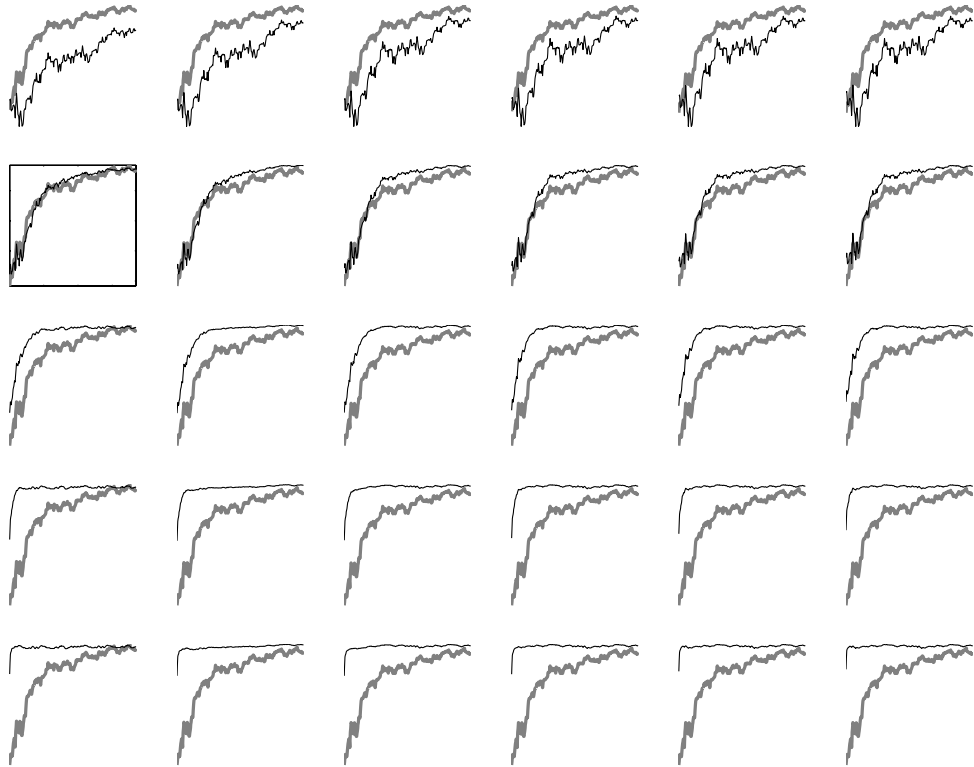Figure 5.19: Adaptation curves for movement jerk ratio

Figure 5.20: Adaptation curves for correlation coefficient
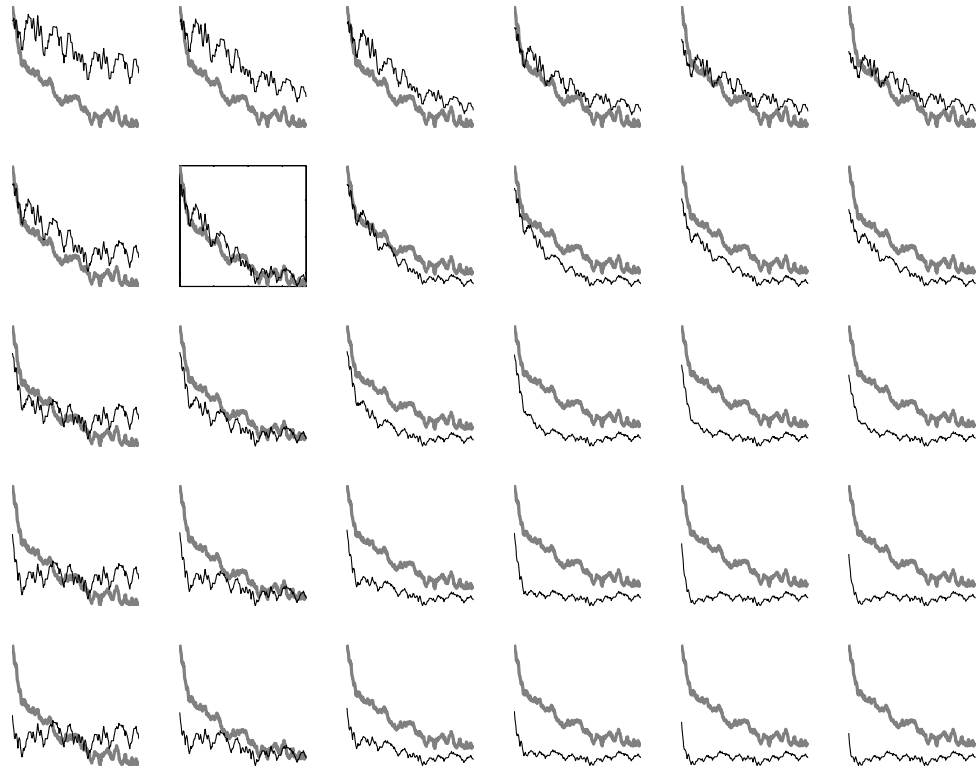
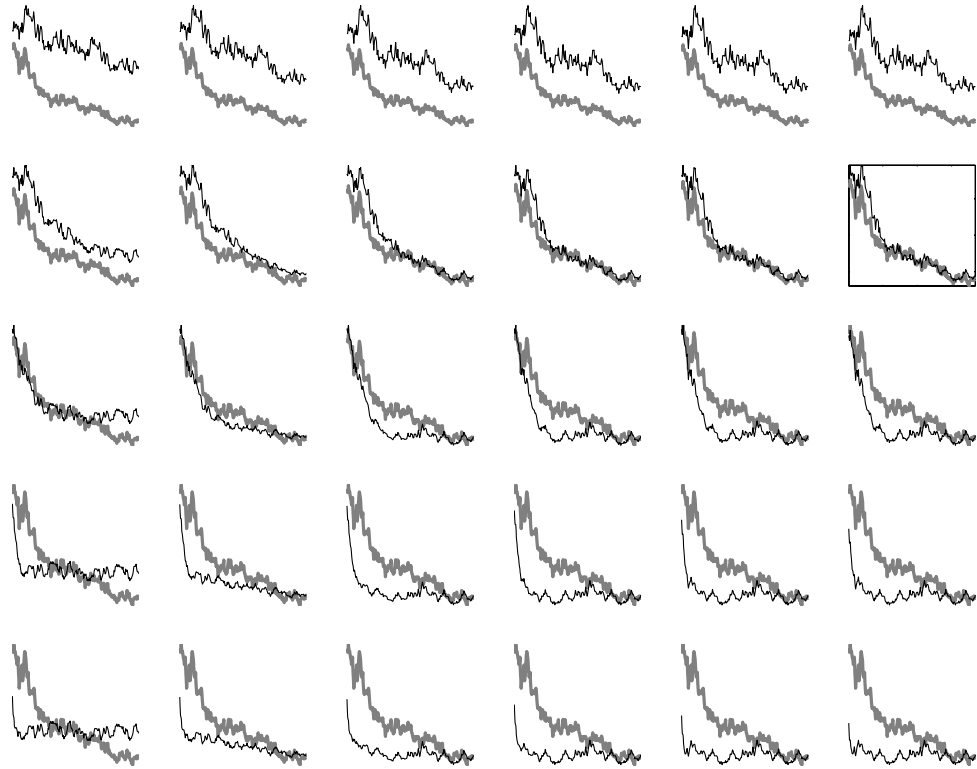Figure 5.21: Adaptation curves for perpendicular displacement at 150 ms

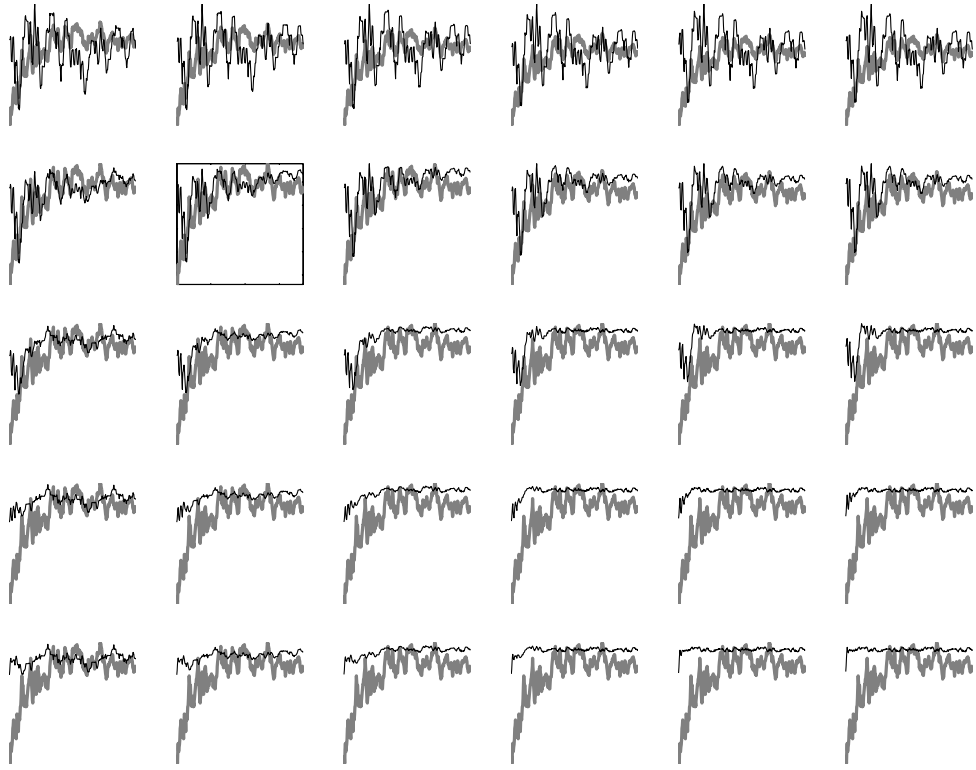Figure 5.22: Adaptation curve for perpendicular velocity power
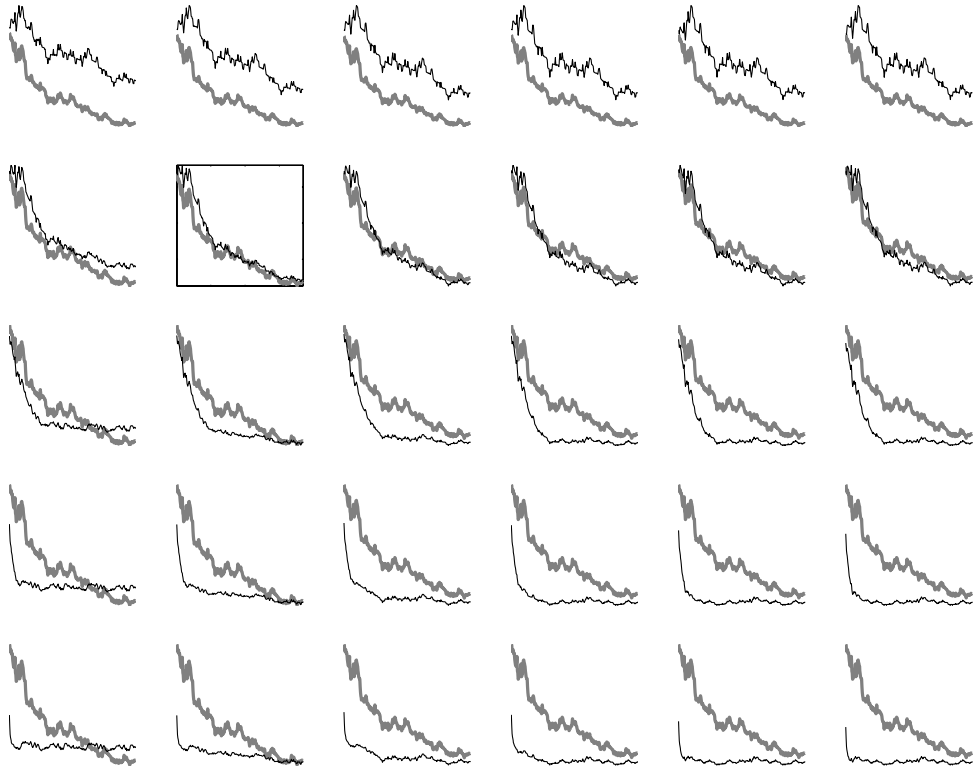
Figure 5.23: Adaptation curve for d_1

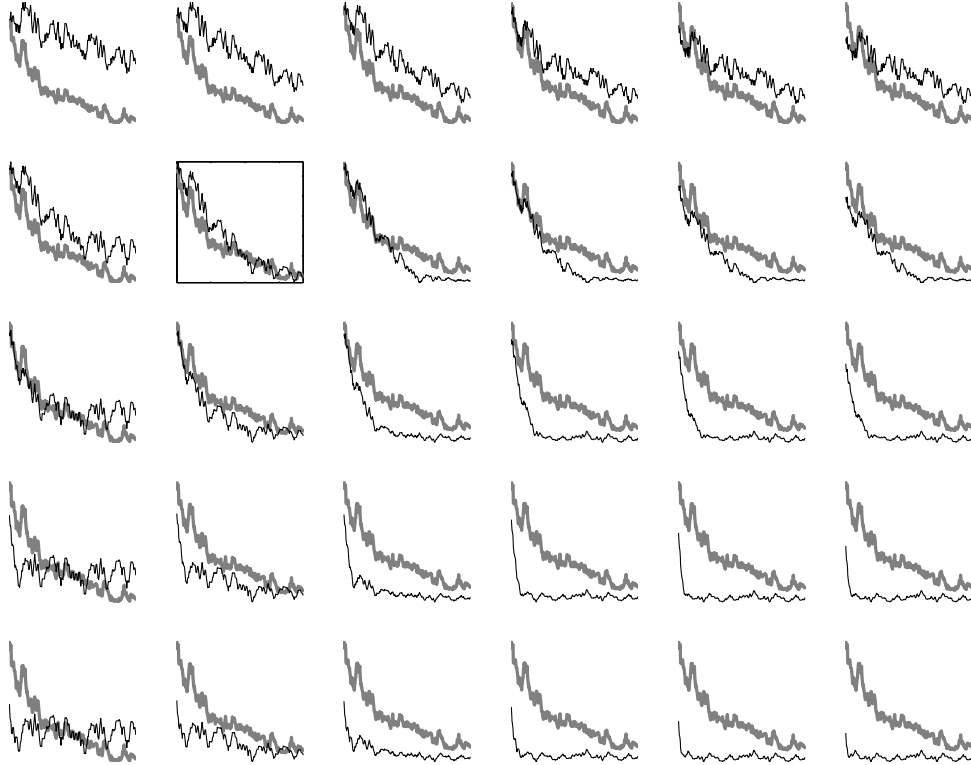Figure 5.24: Adaptation curve for d_2

Figure 5.25: Adaptation curve for speed at first discontinuity $|v|_{SP1}$

of the different adaptation rates for the 16 parameters, mean experimental adaptation curve is plotted with adapatation curves for the 30 combinations from Figs. 5.16-5.25 for the different movement parameters. The errors for each of the parameters is plotted in Fig. 5.26 and the summed error in Fig. 5.27. The region of minimum error is highlighted by the dark line and corresponds to a value of $r_{FM} = 0.01$ and $0.003 < r_{IM} < 0.03$. These values are almost identical to those obtained for training in field B_1, hence it supports the view of fast learning of both the forward and inverse models. The adaptation curves for 20 movement parameters are plotted in Fig. 5.27. for the experimental and simulated movements for rates that show the best fit, $r_{FM} = 0.01$ and $r_{IM} = 0.003$. Again, a very close fit is obtained for most movement parameters.

Note: Null subtracted values for movement parameters are used for all the simulated and experimental results shown here. For the simulations this is achieved by simulating a movement in the null field for all 8 movement directions with the same control parameter set as the fielded movements and then subtracting the value of the movement parameter of the null field from force field. Movement time and correspondingly the peak movement speed, were the only control parameters that were varied between null field and fielded simulations to account for and match the differences seen in experimental data.

From these results it is concretely established that fast adapting internal models are involved
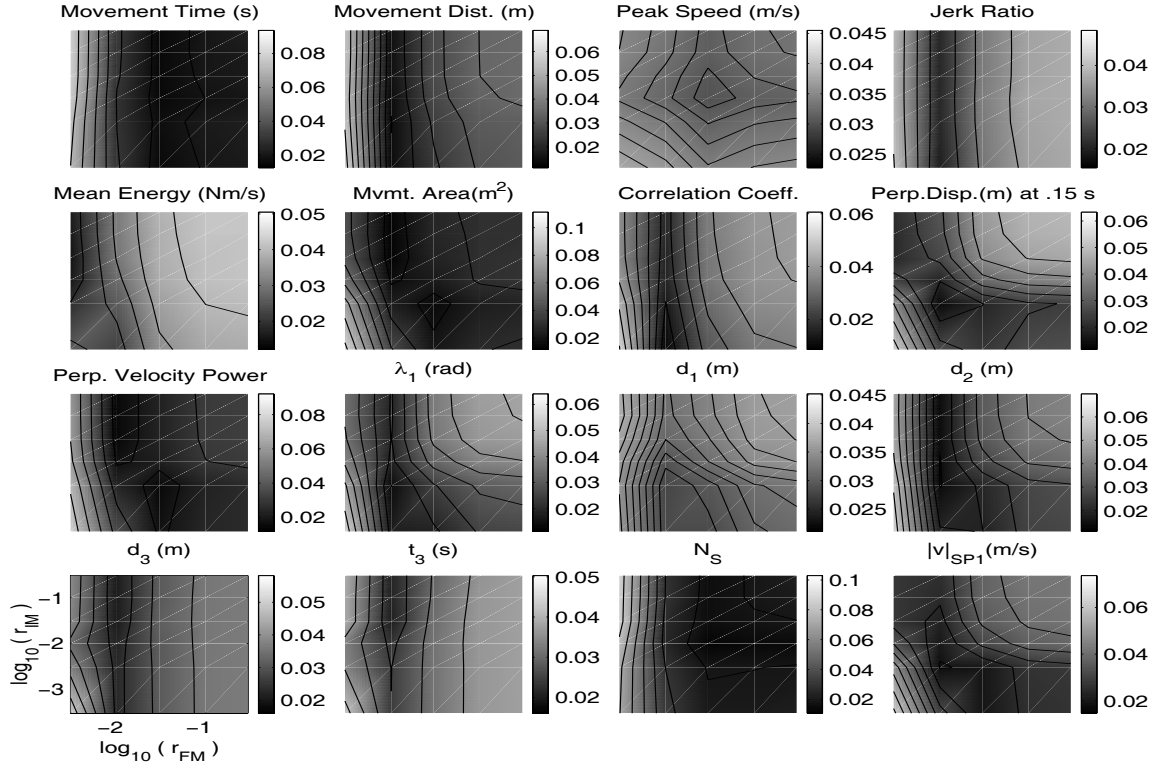
Figure 5.26: 2-D contour plot of normalized errors e_p in movement parameters represented by a gray scale value for five different rates of adaptation of the forward model ($r_{FM} = 0.003, 0.01, 0.03, 0.1, 0.3$) and six rates of inverse model ($r_{IM} = 0.0003, 0.003, 0.01, 0.03, 0.1, 0.3$) in field B_2
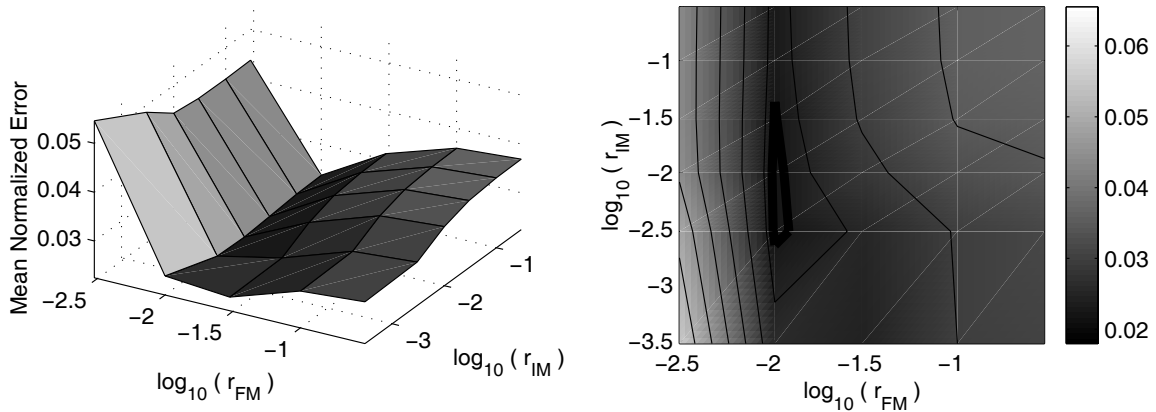
Figure 5.27: Net normalized error E represented by a gray scale value plotted as a 3-D surface and 2-D contour image, for five different rates of adaptation of the forward model ($r_{FM} = 0.003, 0.01, 0.03, 0.1, 0.3$) and six rates of inverse model ($r_{IM} = 0.0003, 0.003, 0.01, 0.03, 0.1, 0.3$). The region of minimum error value is highlighted by the thick black line.

Figure 5.28: Adaptation curve for movement parameters in field B_2 for simulated movements (black) with adaptation constants $r_{FM} = 0.01, r_{IM} = 0.003$, compared to experimental data (gray) plotted as the mean and standard deviation.

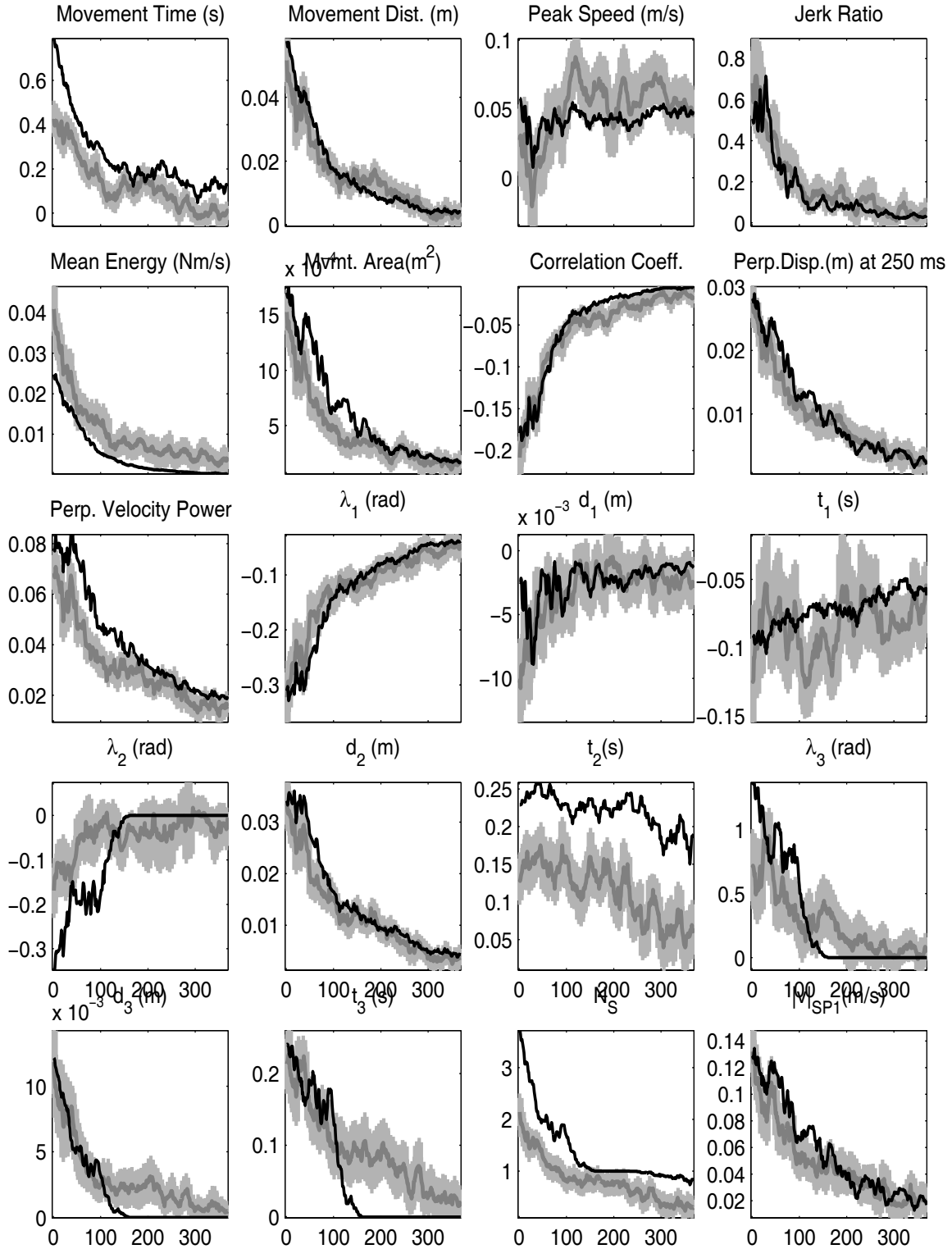in the learning of novel dynamics as presented by force fields. The rate of learning for the forward model is determined with a high certainty, although for the inverse model the rate of lerning cannot be pin-pointed exactly. There is an open possibility that the inverse model may be learnt at a lower rate than the forward model. The possibility that the inverse model is trained during an offline or rest period until after training is over, is ruled out, because adaptation of the inverse model occurs during the course of practice in the field. It however does not rule out the possibilty that a forward model is used to supervise learning of the inverse model which can occur during the course of practice in the force field and during the period in between successive movements.

5.3 Explanation for difference in behavior between zero-hour and six-hour groups

One of the primary objectives of this thesis was to provide a framework to explain the difference observed when subjects returned to perform in the force field after a period of rest. The data is presented from two different groups of subjects when they perform field B_2 after 0 or 6 hours of having trained in field B_1 in chapter 3. It is found that the six hour group of subjects has a better performance in field B_2 than the zero-hour group for most movement parameters. In the previous section the time course of adaptation of the forward and inverse models was determined for all the subjects in field B_1 and the zero hour group in B_2 and showed a reasonably good match with the experimental data. Hence the same analysis can be extended to explain the difference between 0 and 6 hour groups. There are two possible changes that can occur in the internal representation of the models and in the process of adaptation during the period of 6 hours in between the two fields.

The first possibility is a change in the level of internal model adaptation to the first field B_1, so that for the six hour group the initial state of the models is not B_1 exactly, but has shifted from that value. For an improvement in performance, the only change can be a decay in the representation of the force field B_1 towards null field. As an example, consider that both forward and inverse models have decayed by 20% over the period of 6 hours, so that at the beginning of field B_2, the initial states are $FM = IM = 0.8 B_1$ instead of $FM = IM = B_1$. The adaptation rate is assumed to be the same as that computed for the simulated zero hour group. The predicted adaptation curve for this possibility is shown in Fig. 5.28 (gray line) and compared to the simulated adaptation curve for the zero hour group (black line) where $FM = IM = B_1$. The performance is better as seen in experimental data and shows roughly the same change in movement parameters. However, there is a small difference in the experimental and simulated data. Whereas the experimental data shows a shift in the movement parameters towards the null and a *faster* rate of adaptation (given by the slope of the curve) during the
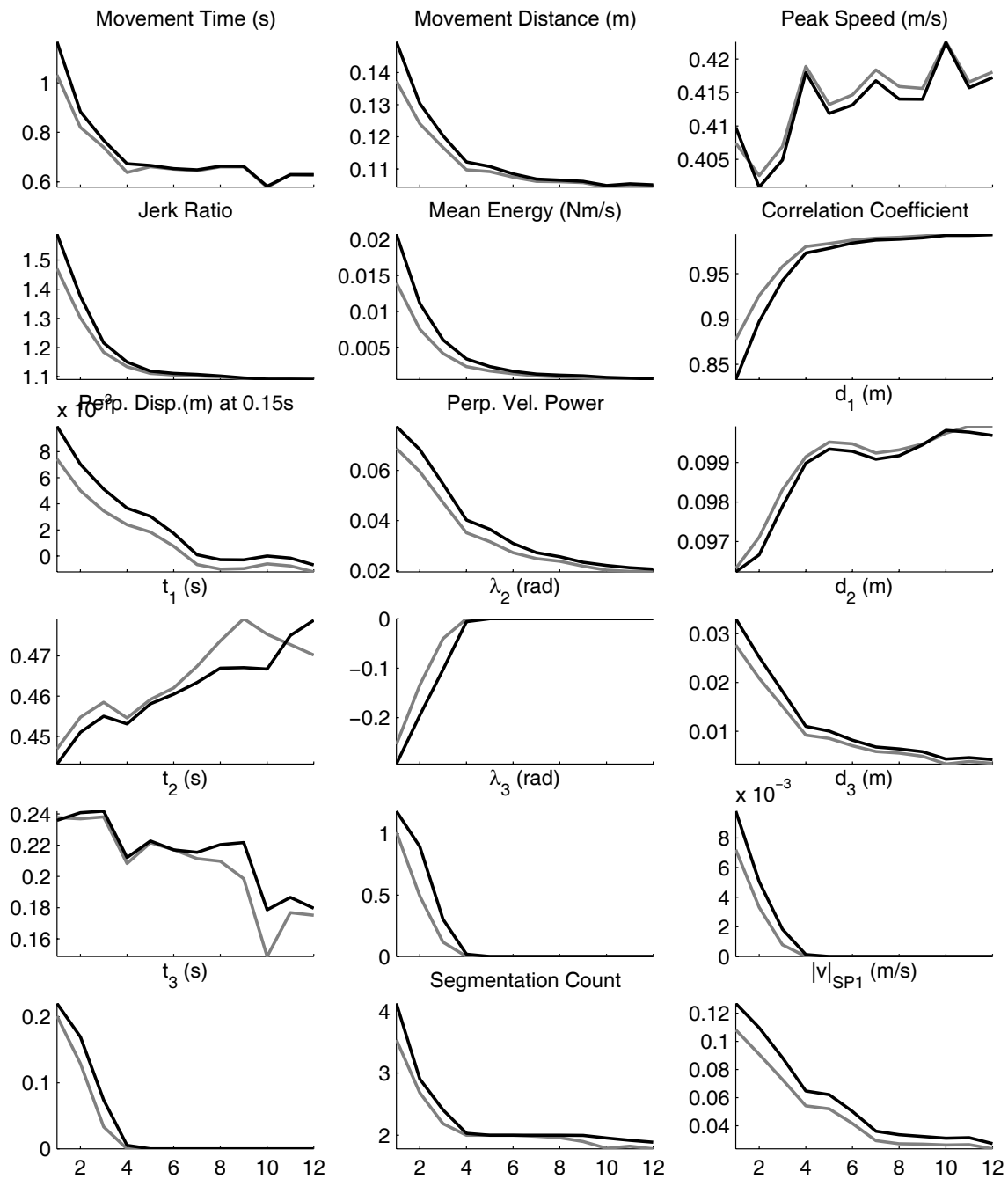
Figure 5.29: Adaptation curve for movement parameters in field B_2 for simulated movements with two different initial levels of forward and inverse models - (1) black, zero hour group with FM(0)=IM(0)=B_1, (2) gray, six hour group with FM(0)=IM(0)=0.8 B_1. Adaptation constants are $r_{FM} = 0.015, r_{IM} = 0.0025$ for both cases
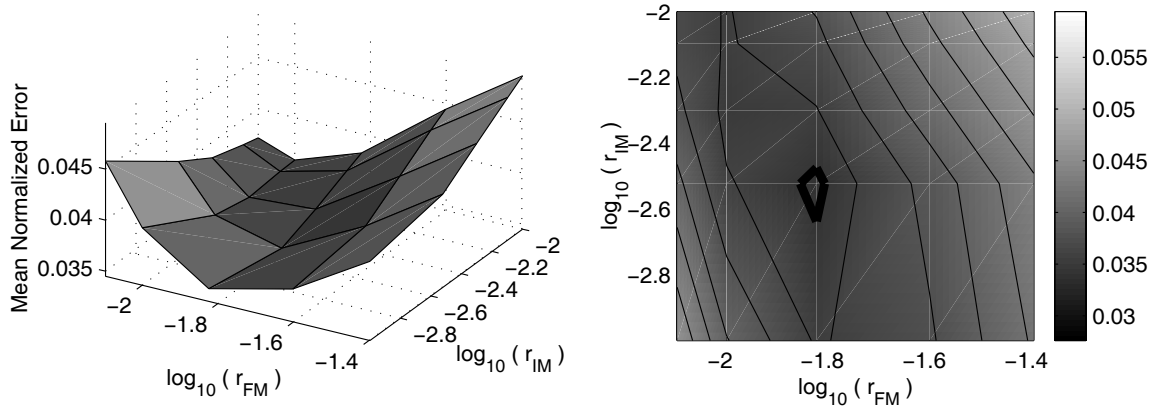
Figure 5.30: Net normalized error E, for five different rates of adaptation of the forward model ($r_{FM} = 0.008, 0.01, 0.015, 0.025, 0.04$) and of inverse model ($r_{IM} = 0.001, 0.003, 0.005, 0.008, 0.01$). The region of minimum error value is highlighted by the thick black line. The error is computed using data from **zero** hour group.

first 32 movements for six-hour group, the simulated data shows the correct shift towards null but a *slower* rate of adaptation.

This leads to the second possibility, that the shift in performance occurs not due to a change in the state of the model, but a change in the rate of adaptation of the models to the new field. To test this hypothesis, the same procedure as the previous section is followed to find the adapatation rates that best fit the experimental data for now the six-hour group when subjects perform in field B_2. The best fit adaptation rates for the zero-hour and six-hour group are shown in Figs. 5.29-5.30 and do show a shift in the rate of adaptation of the two models. Whereas values of $r_{FM} = 0.0158$ and $r_{IM} = 0.0025$ are obtained for the zero hour group, higher values of $r_{FM} = 0.025$ and $r_{IM} = 0.004$ are obtained for the six-hour group. This implies that there is an increase in the rate of adaptation for the six-hour group. The adaptation curves for movement parameters for these two rates of adaptation are shown in Fig. 5.31, and seem to indicate the correct shifts in the values of parameters and the *faster* rate of adaptation observed in experimental data.

The segmenataion data presented in chapter 4 included both the zero-hour and six-hour subjects for the analysis. The two groups did not have significant differences in their segmentation characteristics for the first three movements in the downward direction as shown in Fig. 4.4. This also seems to indicate that the level of internal models has not shifted during the period of rest beacuse the initial behaviour is same for the two groups. Hence the difference is quite likely the result of a faster rate of learning of the new field after 6 hours of rest. This seems to be consistent with the idea of motor interference in the learning of two opposite force fields seperated temporally as proposed by (Shadmehr et al., 1995). The longer the time seperation,

125
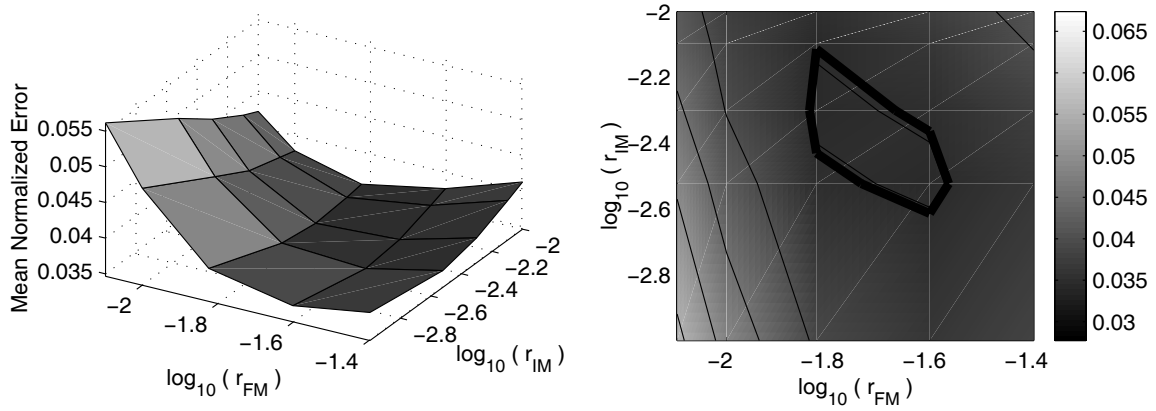
Figure 5.31: Net normalized error E, for five different rates of adaptation of the forward model ($r_{FM} = 0.008, 0.01, 0.015, 0.025, 0.04$) and of inverse model ($r_{IM} = 0.001, 0.003, 0.005, 0.008, 0.01$). The region of minimum error value is highlighted by the thick black line. The error is computed using data from **six** hour group.

the lesser is the interference from a previously learnt task and faster is the rate of adaptation. The process could have something to do with the concept of memory consolidation of the models, a shift from short-term memory to long-term memory over the period of rest, and the possibility that long-term memory has reduced interference when compared to the short-term memory.
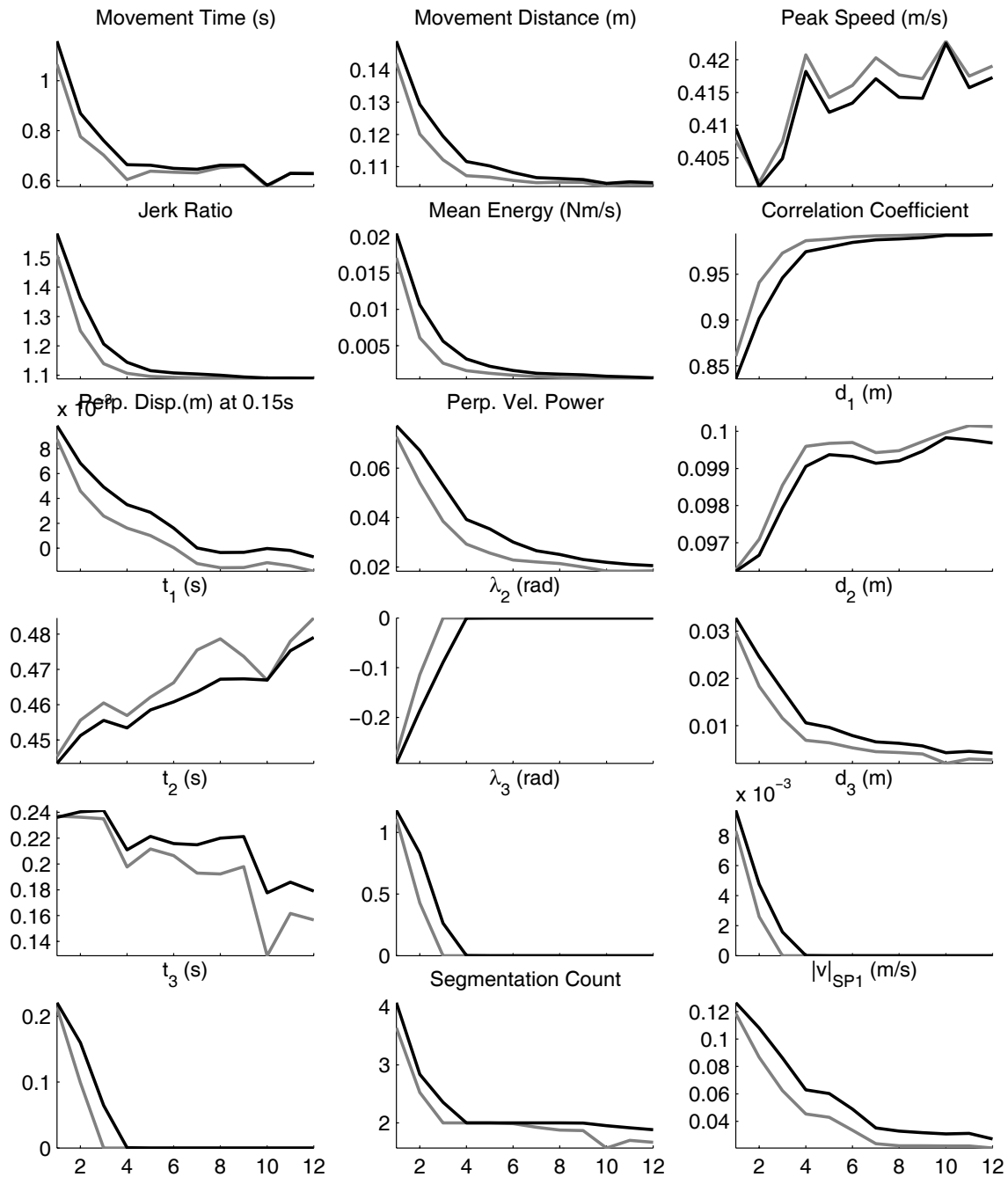
Figure 5.32: Adaptation curve for movement parameters in field B_2 for simulated movements with two different adaptation constants for forward and inverse models - (1) black, zero hour group with $r_{FM} = 0.0158$, $r_{IM} = 0.0025$, (2) gray, six hour group with $r_{FM} = 0.025$, $r_{IM} = 0.004$. The initial states for both are FM(0)=IM(0)=B_1.

Chapter 6

Discussion and Conclusions

The forward-inverse model hand acceleration feedback control seems to achieve the thesis objective of providing a comprehensive framework for study of human motor control and computational processes in the brain. It solves the control problems addressed in the introduction. It provides stable feedback control method for a time-delayed nonlinear system like the human arm and an adaptive control strategy capable of learning novel dynamic interactions. It is also immune to measurement noise in the sensors, particularly so, for velocity signals. In the last two chapters it is shown that simulations with this controller strongly match real human motor behavior in an adaptive control task. This provides validatation for the controller and a strong support for its existence in the brain. By comparing simulated behavior with real human behavior, an insight is also gained into the process of motor adaptation and learning during practice in a novel dynamic environment and during a period of rest after initial training.

Methods for Human Motor Control - Revisited

Let us briefly reconsider the current theories in human motor control. For fast arm movements two feedforward control schemes have been proposed: the equilibrium-point control hypothesis and the inverse dynamics model hypothesis. The equilibrium point hypothesis as proposed by Feldman seeks to get around the problem of nonlinear dynamics of the system by programming a fast feedback loop through the spinal reflex path with positional signals for the muscles. The idea is that if the gain of the feedback is sufficiently high then exact tracking of any desired trajectory is obtained. It suffers from two major drawbacks - delays in the spinal reflex loop that limit the gain of the spinal reflex and the inability to adapt gradually in a novel dynamic environment.

The equilibrium-point hypothesis as proposed by Bizzi, Hogan and Flash is based on programming the activation to muscles using equilibrium properties of a joint connected by several

muscles. Activation to the muscles specifies a particular equilibrium position for the arm. The force-length and force-velocity relations for the muscle provide a zero delay feedback loop. This method also suffers from several disadvantages. It is shown in Sec. 1.3 that the computation involved for determining the activation to the muscles requires knowledge of nonlinear properties of muscles and hence is non-trivial. The feedback gains are limited by physiological limitations on the stiffness of the arm. Infact, as shown by Kawato, the stiffness in human arm movements is much lower than that required for equilibrium-point control. Proof of this is presented in Sec. 2.4 where it is shown that simulation with this control fail to produce desired movements using the measuerd stiffness values. To overcome dynamics of the arm, one requires a virtual equilibrium trajectory (Hogan) that is different from the desired trajectory. This therefore requires existence of two different trajectories. Also the computation of virtual trajectory and its adapatation to novel dynamics is not a trivial problem.

An inverse dynamics model based control seems to overcome the drawbacks of these two methods. It can accurately track any desired trajectory, it is stable and retains equilibrium properties of the arm, and it can adapt to novel dynamics. The computations required for control are inverting the arm dynamics, which is shown to be very simple for unloaded arm movements (Sec. 1.1), and inverting the nonlinear muscle properties. It has been pointed out by Jordan and Kawato that acquiring an inverse model through motor learning is computationallly difficult because the necessary teaching signal for the desired motor command, which is the output of the inverse model, is not available. Kawato has proposed a feedback-error learning model to resolve this difficulty. This feedback is available in the human system from the spinal reflex loop and hence the output of the spinal reflex can be used to adapt the inverse model. The inverse model feedforward control seems to provide an excellent method for control of arm movements. However its major drawback, as with any feedforward system, is that the control signals are determined only by the desired trajectory. The actual trajectory of the arm is ignored and there is no feedback other than limited feedback through spinal reflex and equilibrium muscle properties. This implies that cortical feedback actions like visual corrections to movement are not possible during online control of movement. This is contradictory to atleast two recent observations during visually guided tasks - the segmentation pattern in chapter 4 and an experiment on altered visual feedback by Conditt.

This is the main reason for consideration of feedback methods for control of arm movements. The major problem in the design of a feedback controller is the delay in the feedback loop that tends to destabilize the system. The forward model based Smith predictor method proposed by Miall and Wolpert seeks to overcome the feedback delay. However simulations with the Smith predictor method reveal that this method can be used only for linear systems. The method fails to give stable behavior of the arm for a nonlinear system and for any unmodeled changes in the dynamics of the arm.

The forward-inverse model based feedback control method developed in the current study uses a nonlinear observer based on the forward model to provide stable feedback control. In addition to the forward model it uses the inverse model as the controller in the feedforward path that receives both the desired trajectory and feedback corrections as input. This novel combination of forward and inverse models has several advantages over the methods proposed previously as a result of the following feaures:

- Ability to track any desired trajectory in hand, joint or muscle coordinates

- Compensation for dynamics of arm and muscles through the use of an inverse arm model and an inverse muscle model - this provides the system with a capability to move along a desired trajectory in any dynamic environment once the inverse model adapts to the external dynamics

- A forward model based nonlinear observer that generates current estimates of arm state from delayed visual and proprioceptive feedback and motor commands issued by the inverse model - the state estimates are then used for corrective feedback and as state input to the controller. This provides stable feedback control of a nonlinear dynamic system.

- Correction for errors in the inverse model by a good forward model through feedback action - if the forward model is accurate then the feedbacks gains can be made very high and the system can rely only on feedback to mimic the inverse model and not require an explicit inverse model at all. Therefore a good forward model with high feedback gains allows close to exact tracking of the desired trajectory.

- Cortical feedback gains that are close to five times higher than maximum spinal reflex gains - this allows faster recovery for deviations from desired trajectory caused by external perturbations.

- Visual feedback control of movement - the forward model provides a means of making the feedback current and the inverse model allows the transformation from desired hand trajectory to joint torque that can then be generated by the muscles

- Ability to generate arbitrary static forces and joint torques as an independent variable along with trajectory control

Two advantages of a forward model, other than feedback control, have been hypothesized by Miall and Wolpert. A forward model can be used to in a system that uses motor outflow to cancel the sensory consequences of self-generated movement and by subtraction from actual sensory signals enables the detection of external perturbations. It can also be used for mental

130

rehersal and to predict the outcome of a series of actions thereby allowing motor learning in the absence of action. It has additionally been shown by Narendra that the training of the forward model is easier than the inverse model because it requires conventional backpropogation whereas training of an inverse model requires dynamic backpropogation. Along with Jordan's hypothesis about distal supervised learning where the forward model is used to train the inverse model, it appears that the existence of a forward model is very useful. One of the other advantages that is brought out in the current study is that a fast training of the forward model in an altered external environment allows fast adaptation to that environment and allows the inverse model to be trained more gradually. Although evidence for a slower adapting inverse model is presented in the last chapter, the data is not very strong because of extremely weak reliance of movement parameters on the inverse model. The rate of adaptation of the inverse model cannot be identified very accurately.

While reconsidering the methods of control it is important to mention another approach to human motor control that is different from the ones described above and has been proposed recently by Slotine. This method relies on wave variables to transmit the signals between the master controller and a remote slave. By transforming the motor outflow and the sensory feedback into wave variables before transmitting them, it is shown that stability of the closed loop control is maintained in the presence of time delays in the system. This technique has not been applied for consideration of two-joint arm movements or for adaptation to external dynamics and it will be interesting to find whether or not this method can result in the segmentation pattern observed in the current study.

Open issues in design of the controller

There are a number of open issues in design of the forward-inverse model feedback controller. The first one relates to the control parameters in the controller. The values for feedback gains and muscular co-activation are assumed to be constant through training and within a movement in the current study. It is likely that these control parameters can be modulated by the brain in order to achieve optimal control of the human arm. For instance, co-activation provides greater stability to movements in the presence of unknown perturbations but results in greater energy expenditure by the muscles. Therefore, it is expected that co-activation would be optimized based on a trade-off between stability and energy usage. When a novel dynamic perturbation is introduced, initially the co-activation might be high and then gradually reduce as the internal models adapt to the novel dynamics. Similarly, feedback gains could be optimized based on external perturbations in order to maintain stability and allow maximum gain magnitudes. The other control parameters in the controller are also assumed fixed because a basis for change in their values is not known. It would be interesting to investigate the effect of these control

parameters in different control situations and determine the basis for change in their values.

The other issue relates to the coordinate system of the internal models and the computations in the controller. As formulated in chapter 2, there are atleast three distinct possibilities - cartesian hand coordinates, joint coordinates and muscle coordinates. The behavioral performance of the three methods is very similar in a new dynamic environment and hence identification on the basis of behavior is not possible. However, the computations and the corresponding signals in the controller in the three coordinates are completely different. The coordinates also effect the signals used for learning of the internal models. The muscle coordinates are highly redundant or overspecified because the number of muscles far exceed the degrees of freedom for the arm. However the muscles lengths and forces are directly measured by the sensors and can be directly used in the controller for control and learning. The joint coordinates get rid of the redundancy and allow for coordinated activation of muscles but require transformation from muscle coordinates to joint coordinates. Hand coordinate information is directly available from vision. These three coordinates have to be assessed further in order to establish the differences between them.

A distinction is also not made between proprioceptive and visual feedback and they are both assumed to convey the same information to the brain. In reality, this is certainly not true as evidenced from tasks where a visuomotor transform is introduced[]. The question is how proprioceptive and visual feedback interact with each other and what are the relative roles of the two in control of movement. The experiment by Conditt described in Sec. 1.5.2, where restricting the vision of cursor to a straight line to the target altered the behavior of the movement, could be simulated if the feedback action depended on visually estimated state and the state input to the inverse model depended on proprioceptively estimated state. This either requires two seperate forward models, one in visual space and the other in proprioceptive space, or some transformation from muscle coordinates to hand coordinates or vice versa that incorporates both visual and proprioceptive feedback. This also requires further study.

In the current study, the forward model computes the change in state given the motor command and the current state. It is also possible to use the desired torque or desired acceleration command to compute the change in state. Infact the use of desired acceleration reduces the forward model to an integrator and greatly simplifies the computation involved in state estimation. However, simulations with this method (data not presented) reveal that this form of control can produce the unique kinematic pattern of discontinuities but is much more unstable compared to the forward model using motor commands. The reason is that the observer is not as robust to unmodeled dynamics in the forward model. If a method could be found to stabilize the system in the case of a forward model based on desired acceleration, then the compuatations involved in the controller could be greatly reduced. A possibility is the use of intermittent feedback control hypothesized by (Ronco et al., 1998) where the system is under

open loop control and only intermittently corrected by feedback to maintain stability. It is possible that this intermittent feedback is the cause of segmentation behavior observed in our subjects and needs further investigation.

Implementation of the controller in the brain

In the current study the controllers have been implemented as mathematical equations and relations with certain predetermined structures. During adaptation, for example, the change is assumed to take place in one parameter of such a structure. In the brain however, it is unlikely that the controller exists in a mathematically pre-structured manner. It is much more likely that as children grow and learn to move their arms and legs, they build neural connections in the brain from input-output signals for different functions in the controller, and later modify or adapt these connections to different environments. There are at present a number of unanswered questions. How are the internal models expressed in terms of neural networks? What is the size of such a network? What are the actual signals used for training of the internal models? A greater insight into the processes involved in the controller can be gained by actually implementing the forward and inverse models as neural networks and then studying the adaptation of the neural networks for the two models based on error signals.

It has been hypothesized that these internal models could reside in the cerebellum (Shidara et al., 1993; Miall et al., 1993). Two other brain structures - the basal ganglia and the motor cortex are involved in movement contol. What part of the controller is represented in these regions? A knowlege of the regions of the brain where different components of the controller exist, might help explain deficits seen in certain neural diseases and disorders. In recent work in our lab, it has been shown by (Smith et al., 1997) that Huntingdon's disease could be related to deficits in feedback control of the human arm and clinically it is believed that HD patients suffer from damage to the basal ganglia. Therefore if a link can be made between the affected regions of the brain and components of the controller, then it would provide a much better understanding of the neural disorder itself.

Conclusion

Several avenues for research can arise through the use of the controller developed in this thesis as mentioned in the preceding sections. This control method is developed and tested in the specific context of point-to-point reaching movements of the arm, but can also be applied to a much broader range of motor control situations. But before that, the evidence for control of human arm with this controller needs to be verified further and the issues related to its design resolved.

In conclusion, a method of control of the human arm is developed that uses a combination of feedforward control through an inverse model and feedback control through a forward model. This method provides a means for stable adaptive feedback control of a time-delayed nonlinear system. Evidence for the existence of this control comes from comparison of simulations using this controller and the performance of human subjects in a novel force field. The simulations are able to mimic a unique pattern of near-discontinuities observed in the hand path of our subjects. It is further established that this can occur only with an adaptive forward model. The adapatation data from the subjects fits an exponentially-decaying learning curve for the forward and inverse models as they gradually adapt to the force field. The best fit curve to experimental data points to fast adapting forward and inverse models. The rate constant for the exponential curve of adaptation of the forward model is further established as 0.01 per movement, implying that the forward model learns 63% of the novel force field in 100 movements. The rate of adaptation for the inverse model is determined to be close to 0.003 per movement, but not with great accuracy and hence can lie anywhere in the range from 0.001 to 0.03. Although the rate of adaptation for the inverse model is found to be 3 times slower than the forward model, this result cannot be concretely established. Within the framework of this controller, the discrepancy in behavior between the zero-hour and six-hour group of subjects can be explained by a change in the rate of adaptation of the internal models. For the six-hour group, the adaptation rates are found to be close to 60% higher than the zero-hour group for both the forward and inverse models. This change in the adaptation rate can be attributed to a reduced interference in learning by temporal seperation between learning of two anti-correlated force fields.

Future work on the forward-inverse model feedback controller can provide an even better understanding of the computational processes involved in the brain during control of arm movements and adaptation to novel dynamic environments, as well as the changes in adaptive representation of tasks after active practice.

Bibliography

Bizzi, E., Mussa-Ivaldi, F. A., and Giszter, S. (1982). Arm trajectory formation in monkeys. *Exp Brain Res*, 46:139–143.

Conditt, M. A., Scheidt, R. A., and Mussa-Ivaldi, F. A. (1997). Visual influence on learning arm dynamics. *Soc Neurosci Abs*, 23.

Feldman, A. G. (1966). Functional tuning of the nervous system with control of movement or maintenance of a steady posture- ii. controllable parameters of the muscle. *Biophysics*, 11:565–578.

Flanagan, J. R. and Rao, A. K. (1995). Trajectory adaptation to a nonlinear visuomotor transformation: Evidence of motion planning in visually perceived space. *J Neurophysiol*, 74:2174–2178.

Flash, T. (1987). The control of hand equilibrium trajectories in multi-joint arm movements. *Biol Cybern*, 57:257–274.

Flash, T. and Hogan, N. (1985). The coordination of arm movements: an experimentally confirmed mathematical model. *J Neurosci*, 5:1688–1703.

Fu, Q.-G., Flament, D., Coltz, J. D., and J., E. T. (1997). Relationship of cerebellar purkinje cell simple spike discharge to movement kinematics in the monkey. *J Neurophysiol*, 78:478–491.

Georgopoulos, A. P., Kalaska, J. F., Caminiti, R., and Massey, J. (1982). On the relations between the direction of two-dimensional arm movements and cell discharge in primate motor cortex. *J Neurosci*, 2:1527–1537.

Gielen, C. C. A. M. and Houk, J. C. (1987). A model of the motor servo: Incorporating nonlinear spindle receptor and muscle mechanical properties. *Biol Cybern*, 57:217–231.

Gomi, H. and Kawato, M. (1996). Equilibrium-point control hypothesis examined by measured arm stiffness during multijoint movement. *Science*, 272:117–20.

Gordon, J., Ghilardi, M. F., and Ghez, C. (1995). Impairments of reaching movements in patients without proprioception: I. Spatial errors. *J Neurophysiol*, 73:347–60.

Gribble, P. L., Ostry, D. J., Sanguineti, V., and LaBoissiere, R. (1998). Are complex control signals required for human arm movement? *J Neurophysiol*, 79:1409–24.

Hogan, N. (1984). An organizing principle for a class of voluntary movements. *J Neurosci*, 4:2745–54.

Jordan, M. I. (1995). Computational aspects of motor control and motor learning. In Heuer, H. and Keele, S., editors, *Handbook of Perception and Action: Motor Skills*. Academic Press, New York.

Jordan, M. I., Flash, T., and Arnon, Y. (1994). A model of the learning of arm trajectories from spatial deviations. *J. Cognitive Neuroscience*, 6(4):359–376.

Jordan, M. I. and Rumelhart, D. E. (1992). Forward models: supervised learning with a distal teacher. *Cognitive Science*, 16:307–54.

Karniel, A. and Inbar, G. F. (1997). A model for learning human reaching movements. *Biol Cybern*, 77:173–83.

Kawato, M., Furukawa, K., and Suzuki, R. (1987). A hierarchical neural network model for control and learning of voluntary movement. *Biol Cybern*, 57:169–185.

Kawato, M. and Gomi, H. (1992). A computational model of four regions of the cerebellum based on feedback-error learning. *Biol Cybern*, 68:95–103.

Krylow, A. M., Sandercock, T. G., and Rymer, W. Z. (1995). Muscle models. In Arbib, M. A., editor, *The handbook of brain theory and neural networks*, pages 609–13. MIT Press, Cambridge, MA.

Lohmiller, W. and Slotine, J. (1996). Metric observers for nonlinear systems. *IEEE Int Conf on Control Applications, Dearborn, MI*.

Massaquoi, S. G. and Slotine, J.-J. E. (1996). The intermediate cerebellum may function as a wave-variable processor. *Neurosci Letters*, 215:60–64.

Miall, R. C., Weir, D. J., Wolpert, D. M., and Stein, J. F. (1993). Is the cerebellum a Smith predictor? *J Motor Behav*, 25:203–16.

Miall, R. C. and Wolpert, D. M. (1996). Forward models for physiological motor control. *Neural Networks*, 9:1265–79.

Murray, W. M., Delp, S. L., and Buchanan, T. S. (1995). Variation of muscle moment arms with elbow and forearm position. *J Biomech*, 28:513–525.

Mussa-Ivaldi, F. A., Hogan, N., and Bizzi, E. (1985). Neural, mechanical and geometric factors subserving arm posture in humans. *J Neurosci*, 5:2732–2743.

Narendra, K. S. (1990). Identification and control of dynamical systems using neural networks. *IEEE Trans Neural Netw*, 1:4–27.

Ronco, E., Arsan, T., Gawthrop, P. J., and Hill, D. J. (1998). Open-loop intermittent feedback optimization control: a model of the human motor control system. *IEEE*, submitted.

Sanes, J. N. and Shadmehr, R. (1995). Sense of muscular effort and somesthetic afferent information in huamns. *Can J Physiol Pharmacol*, 73:223–233.

Scott, S. H. and Kalaska, J. F. (1997). Reaching movements with similar hand paths but different arm orientation: I. activity of individual cells in motor cortex. *J Neurophysiol*, 77:826–852.

Sergio, L. E. and Kalaska, J. F. (1997). Systematic changes in directional tuning of motor cortex cell activity with hand location in the workspace during generation of static isometric forces in constant spatial directions. *J Neurophysiol*, 78:1170–74.

Shadmehr, R., Brashers-Krug, T., and Mussa-Ivaldi, F. A. (1995). Interference in learning internal models of inverse dynamics in humans. In Tesauro, G., Touretzky, D. S., and Leen, T. K., editors, *Advances in Neural Information Processing Systems*, volume 7, pages 1117–1124. MIT Press, Boston.

Shadmehr, R. and Holcomb, H. H. (1997). Neural correlates of motor memory consolidation. *Science*, 277:821–825.

Shadmehr, R. and Mussa-Ivaldi, F. A. (1994). Adaptive representation of dynamics during learning of a motor task. *J Neurosci*, 14(5):3208–3224.

Shidara, M., Kawano, K., Gomi, H., and Kawato, M. (1993). Inverse dynamics model eye movement control by purkinje cells in the cerebellum. *Nature*, 365:50–52.

Slotine, J. E. and Li, W. (1987). On the adaptive control of robot manipulators. *Int J Robot Res*, 6:49–59.

Smith, M., Shadmehr, R., and Brandt, J. (1997). Motor learning disorders in gene-positive but pre-symptomatic Huntington's disease. *Soc Neurosci Abs*, 23:203.

Soechting, J. F. and Flanders, M. (1997). Evaluating an integrated musculoskeletal model of the human arm. *J Biomech Eng*, 119:93–102.

Turrell, Y., Bard, C., Fleury, M., Teasdale, N., and Martin, O. (1998). Corrective loops involved in fast aiming movements: effect of task and environment. *Exp Brain Res*, 120:41–51.

Wolpert, D. M., Ghahramani, Z., and Jordan, M. I. (1994). Perceptual distortion contributes to the curvature of human reaching movements. *Exp Brain Res*, 98:153–6.

Wolpert, D. M., Ghahramani, Z., and Jordan, M. I. (1995). An internal model for sensorimotor integration. *Science*, 269:1880–82.